5 MECHANICAL STABILITY MODEL

Rock mechanics evaluation was performed for the Äspö HRL based on the results from rock stress measurements in three boreholes on Äspö, the laboratory testing on core samples and geological pre-investigations */Stille and Olsson, 1990/*. During excavation of the tunnel a number of overcoring measurements for rock stress determination were made underground. After each excavating sequence a rock mass classification was carried out for the latest excavated part of the tunnel. Complementary laboratory tests of rock samples from the tunnel were also made. The report, *Stille and Olsson /1996/* summarize rock mechanics experience and discuss the situation in more general terms from the viewpoint of the specific conditions at Äspö HRL.

The mechanical stability model comprises:

- the rock stress situation
- mechanical properties
- rock mass classification

5.1 ROCK STRESS CONDITIONS

5.1.1 Results from deep surface boreholes

During the site investigation phase, stress measurements were made in surface boreholes KAS02, KAS03 and KAS05 see *Figure 5-1*. KAS02 and KAS05 were drilled near-vertical, within and below the rock volume later enveloped by the ramp loops. KAS03 is also near-vertical, but located some 500 m to the north-west of the ramp area.

The surface borehole measurements employed both hydraulic fracturing and overcoring. Hydraulic fracturing was used in holes KAS02 and KAS03, and provided a total of 41 point measurements, distributed over depths down about 950 m. Hydraulic fracturing is a two-dimensional method that provides information on stress conditions in the plane perpendicular to the borehole (i.e. in this case horizontal stress components).

In KAS05, an early version of the three-dimensional deep-hole overcoring method developed by the Swedish State Power Board was used. A total of 7 tests were reported from the overcoring work. Three points were located at a depth of 195 metres and the remaining four at about 355 metres.

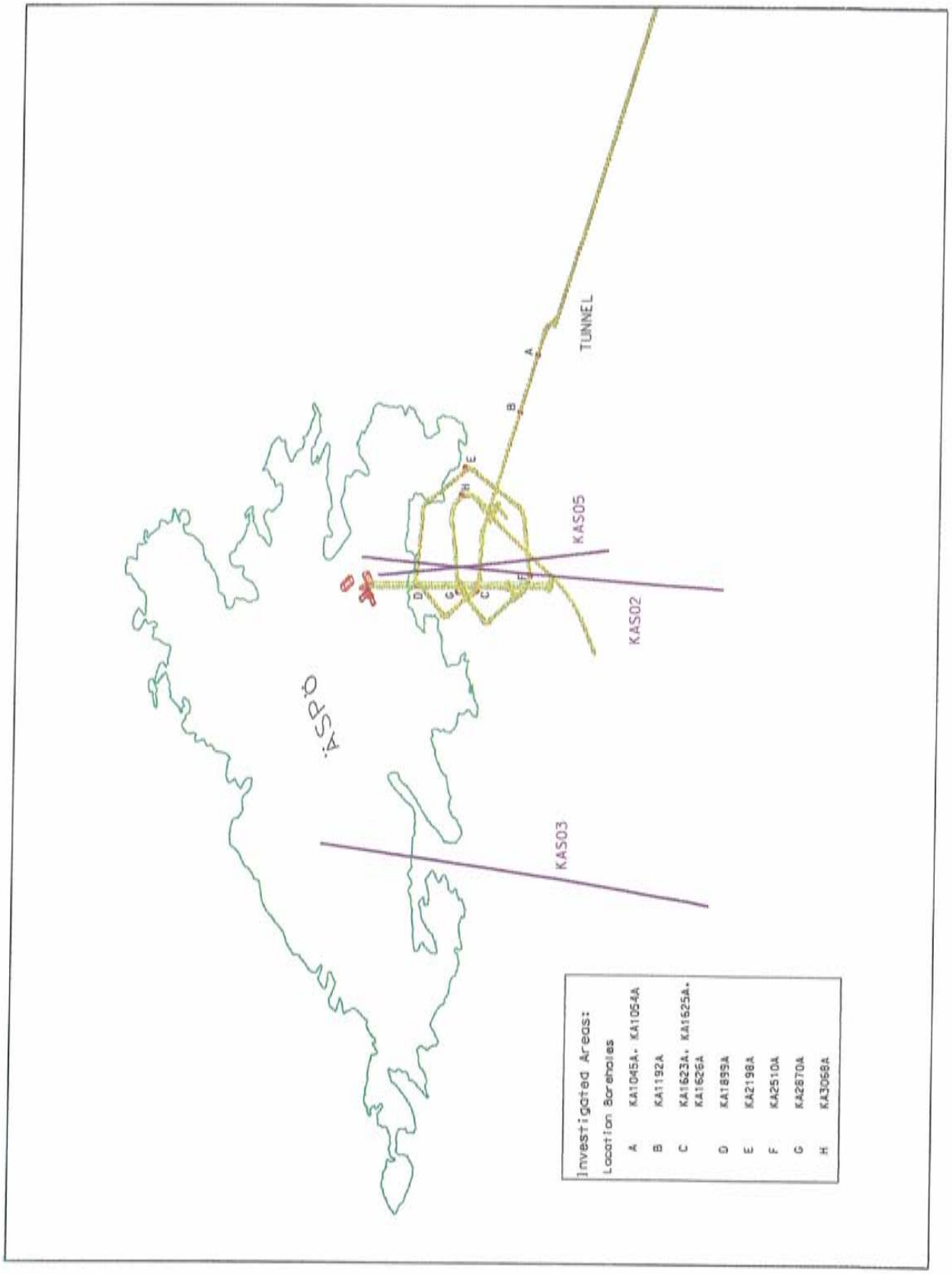

Figure 5-1. *Surface boreholes and locations along the ramp where stress measurements were made /Leijon, 1995/.*

5.1.2 Results from short underground boreholes

Concurrent with the excavation of the access ramp, overcoring measurements were made in a series of 12-18 m long, near-horizontal boreholes drilled from suitable locations along the ramp. The main objective was to evaluate predictions of local rock stresses made prior to excavation. An additional objective was to provide background data required to establish stress ranges on a site scale. The overall state of stress determines the mechanical boundary conditions for the various experiments to be conducted at Äspö */Leijon, 1995/*.

Starting at a depth of 143 m, measurements were made in a total of 11 boreholes, representing 8 locations along the ramp, the deepest at 408 metres. As indicated in *Figure 5-1*, two measurement locations are located in the first, straight part of the ramp. The remaining locations are distributed along the spiral part.

The measurements prove a dominating NW-SE orientation, which corresponds to the prediction see *Figure 5-2*.

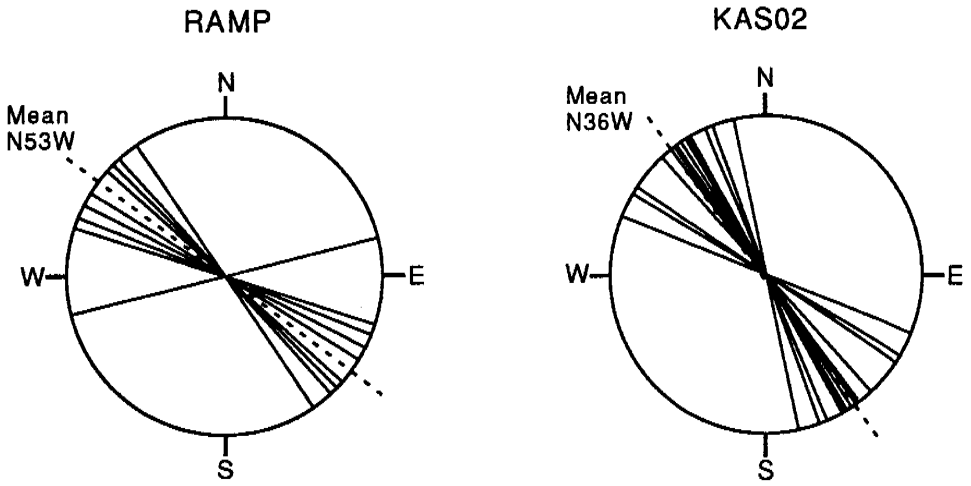

Figure 5-2. *Orientation of maximum horizontal stress, from overcoring holes in the ramp (hole averages) and hydraulic fracturing in KAS02 (test points) /Leijon, 1995/.*

The measurements made in the tunnel proved the presence of a considerably higher stress level than was anticipated, based on the measurements made in the deep surface boreholes. The estimated mean Ko-value (Ko is the ratio between the maximum horizontal stress (σ_H) and the theoretical vertical stress (σ_V)) for all boreholes, is 2.9, with the average for individual boreholes ranging between 1.7 and 4.0. Single measurements in the individual boreholes varied

between 1.5 and 4.0. The Ko-values at different depths are presented in *Figure 5-3 /Stille and Olsson, 1996/.*

The maximum horizontal stress component proved to be significantly higher for the measurements made in the tunnel. The maximum horizontal stress component measured at different depths in surface boreholes and in the tunnel are presented in *Figure 5-4.*

The relationship between the highest horizontal stress and the lowest horizontal stress is presented in *Figure 5-5* for the same measurements as in the figure above.

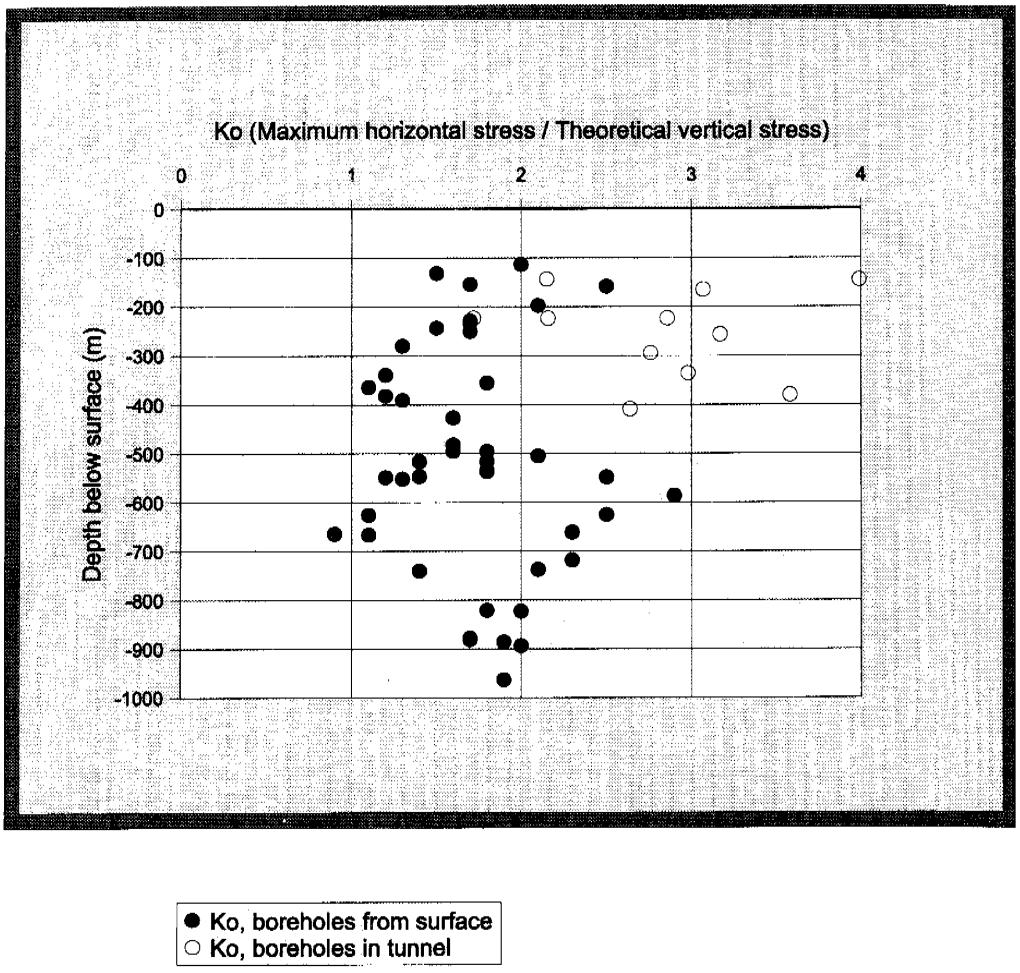

Figure 5-3. *Ko-values at different depths /Stille and Olsson, 1996/.*

The difference between the results from rock stress measurements made from the surface and in the tunnel can not be explained by geometrical factors, for example that measurements in the tunnel were made too close to the tunnel. Some differences may possibly be explained by natural variations in the rock mass.

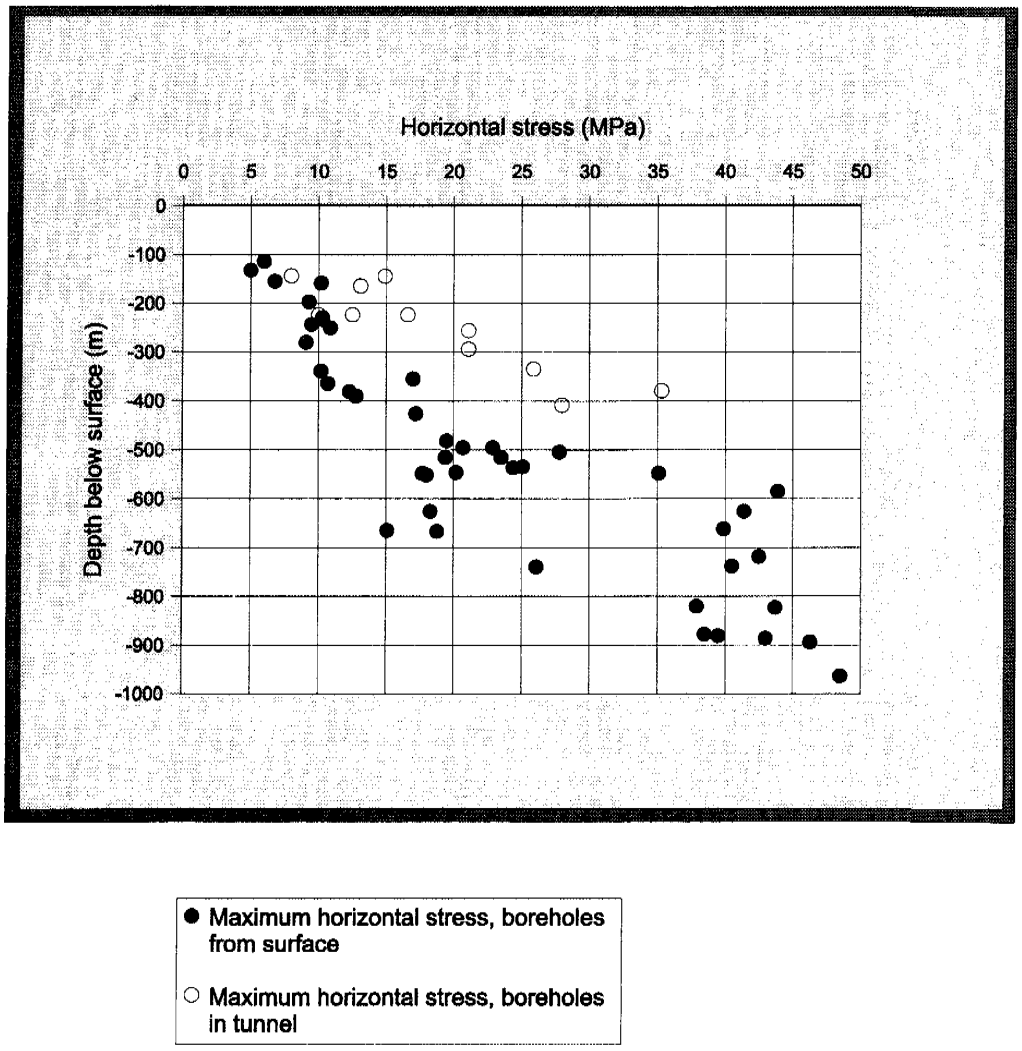

Figure 5-4. *Measured maximum horizontal stress /Stille and Olsson, 1996/.*

It is, however, probable that a large portion of the differences is due to the two different methods for making the measurements, i.e. overcoring and hydraulic fracturing. A brief review of all measurements shows that hydraulic fracturing provides significantly lower stress levels. In the pre-investigation phase the majority of the measurements were made using hydraulic fracturing, while overcoring was used for all measurements in the tunnel.

A more comprehensive analysis of the rock stress conditions at Äspö are needed to give a clear explanation of the significant difference between the rock stress magnitude measured from the surface and that measured from the tunnel. It is recommended that such study be performed.

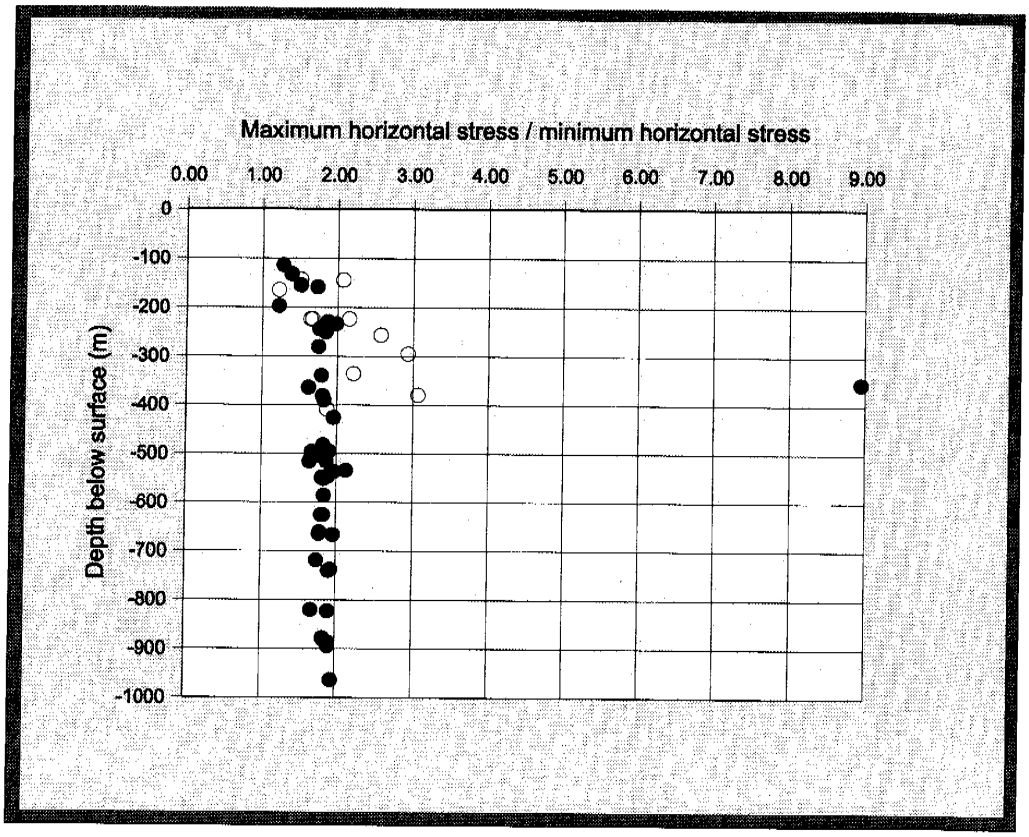

Figure 5-5. *Relationship between maximum and minimum horizontal stress /Stille and Olsson, 1996/.*

5.2 MECHANICAL PROPERTIES

The laboratory testing comprised uniaxial compressive strength, Young's moduli, Poisson's ratio and an estimate of the degree of brittleness. A few results from testing of joints were also presented in *Stille and Olsson /1996/.*

The tests were performed on cores selected from one single borehole. A total of four tests were carried out for each of the four rock types.

Laboratory testing of mechanical properties is usually of less importance for predictions of rock stability conditions in Swedish underground facilities. The results from compressive strength testing are used to ensure that the correct magnitude of compressive strength is applied in the rock classification system. The testing of brittleness is important for further evaluations on the potential for rock burst. The number of tests usually performed prior to excavation is normally small and the result usually exhibit rather big variations.

During the excavation period cores were drilled out in the tunnel and selected for laboratory testing. Similar testing was carried out during the prediction phase. The testing of joint surface parameters was, however, not performed and is not further discussed here. A total of ten tests were generally performed for each parameter and rock type. Only nine tests were performed for fine-grained granite. The cores for each rock type were selected from 2-8 different boreholes, mainly located in the first part of the tunnel. The results of the testing are further described by *Lee et al /1993/* and *Delin et al /1993/.*

A summary of the results from the testing performed during the pre-investigation and excavation phases is presented in *Table 5-1 /Stille and Olsson, 1996/.*

The variations between the results from the pre-investigation phase and those from the excavation phase are significant. Significant variations were also observed between tests performed during the same phase. The significant variations may possibly be explained by the small number of tests performed and also by natural variations in the rock mass. The samples were also collected from different levels. Earlier experience also proved that a large number of tests must be performed to achieve high statistical accuracy in the material.

For design of underground constructions in similar rock types in Sweden, a large part of the laboratory testing may be replaced by general experience from other sites. The testing should mainly be concentrated to specific rock types of major importance for indications of, for example, spalling, slaking, rock burst and poor rock.

For investigations and undisturbed testing of rock of poor quality drilling techniques other than those used at the Äspö Hard Rock Laboratory are necessary, like triple-barrel core drilling.

5.3 CLASSIFICATION OF ROCK MASS

A well established rock classification is of great importance when planning of a new underground project. Time and cost conditions will be influenced to a high degree by the rock quality, especially the amount of rock of poor quality which will require to comprehensive rock support and grouting */Stille and Olsson, 1996/.*

The demand for establishing an acceptable prediction for rock qualities is extremely important for underground constructions at great depth, where the groundwater pressure present will raise difficulties in stability and sealing matters.

Table 5-1. Laboratory testing of mechanical parameters. From *Stille and Olsson, 1996/.* Data based on surface boreholes or tunnel boreholes.

	Greenstone	Fine-grained granite	Äspö diorite	Småland (Ävrö) granite
Unconfined compressive strength (MPa)	**(MPa)**	**(MPa)**	**(MPa)**	**(MPa)**
Surface boreholes				
-mean	119	236	184	189
-range	103-168	152-336	164-217	147-260
No of tests	4	4	4	4
Tunnel boreholes				
-mean	207	258	171	255
-range	121-274	103-329	103-210	197-275
No of tests	10	9	10	10
Young's modulus (Gpa)	**(GPa)**	**(GPa)**	**(GPa)**	**(GPa)**
Surface boreholes				
-mean	53	65	60	62
-range	32-74	59-70	54-65	62-63
No of tests	4	4	4	4
Tunnel boreholes				
-mean	78	77	73	74
-range	71-96	72-80	65-80	63-79
No of tests	10	9	10	10
Poisson's ratio	**(-)**	**(-)**	**(-)**	**(-)**
Surface boreholes				
-mean	0.25	0.22	0.23	0.24
-range	0.24-0.26	0.20-0.22	0.20-0.25	0.24
No of tests	4	4	4	4
Tunnel boreholes				
-mean	0.24	0.23	0.24	0.23
-range	0.18-0.31	0.21-0.25	0.22-0.29	0.20-0.26
No of tests	10	9	10	10
Brittleness				
Surface boreholes				
-degree of brittleness	more brittle	less brittle	brittle	brittle
No of tests	4	4	4	4
Tunnel boreholes				
-degree of brittleness	brittle	more brittle	more brittle	more brittle
No of tests	10	9	10	10

Table 5-2. Summary of predicted and observed RMR-values along the tunnel 431-2875 m /Stille and Olsson, 1996/. 'Prediction' was based on surface borehole data. 'Outcome' in the table is based on tunnel mapping data.

Class	RMR-value	Predicted distribution (%)	Outcome distribution (%)
A	RMR >72	23	28
B	RMR 60-72	50	40
C	RMR 40-60	19	28
D	RMR <40	3	4
E	RMR <40	5	

The distributions of individual RMR-values are presented in *Figure 5-7.*

For the classification of the rock mass in the Äspö tunnel the RMR-system was applied. This system employs five parameters describing the rock mass and is more simple to use when the classification is based on pre-investigation data. If any parameter is missing, it is possible to estimate the value of the missing parameter. The Q-system is more complex and employs more parameters. The RMR-system is usually divided into five different groups which correspond to 'very good rock' to 'very poor rock'. To get a more accurate prediction for the Äspö tunnel the rock mass was divided into five groups which were estimated to better apply to the different stability conditions expected to be significant */Stille and Olsson, 1996/.*

The following stability conditions were in the prediction estimated to apply to the different rock mass classes:

Class A Instability of single blocks.

Class B Instability of single key blocks which may progress to failure of the roof arch. Orientation of joints will determine the amount of rock support necessary.

Class C Instability in the roof. Difficult to locate all unstable areas. Both small and large blocks have to be supported. Large blocks are supported by bolts and smaller blocks by shotcretes. Bolts and shotcretes are applied systematically.

Class D General instability in walls and roof. A rock arch has to be established to make the tunnel stable. This necessitates systematic installation of bolts and shotcretes.

Class E As class D.

A summary of the predicted and observed RMR-values is presented in *Table 5-2*. The variations in observed RMR-values along the tunnel are presented in *Figure 5-6*.

To analyse the effect of major fracture zones, that can probably be identified during the pre-investigation phase, the distribution of RMR-values in % of tunnel length were plotted including the zones, see *Figure 5-7*. *Figure 5-8* shows the distribution of individual RMR-values along the tunnel excluding the parts that have been geologically defined as fracture zones wider than 5 m. The geological definition of zones is further described by *Annertz, K* in *Rhén and Stanfors /1995/*.

The RMR-values for different rock types were also analysed. The distributions of RMR-values in respective rock types are shown in *Figures 5-9* to *5-12*.

A summary of RMR-values in the different rock types is also presented in *Table 5-3*.

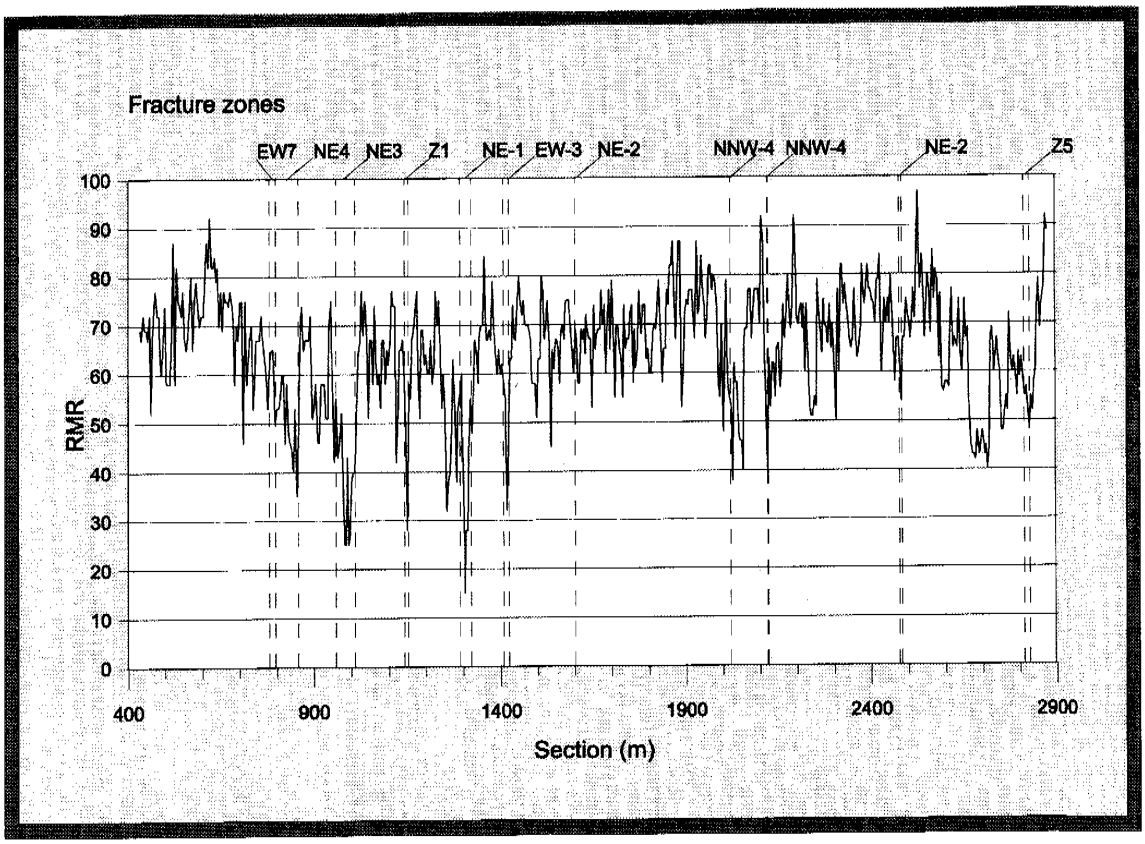

Figure 5-6. *Distribution of RMR-values along the tunnel /Stille and Olsson, 1996/.*

Table 5-3. Summary of RMR-value in different rock types *Stille and Olsson, 1996/*. Tunnel mapping data.

	Greenstone	Fine-grained granite	Äspö diorite	Småland (Ävrö) granite
Mean RMR-value	64	48	69	65
Interval	53-74	15-89	28-97	35-92
Standard dev.	6	13	10	11
No. of values	18	69	289	202

The predicted RMR-values for the tunnel show acceptable correspondence with the observations made in the tunnel.

The portion of poor rock will have a determining influence on cost and time factors for the tunnelling work. It is therefore important that the prediction of poor rock correspond well to the outcome. For the Äspö tunnel poor rock was predicted to 8 % while the outcome was 4 %. While establishing a prediction of rock quality a rock classification system is commonly applied to core samples. General experience from this is that the prediction will be somewhat conservative, i.e. lower RMR-values will be predicted than what actually will be found in the tunnel.

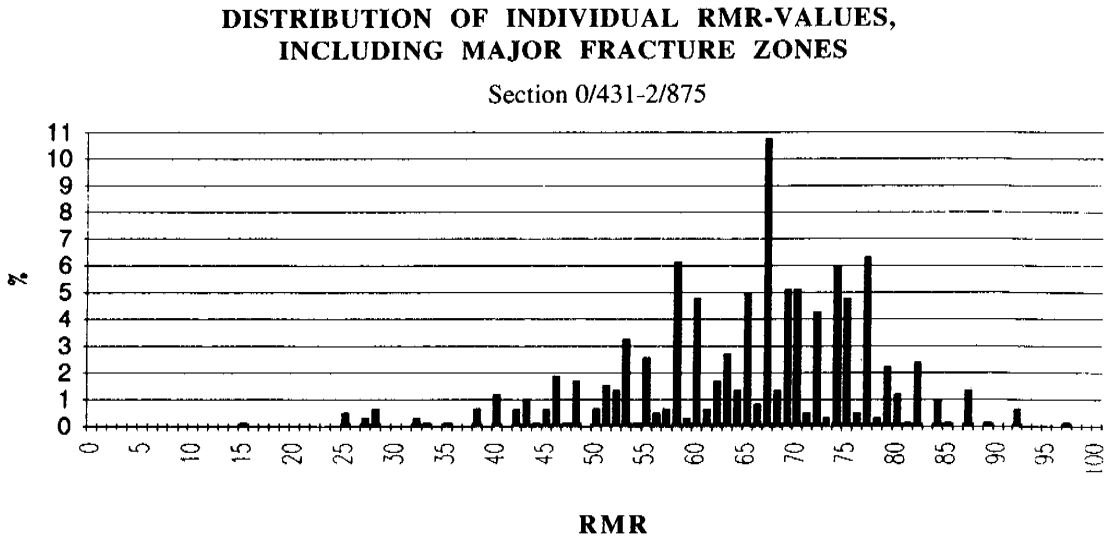

Figure 5-7. *Distribution of individual RMR-values in % of tunnel length, major fracture zones included. Tunnel section 431 - 2875 m /Stille and Olsson, 1996/.*

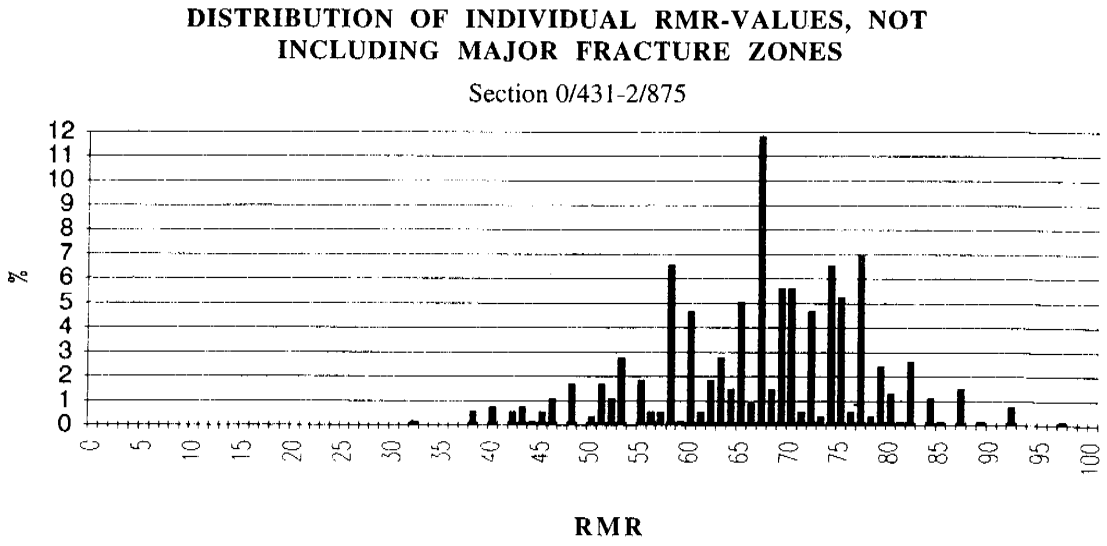

Figure 5-8. *Distribution of individual RMR-values in % of tunnel length, major fracture zones not included. Tunnel section 431 - 2875 m /Stille and Olsson, 1996/.*

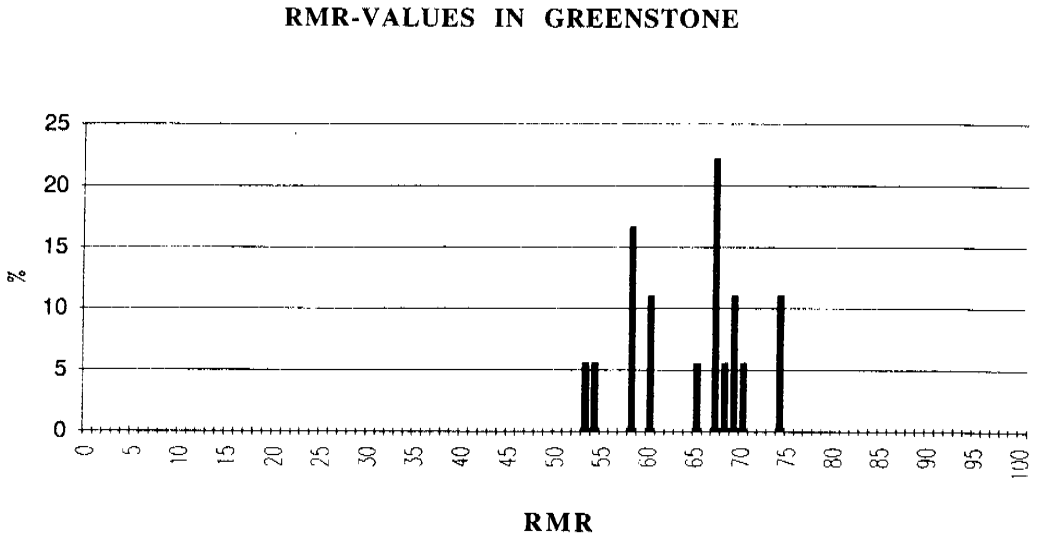

Figure 5-9. *RMR-values in % of tunnel length in greenstone. Tunnel section 431 - 2875 m /Stille and Olsson, 1996/.*

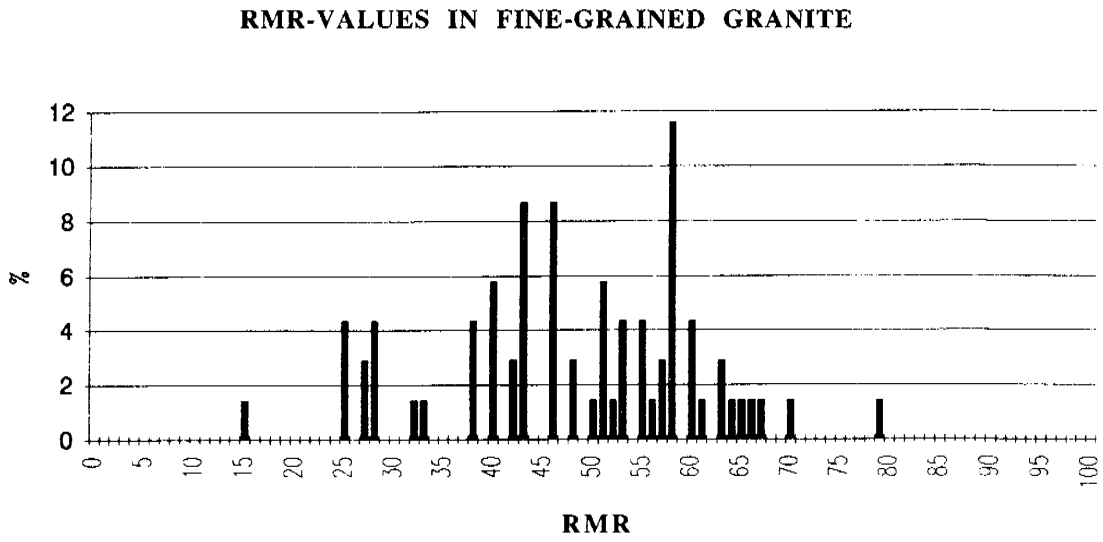

Figure 5-10. *RMR-values in % of tunnel length in fine-grained granite. Tunnel section 431 - 2875 m /Stille and Olsson, 1996/.*

Experience from the Äspö tunnel prove that the rock quality is very dependent on the rock type. Fine-grained granite, which is often fractured, exhibits both significantly lower mean RMR-values and larger variations.

The differences between greenstone, Småland (Ävrö) granite and Äspö diorite are smaller and they also show smaller variations.

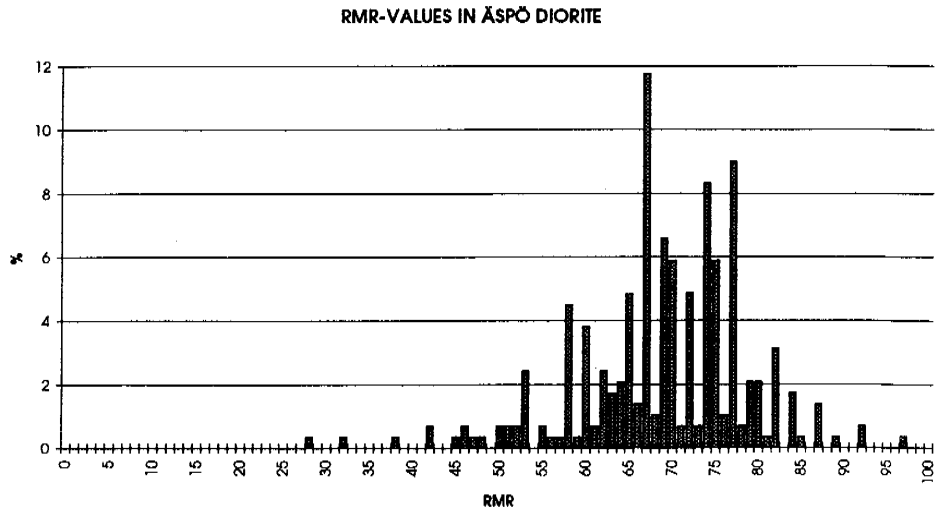

Figure 5-11. *RMR-values in % of tunnel length in Äspö diorite. Tunnel section 431 - 2875 m /Stille and Olsson, 1996/.*

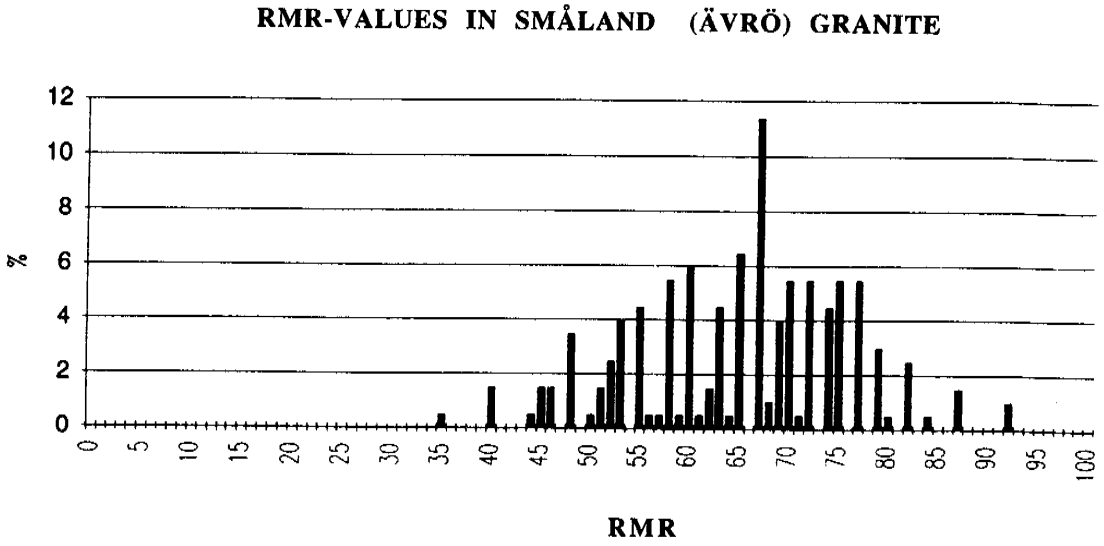

Figure 5-12. *RMR-values in % of tunnel length in Småland (Ävrö) granite. Tunnel section 431 - 2875 m /Stille and Olsson, 1996/.*

5.4 RISK OF SPALLING, SLAKING AND ROCK BURST

Since parts of the tunnel was located at a very considerable depth there was a possible risk of rock burst. Rock burst usually occurs at great depth where rock stresses are high, but it may also be observed at lesser depths under some conditions. Rock stress problems with frequent rock burst are very difficult to foresee with certainty */Stille and Olsson, 1996/.*

Rock burst is an explosion-like failure in virgin rock, and depends on a number of factors such as:

- High stresses in the rock
- Residual stresses
- Anisotropic stress conditions
- Mechanical properties of the rock (structure, compressive strength, brittleness)
- Fracture pattern in the rock.

To enable an evaluation of rock-burst activity to be made, some empirical relationships were used for the prediction.

It was predicted that no rock burst to just minor rock burst should occur and if rock burst should occur it would only be of minor intensity, like spalling and mainly connected to greenstone. As already mentioned, much higher maximum horizontal stresses were measured, up to around 30 MPa, from the tunnel than in the pre-investigation (~20 MPa).

The laboratory testing of the rock has shown that the strength is a little higher than was predicted. The higher horizontal stresses, that were measured, will however increase the risk for rock burst.

An updated prediction of rock burst, based on both the higher rock strength and the higher stress level, indicates that minor spalling may occur both in the greenstone and Äspö diorite at depth greater than 400 m.

No rock burst was observed during the tunnelling operation. Occasional cracking was heard after excavation and some tendency to spalling was noted. The rock burst problem was thus less than expected from the updated prediction. The result emphasises the difficulties of foreseeing rock burst activity.

5.5 ROCK SUPPORT

The rock support performed in the tunnel has comprised rock bolting, shotcrete and grouting. The rock support work performed is presented and further discussed below.

Bolts

Rock support with bolts comprised three different types of bolt:

- Coated Swellex length L = 3 - 4 m
- Örsta CT-bolt length L = 3 - 4 m
- Grouted rebars, non-tensioned without plates length L = 2.4 - 3 m

In general, Swellex bolts and grouted rebars were used as temporary support installed during the excavating process, while the CT-bolts were used as permanent support and installed after excavation.

Shotcrete

Shotcreting was done using both the wet mix and dry mix methods. For the part of the tunnel where the most intensive fracture zones are located, stretching to section 2600 m, the contractor Siab selected the wet mix method. This also permitted the application of shotcrete containing fibres. For the rest of the tunnel, which were excavated by a contractor Skanska, the dry mix method was used.

Shotcrete were predominately used as permanent support installed after tunnel excavation. In the major fracture zones, NE-3 and NE-1, intensive support with shotcrete with fibres and bolts was applied during the excavation cycle.

The amount of rock support work performed in the tunnel is presented in *Table 5.4*. Support work performed in connection with the caverns established for the hoist and ventilation shafts is not included. The shotcreted areas refer to the theoretical (or calculated) areas.

Rock support installed in connection with major fracture zones, defined as being more than 5 m wide, is presented separately. Rock support in connection with these zones has usually been applied over a larger area than the area geologically defined as a zone. The total length of the zones is 225 m. With the adjacent areas, where support work has been performed and obviously needed, the total length is 350 m, which is approximately 11% of the tunnel length. As much as 55% of all bolting and 77% of all shotcrete in the tunnel have been performed in connection with these zones.

Table 5-4. Summary of rock support work performed.

		Tunnel portal	**Fracture zones width >5 m (11% of tunnel length)**	**Remaining tunnel**	**Total**
Bolts	(no)	56	396	267	718
	(%)	8	55	37	100
Shotcrete	(m^2)	120	3377	900	4397
	(%)	3	77	20	100

For the rock bolting it has not been possible, except for the zones, to identify a relationship between the rock quality or rock type and the amount of rock bolts. Rock bolts have predominantly been installed as spot bolts in the roof and walls in all different rock qualities and rock types.

Systematic bolting has only been performed in the most intensive parts of NE-3 and NE-1. The typical rock quality in the zones is fair and poor, i.e. Classes C, D and E (RMR 20-60).

Shotcreting was performed predominantly in connection with the zones and in other areas in the tunnel with RMR values less than 60. According to the geological follow up, 32% of rock belonged to Classes C, D and E. The predicted rock support for these classes was a general shotcreting of the roof. However, just 8% of the tunnel length has been supported with shotcrete.

The problem of identifying a more distinct relationship between rock support and rock quality outside the zones can partly be explained by the generally very low support intensity in the tunnel.

The stability conditions in the tunnel are in general good. In the dominating part of the tunnel the stability conditions only required spot bolting of single blocks in the roof. Large areas of the tunnel have no rock support. More intensive rock support work has only been performed in connection with major fracture zones.

A favourable geometry and size of tunnel, as well as the future activities in the tunnel which will permit the installation of complementary support, have probably influenced the amount of support installed.

In relation to the rock classification, however, the amount of rock support has been small. However, no observation has been made during the construction period, and first year of the operation, that indicates a low stability in the tunnel. There is therefore no present information that indicates that the tunnel possibly is under-supported, i.e. the tunnel has not been made with too little support.

It is also important to point out that most of the rock support has been applied in the major fracture zones. One of the main objectives during the pre-investigation stage must, from a rock mechanics point of view, be to identify major fracture zones.

5.6 GROUTING

The experience from the grouting work in the tunnel has been evaluated in detail and the results are presented in two separate reports */Stille et al, 1993 and 1994, Gustafson and Stille, 1996/.*

The difficult hydrogeological conditions for the tunnelling work, with high water pressure and locally high transmissivities in the rock mass, made the grouting operations very important for the tunnelling work.

At an early stage of the project there was a desire to avoid grouting operations in the tunnel due to planned future research activities concerning hydrogeology and groundwater chemistry. It was, however, obvious at an early stage that the amount of grouting work would be significant. Three objectives were therefore set up for the grouting work:

- the total allowed flow of water into the tunnel was specified at 3000 l/min (approximately 80 l per minute per 100 m)
- the grouting work should fulfil the demands of not jeopardizing the stability conditions
- the grout spread around the tunnel should be limited to 10 m.

The results of the grouting work correspond well to these requirements.

A total of 150 grouting operations were performed in the tunnel along section 0-3137 m. The grouting were predominantly performed as pregrouting, i.e. before the excavation sequence. Regrouting, (more than one pregrouting at the same tunnel front) was performed 50 times out of the total of 150. Regrouting was performed mainly in the most extensively fractured zones (NE-1 and NE-3) which represent 36 out of 50 regroutings.

The total pre-grouted length of the tunnel is approximately 841 m which corresponds to 27%. The total length of grout fans are approximately 10% higher, since a certain overlap is desired between grout fans.

Complementary grouting was also performed in probe holes and core boreholes which have been drilled for the research programme. These groutings are not further discussed here.

During the first part of the tunnel, grouting was performed with a cement-silicate grout. During the extensive grouting work at NE-1 difficulties were encountered in achieving required strength of the grout to withstand the water pressure. To be able to remove the packers after a few hours grouts were used to which calcium chloride had been added. The amount of calcium chloride varied between 8% and 12%. Grouted volumes for different categories are presented in *Table 5-5*. The distribution of grout volumes along the tunnel is presented in *Figure 5-13*.

The table shows that 40% of the grouted volume was in parts of the tunnel not being characterized as zones. In zones wider than 5 m, 44% of the grout volume was consumed. These zones are of a size that both their position and nature can be identified and predicted in the pre-investigation stage. Smaller zones, less than 5 m, and the single fractures that consumed the remainder of the grout are more difficult to localize prior to excavation. In the pre-investigation phase the hydrogeological conditions will, however, be characterized and the presence of single fractures can be predicted. The position of single conductive fractures is however very difficult to predict.

For construction of tunnels at shallow depth the water pressure is usually not considered. Tunnels at great depth, with high water pressure, are exposed to greater stability risks than other tunnels. The stability problems can result in rapidly increased loads on tunnel support. Special attention must be given the design of rock support in tunnels with high water pressure.

Table 5-5. Summary of grouted volumes and drilled grout holes. (l = litre).

	Grouted volume (l)	Total length of grout holes (m)	Grouted volume per drilled borehole metre (l/m)
Zones width <5 m (23 no)	76 500 (16%)	2 400	32.0
Zones width >5 m (12 no, 225 m)	205 000 (44%)	14 400	14.2
Remaining parts of tunnel	189 500 (40%)	700	27.0
Total	471 000	23 800	19.8

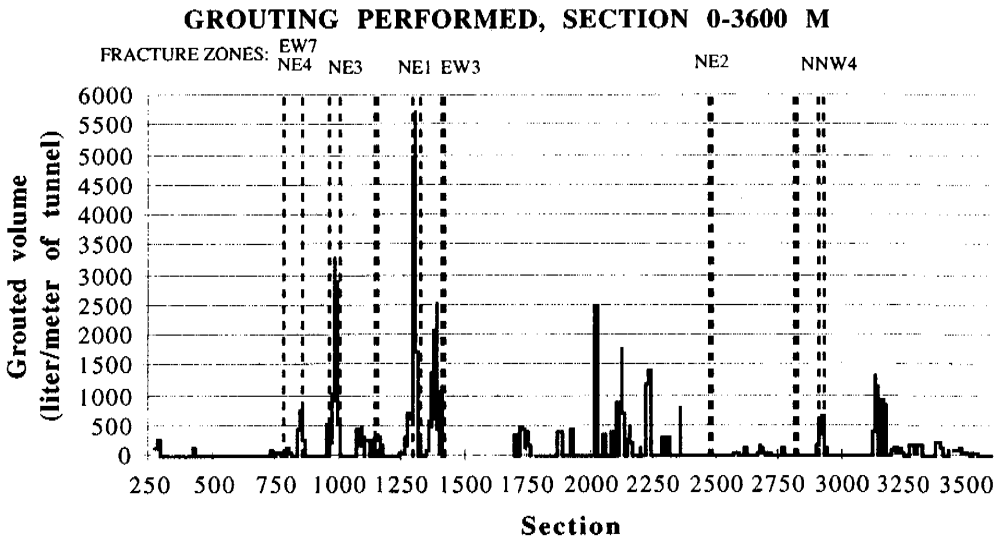

Figure 5-13. Grout volumes along the tunnel.

6 GEOHYDROLOGY

6.1 INTRODUCTION

The geohydrological model presented in this *Chapter 6* comprises evaluated and compiled geohydrological data. A number of the different data sets have been analysed statistically and the results are presented in tables and figures. As regards the properties of the rock mass, the results presented focus mainly on concepts for stochastic continuum modelling as the PHOENICS numerical code used in most cases is a code for continuum models. Due to this, effective hydraulic conductivities have been estimated as the transmissivity divided by the test section length. When using the data and statistics it is necessary to be aware of the fact that the hydraulic conductivities presented involve a scale dependency and the way in which these data should be used is dependent on the concepts used in the numerical model.

As described in *Chapter 3* the rock mass is divided into hydraulic conductor domains, mainly defined as major fracture zones, and hydraulic rock mass domains representing defined volumes in space with properties different from surrounding hydraulic conductor and rock mass domains. This is schematically shown in *Figure 6-1*. As an introduction to this chapter it can also be said that the data, mainly from Äspö, show that there are four main fracture sets in the rock mass domains, one subhorizontal set and the subvertical sets striking WNW-NW, approximately N-S and NE. WNW-NW has the highest fracture frequency of all sets, but hydraulic tests indicate that both the WNW-NW and N-S sets are more transmissive than the other sets. Occasionally single fractures in the rock mass domains can be very transmissive and cause high flow rates into drilled boreholes.

6.2 MODELS ON A REGIONAL SCALE

6.2.1 General

The regional scale model covers an area of approximately 100 km^2 (see *Figure 6-2*) and the interpretation is based on data mainly from the pre-investigation phase, such as data from the Swedish Geological Survey (SGU) Well Archive, the hydraulic tests performed at the Äspö HRL and the hydrology of the area around Äspö compiled by the Swedish Meterological and Hydrological Institute (SMHI). A base for the regional scale model is also the geological-structural model presented in *Chapter 4*. The regional model comprises concepts for:

- boundary conditions
- hydraulic conductor domains
- hydraulic rock mass domains

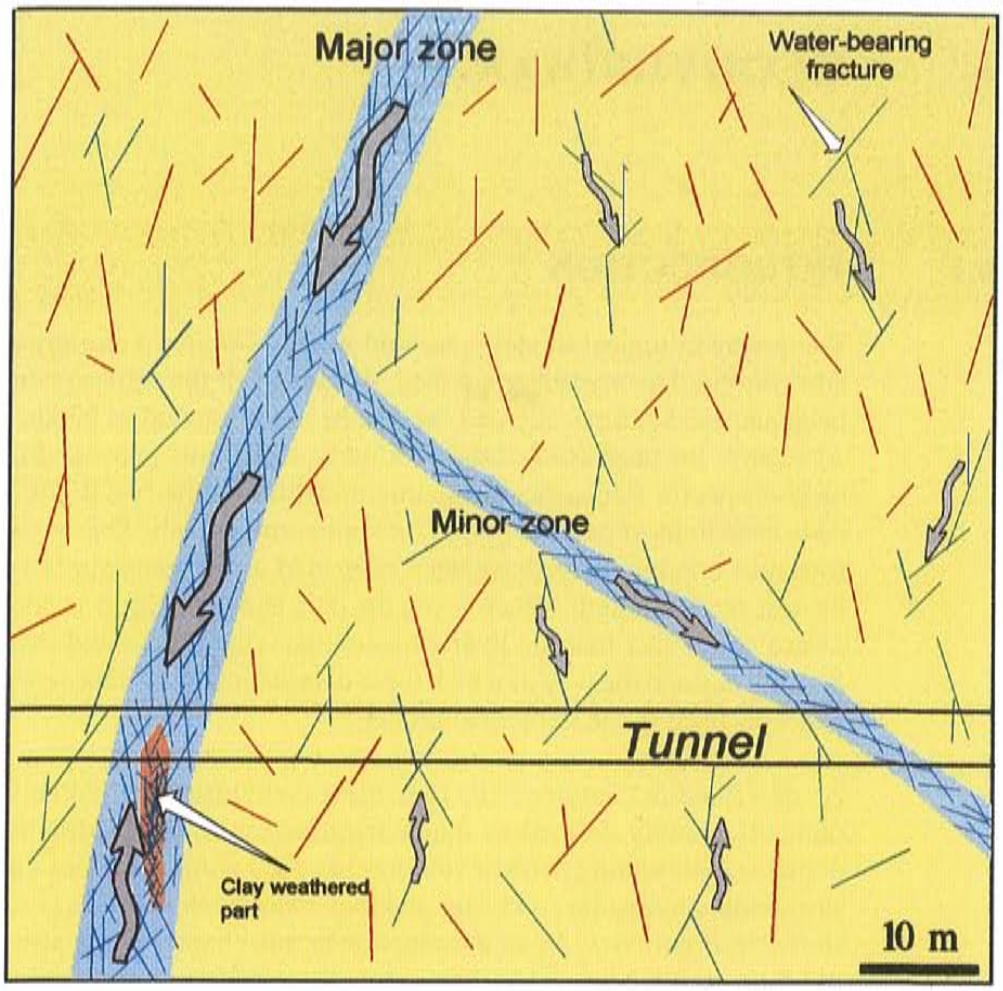

Figure 6-1. *A schematic description of hydraulic conductor domains (generally major zones) and the rock mass domains.*

Data for these concepts for the Äspö region are presented below.

6.2.2 Boundary conditions

Hydrological setting of the Simpevarp area

The hydrology of the area around Äspö and on Äspö was compiled during 1986-1987 in the siting stage. No new measurement stations were established as it was judged that it was no need for investigations for the Äspö HRL. Drainage basins, rivers, lakes and peatlands for areas nearby Äspö are shown in *Figure 6-2*. The topography is also shown but for a smaller area, which is the area for the regional model.

The mean precipitation in the Kalmar County area is about 675 mm/year */Svensson, 1987/*. About 18 % falls as snow. The durability of the snow cover is on average 91 days from 30 November to 7 April. The calculated actual evapotranspiration is 490 mm/year and the potential evapotranspiration

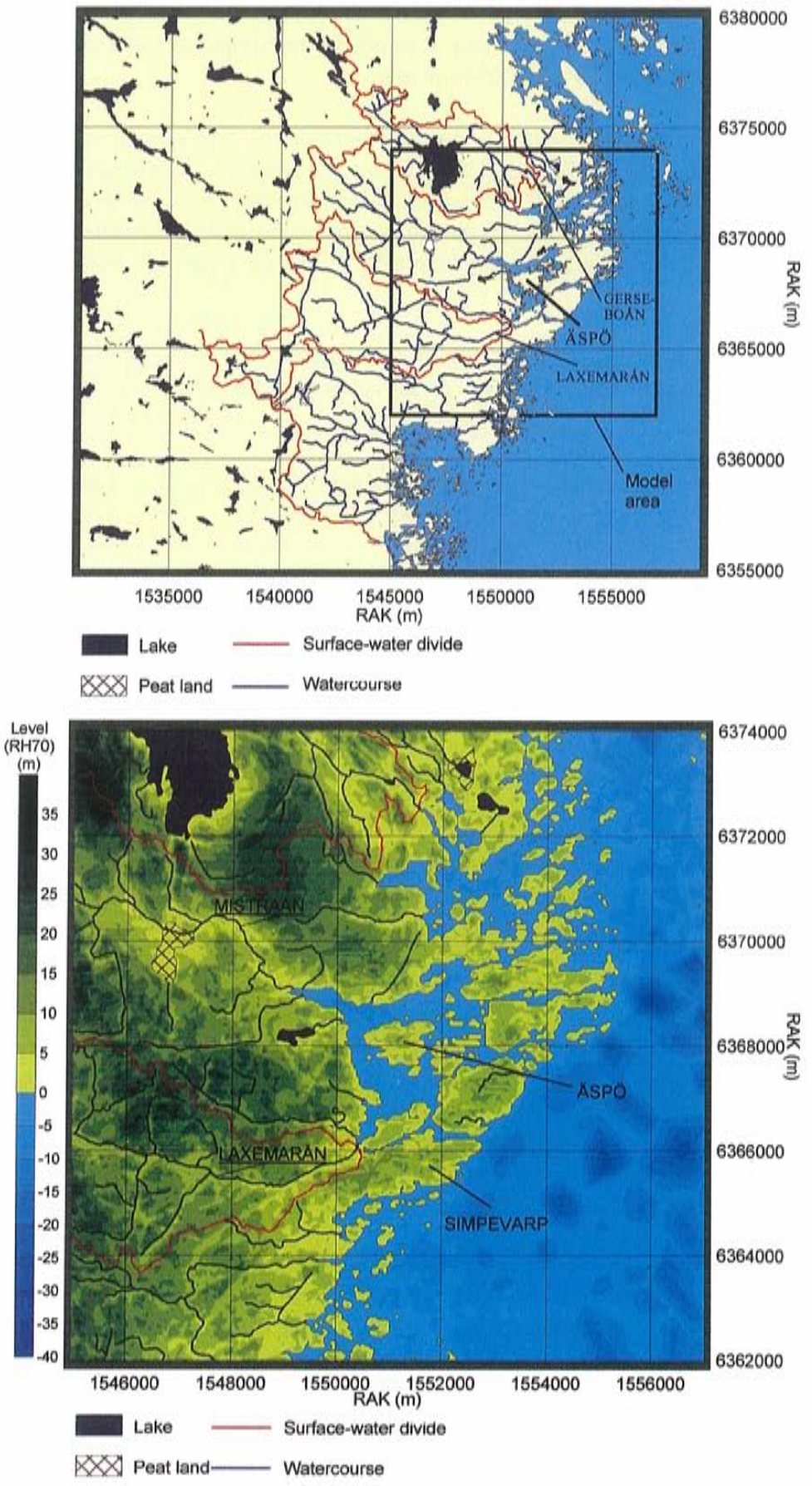

Figure 6-2. *Top: Hydrology of the area around Äspö (rivers outside the drainage basins are not shown). (Coordinate system: RAK).*
Bottom: Hydrology and topography of the area around Äspö. (Model area shown in top figure) (Coordinate system: RAK).

amounts to 616 mm/year. Run-off for the Simpevarp area was estimated to be between 150 and 200 mm/year.

In the region around Simpevarp there are two major catchment areas, Virsboån and Marströmmen. Two streams, Laxemarån and Gerseboån, between the major streams Virsboån and Marströmmen, were chosen to represent the coastal area. The estimated run-off per square kilometre for the last two catchment areas is approximately 0.006 $m^3/(s\ km^2)$ */Svensson, 1987/.*

Table 6-1. Data for major catchment areas in the region around Simpevarp. Lake area as percentage of the catchment area.

Water course	Annual mean run-off (m^3/s)	Catchment area (km^2)	Lake area (%)
Virsboån	3.6	601	8
Marströmmen	2.9	486	7
Laxemarån	-	41	1.2
Gerseboån	-	25	12

The small local catchment areas, which can be seen in *Figure 6-2* imply that the terrain may be subdivided into a mosaic of recharge and discharge areas and that the annual recharge of ground water to deeper levels is small as long as the ground water is not utilized or drained to an underground facility .

In *Figure 6-3* the annual mean temperature and precipitation for Oskarshamn (until June 1994) and Västervik (after July 1994) are shown. The annual mean potential evapotranspiration as an average for Ölands Norra Udde and Västervik is also presented. In *Figure 6-4* the 30-day means and daily variation of precipitation, potential evapotranspiration and temperature are exemplified by measurements from a period of approximately two years. Potential evapotranspiration is calculated using the Penman formula */Nyberg et al, 1996/.*

The most important error in point measurements of precipitation is due to the wind. The wind error varies with the type of precipitation, wind speed and site, but always results in a deficiency of catch. The error due to evaporation from the gauge is largest during warm summer days with showers. The loss is estimated to be some 1.5 mm/month */Gottschalk, 1980/* as a mean, although depending greatly on meteorological factors. All types of error cause precipitation to be underestimated. For the Oskarshamn station the total correction needed has been estimated at +18 % */Eriksson, 1980/* for the annual precipitation. All precipitation values for Oskarshamn and Västervik in *Figures 6-3* and

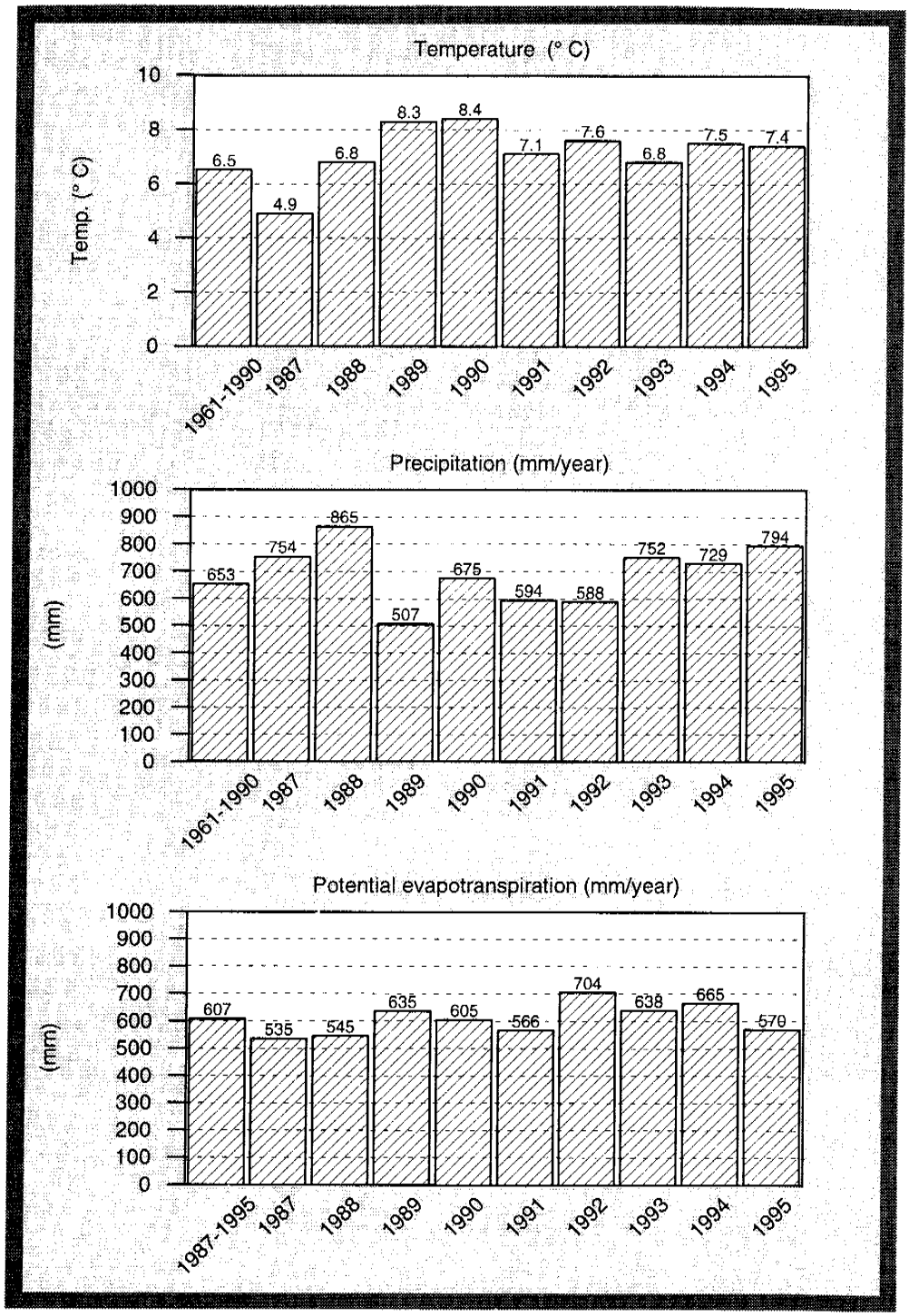

Figure 6-3. *Top: Temperature at Oskarshamn. Annual values 1987-1995 and annual mean 1961-1990.*
Middle: Precipitation at Oskarshamn. Annual values 1987-1995 and annual mean 1961-1990. (Corrected values: 18 % added to measured values).
Bottom: Potential evapotranspiration as average from Västervik and Ölands Norra Udde. Annual values and annual mean 1987-1995.

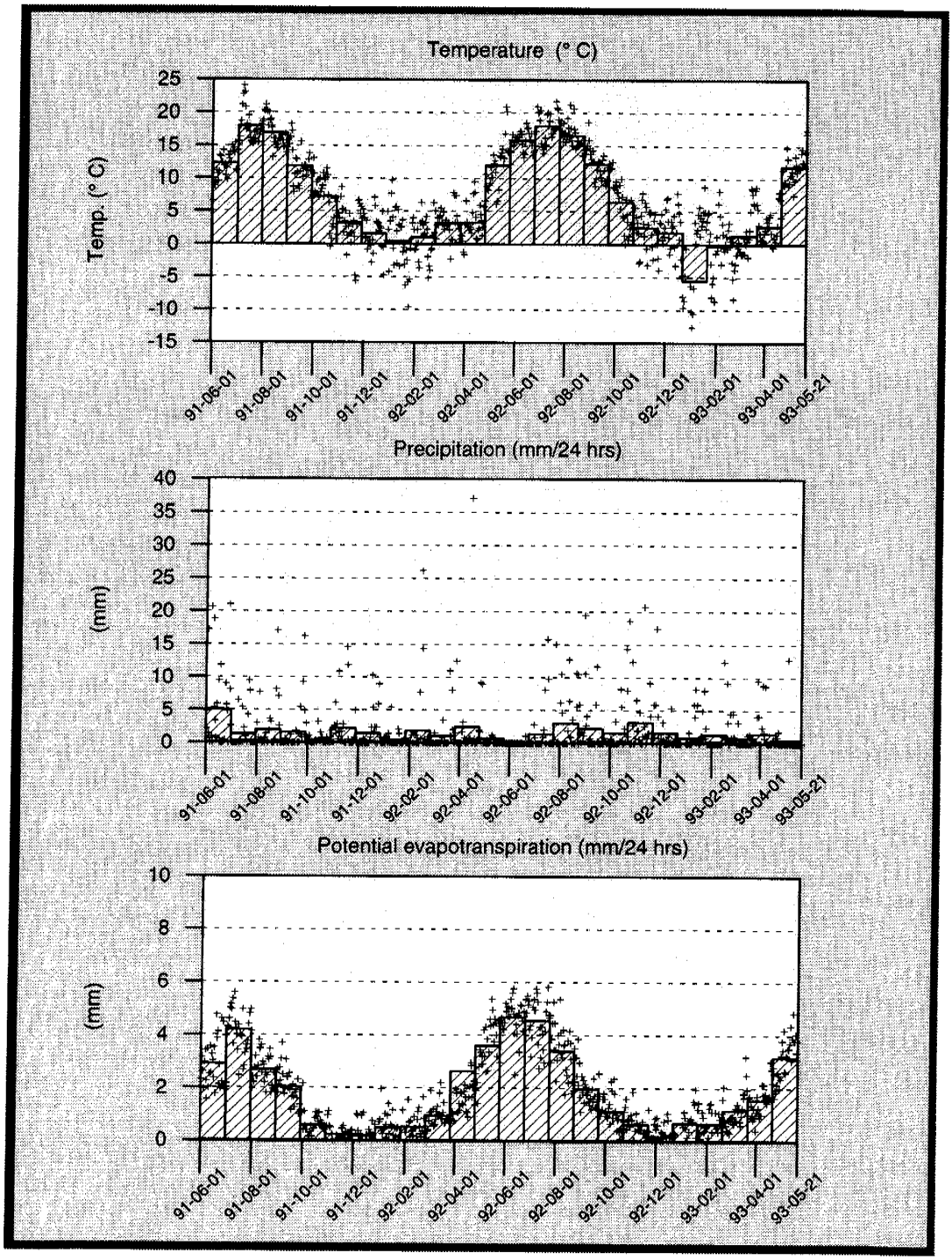

Figure 6-4. *Top: Temperature at Oskarshamn. Daily values (+) and the 30-day mean values.*
Middle: Precipitation at Oskarshamn. Daily values(+) and the 30-day mean values. (Corrected values: 18 % added to measured values).
Bottom: Potential evapotranspiration as average from Västervik and Ölands Norra Udde. Daily values(+) and the 30-day mean values.

6-4 are corrected values, not measured ones. The values reported by *Svensson /1987/* presented above in the text were corrected by an addition of 15-20 %.

A much more difficult problem when dealing with precipitation data is the poor areal representativeness of precipitation measurements, especially during showery conditions in the summer. No correction has been made for this. However, as the ground water recharge is limited during the summer season this is considered to be a minor problem.

Quaternary deposits

The ice of the last glaciation melted in the area about 11900 years ago and the ice left deposits, mainly till but also sand, silt and clay. Peatlands and fine grained sediments are also found within the area in some of the depressions in the landscape. The soil cover is usually thin.

Water table

The main recharge takes place in conjunction with the melting of snow, thereby giving a maximum elevation of the water table in the spring and a minimum in late summer */Svensson, 1987/.*

Levels are only known from boreholes on Äspö, Laxemar, Hålö and Ävrö. The data indicate that the undisturbed water table follows the topography rather well. The surface of the water table is very irregular because the hydraulically active fractures are sparsely distributed and not very well interconnected hydraulically, see *Figure 6-5*. Measured levels near the surface may in some cases represent more or less local flow systems.

At some depths below the water table the irregular pressure distribution is levelled out and probably to a large extent governed by the fracture zones and large fractures with high transmissivities. This levelled out pressure distribution also controls to some extent the depth to the saline interface.

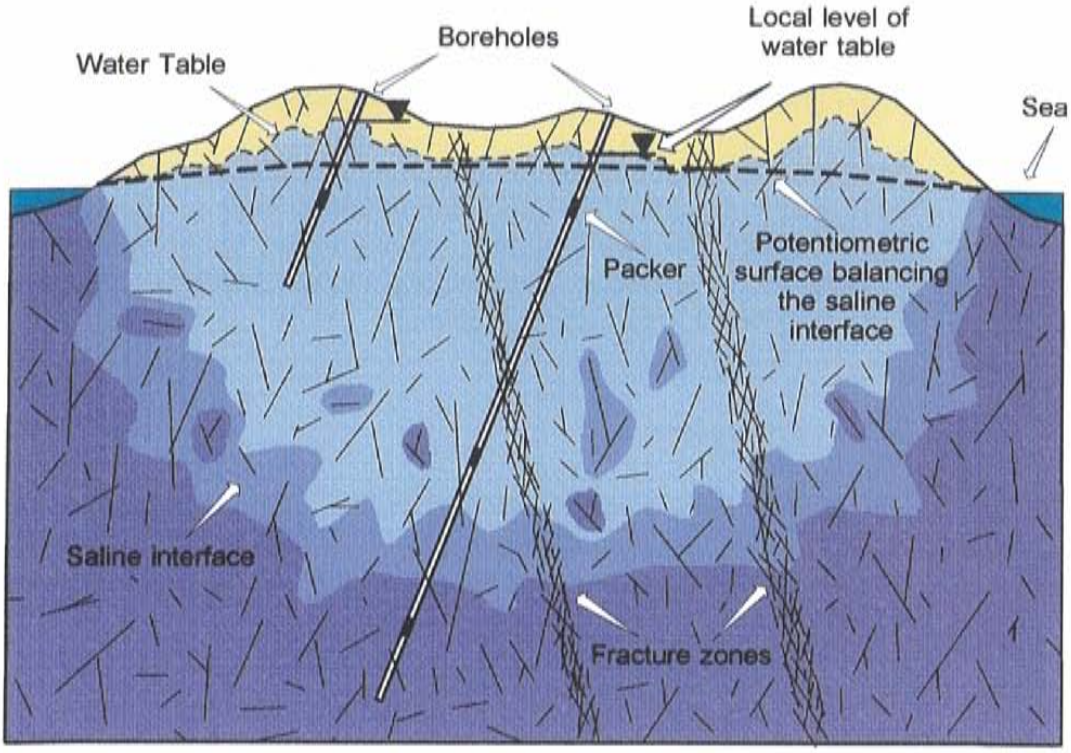

Figure 6-5. *Water table and saline interface in a fractured medium. The hydraulically active fractures are sparsely distributed and not well interconnected hydraulically. At some depth below the water table the irregular pressure is levelled because of transmissive fracture zones.*

The annual fluctuation of the water table is greater for areas near surface-water divides compared to areas close to discharge areas, see *Figure 6-6.*

Figure 6-7 shows the relationship between the elevation of the topography and the water table above mean sea level for the wells in the Äspö HRL area, except wells in Laxemar area. It should be pointed out that the relationship shown in *Figure 6-7* is only valid close to the coast as the discharge from the superficial bedrock takes place at the water courses. (This is why the Laxemar wells were excluded from the regression in *Figure 6-7*). The relationship can possibly be used if the local elevations of the water courses are used instead of sea level for local estimates of the elevation of the water table.

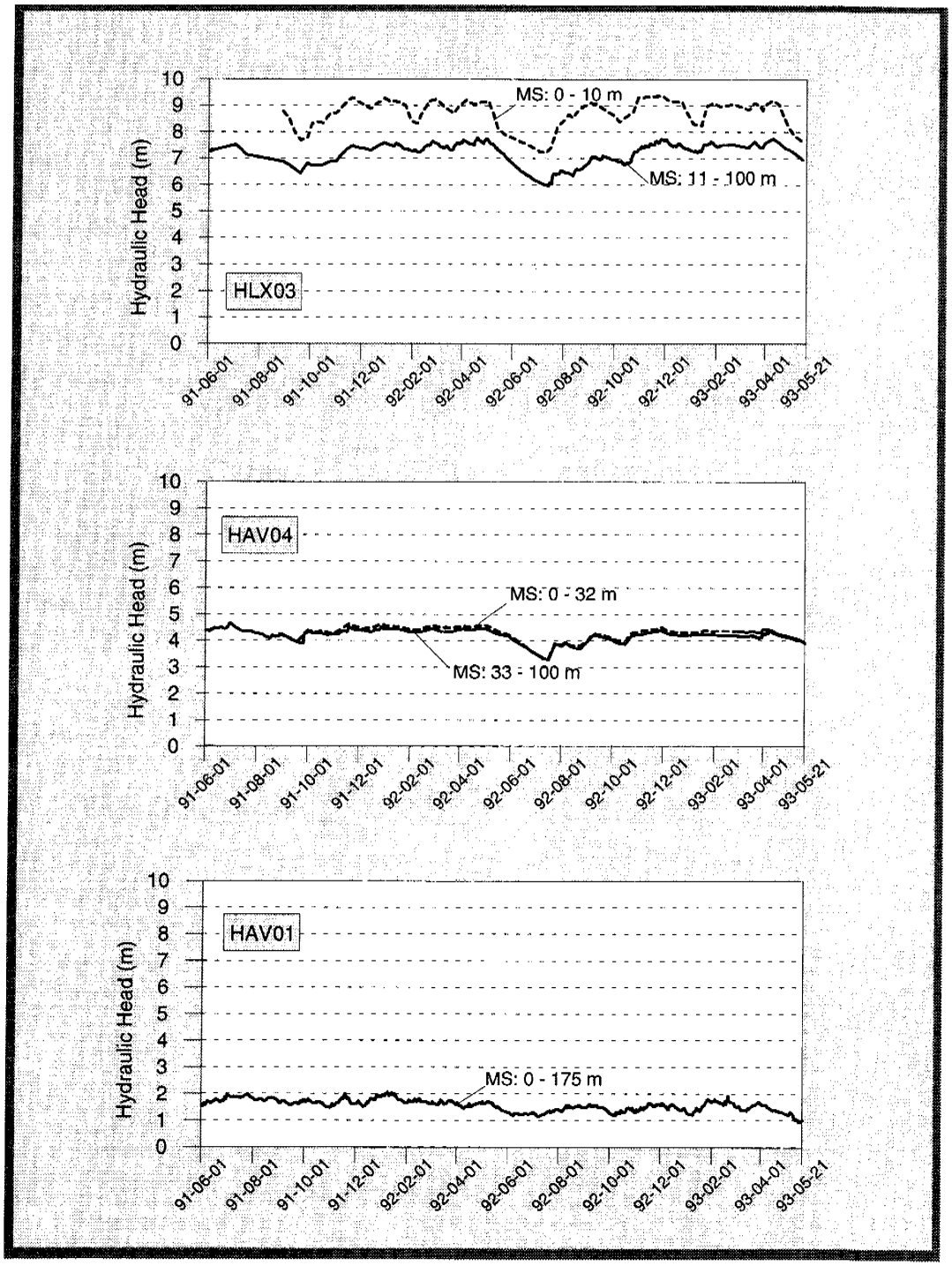

Figure 6-6. *Undisturbed piezometric levels for boreholes HLX03, HAV01 and HAV02. The location of the boreholes is shown in Figure 2-3. (MS: Measurement section).*

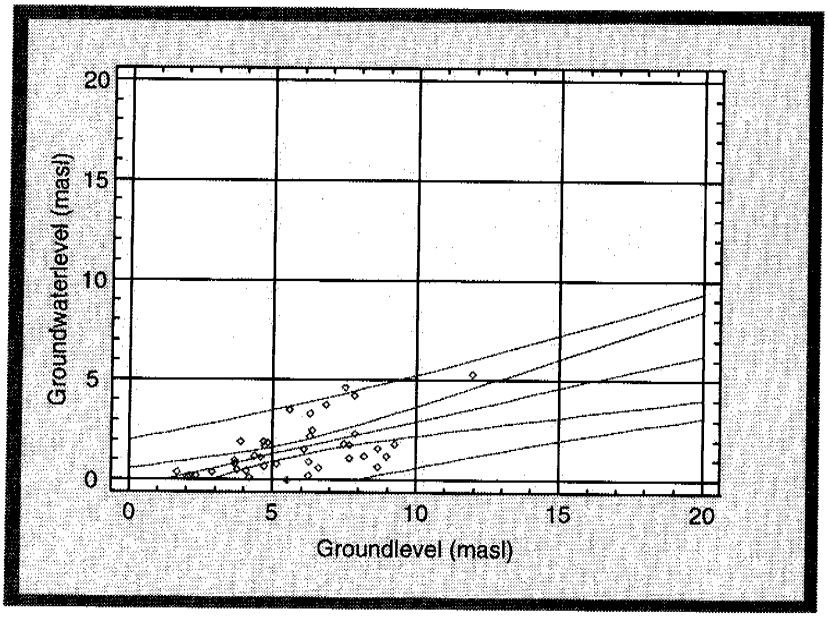

Figure 6-7. *Elevation of water table above mean sea level as a function of the elevation of the topography above mean sea level. Valid for areas close to the coast. Data: Boreholes on Äspö, Bockholmen, and Ävrö. Middle line: Mean water table elevation = -0.39+0.333 masl. Inner lines: 95 % confidence band on mean water table elevation. Outermost lines: 95 % prediction band on the water table elevation as a function of the topography. (masl = metres above mean sea level).*

Piezometric levels

A number of factors influence the measured piezometric levels, which is illustrated in *Figures 6-9* to *6-14*. A few of the upmost measurement sections respond fast to precipitation, see *Figure 6-9*. The present measurement sections at Äspö HRL do not seem to be influenced to any greater extent by sea level fluctuations. However, if a measurement section is in good hydraulic contact with the sea, the section should show rather clear responses to sea level changes.

Short time fluctuations due to earth tides, which are caused the tidal forces of the moon and the sun, is seen in most measurement section except for some of the uppermost sections. The fluctuations are up to about ± 0.1 m, see *Figure 6-12*.

The calculated earth tides indicate that the maximum change of the level of the ground surface relative to mean level of the ground surface is about ± 0.25 m, see *Figure 6-8*. These fluctuations may influence the possibilities to interpret responses in observation sections seen during an interference test if the responses are small.

The tidal force causes a strain of the crust that possibly creates a small pumping effect, that in turn may be responsible for some of the mixing of the groundwater. Possibly the dynamic load of the tidal forces and the more static stress field

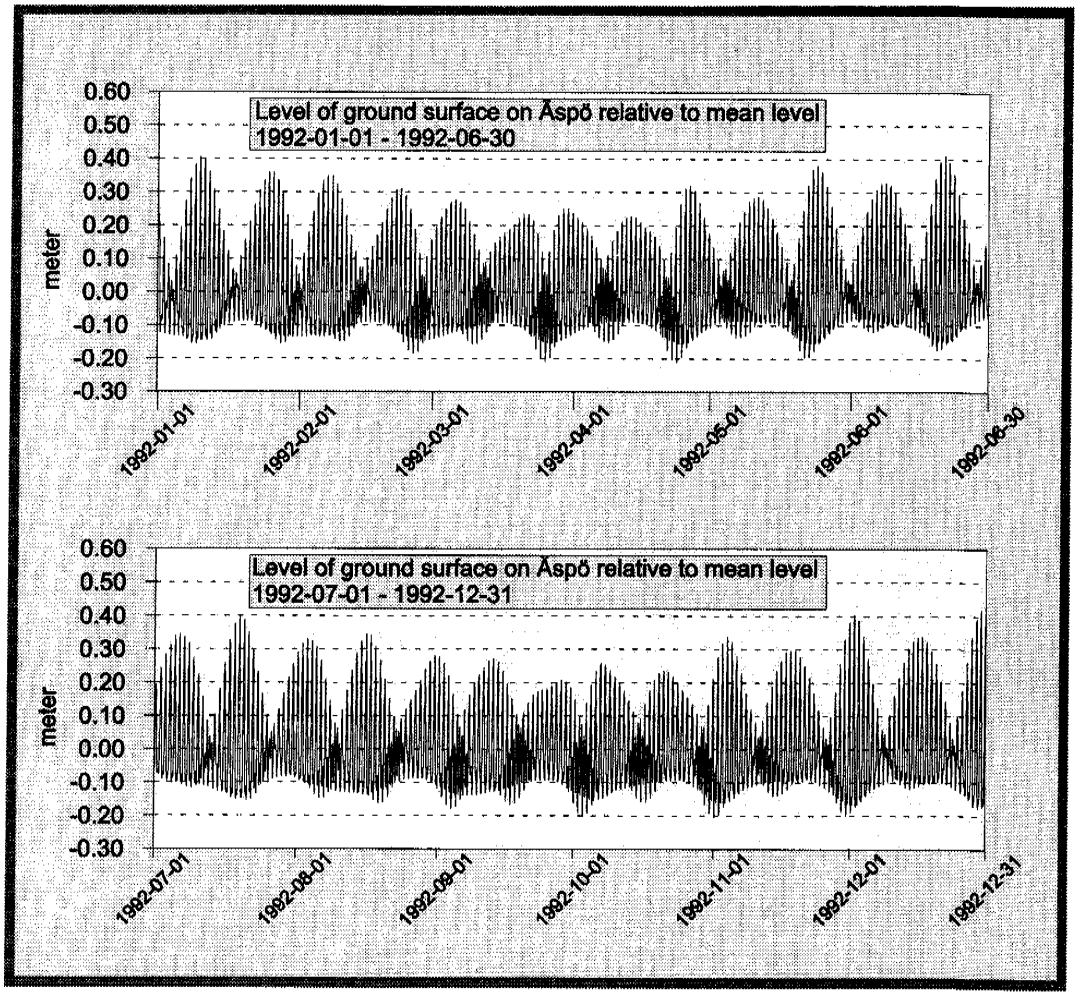

Figure 6-8. *Calculated earth tides for 1992.*

due to the continental drift and the weight of the rock also influence which sets of fractures that are found most transmissive. The effect of the tidal forces on the hydraulic properties and the transport processes remains to be studied in more detail. (The earth tides were calculated by Scherneck by a method reported in *Scherneck /1991/*).

The influence of barometric pressure is seen in some borehole sections, see *Figure 6-14.*

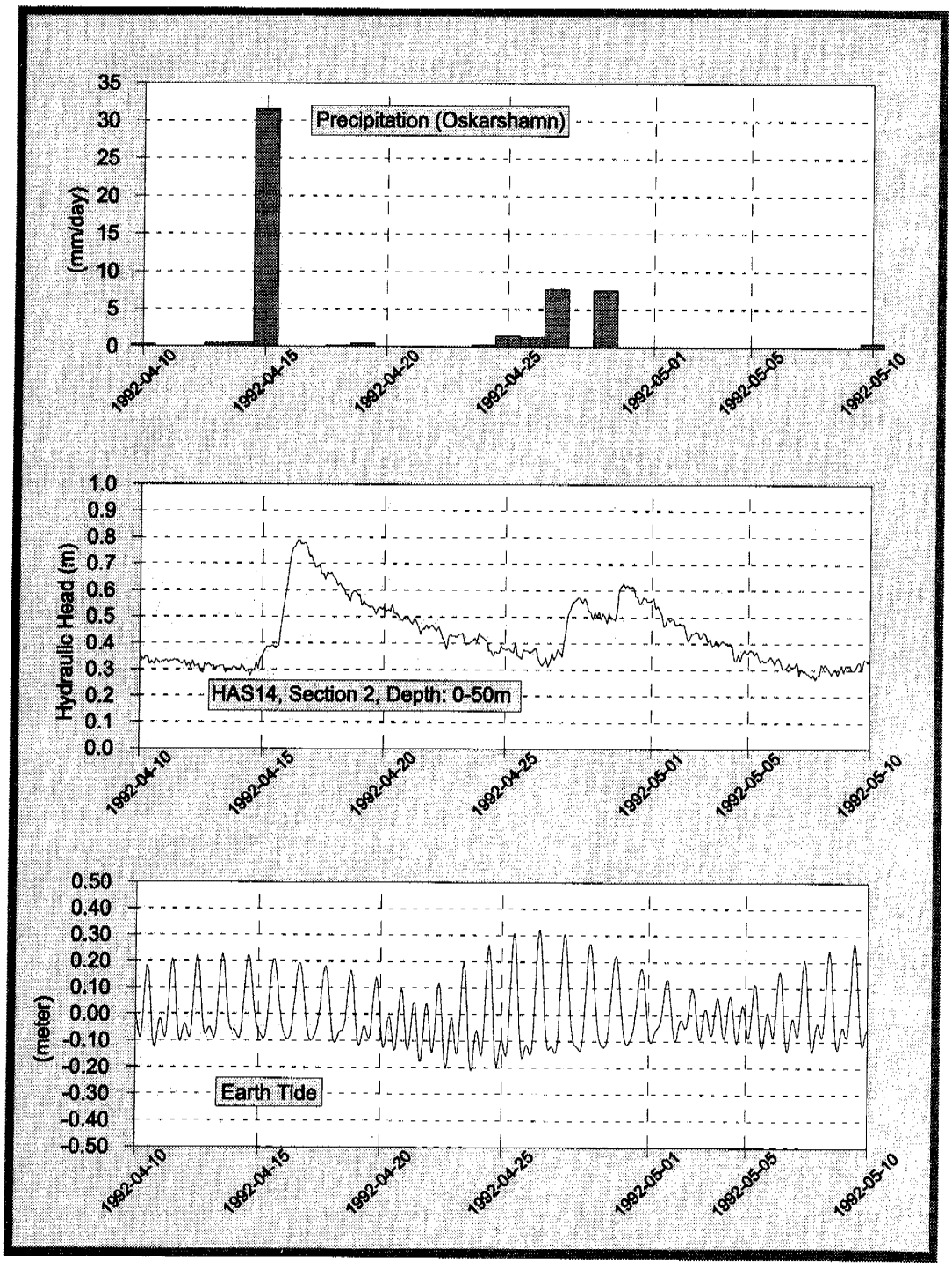

Figure 6-9. *Measured piezometric level in HAS14 (measurement section 2), measured precipitation (Oskarshamn) and calculated earth tide.*

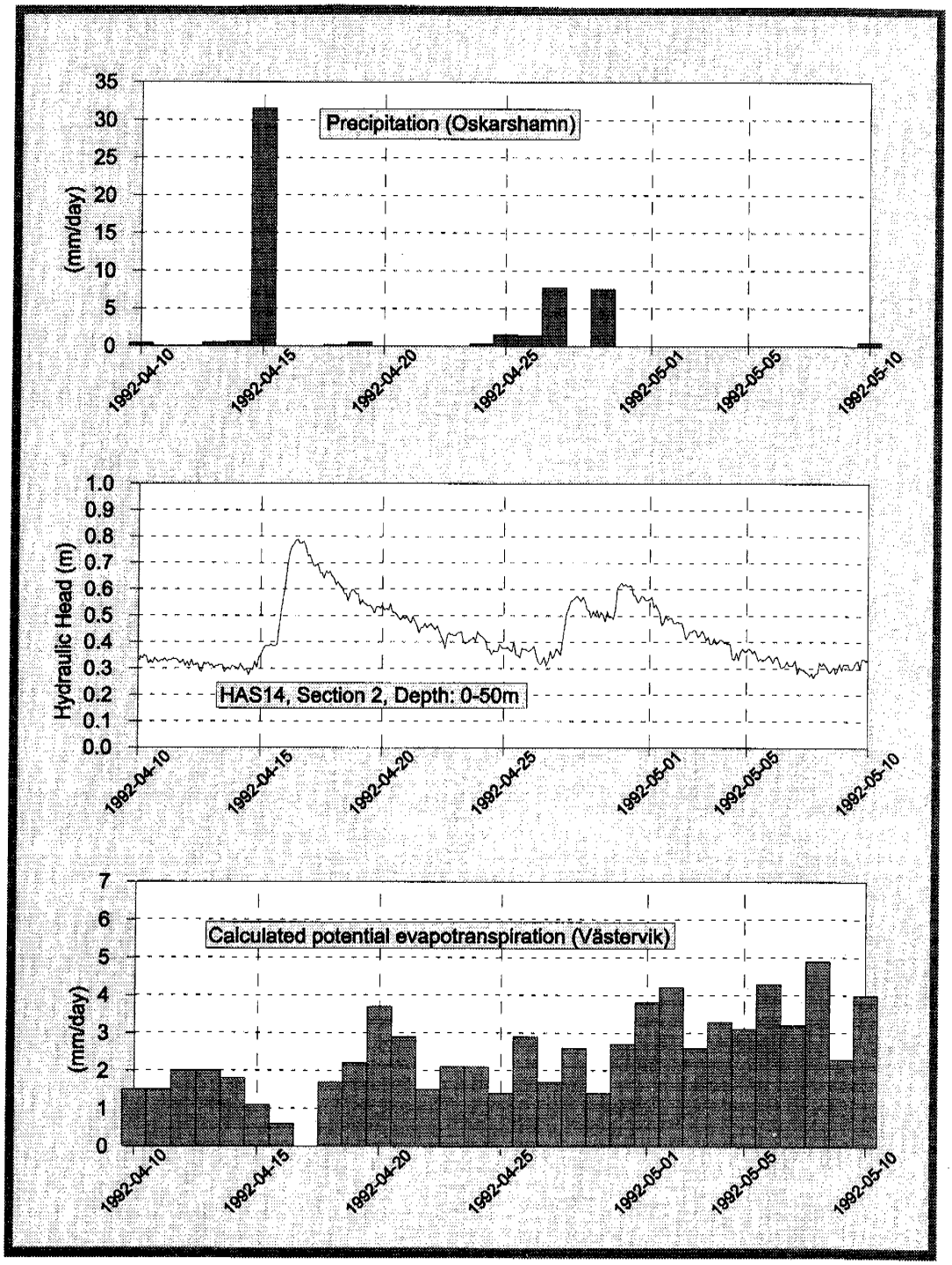

Figure 6-10. *Measured piezometric level in HAS14 (measurement section 2), measured precipitation (Oskarshamn) and calculated potential evapotranspiration (Västervik).*

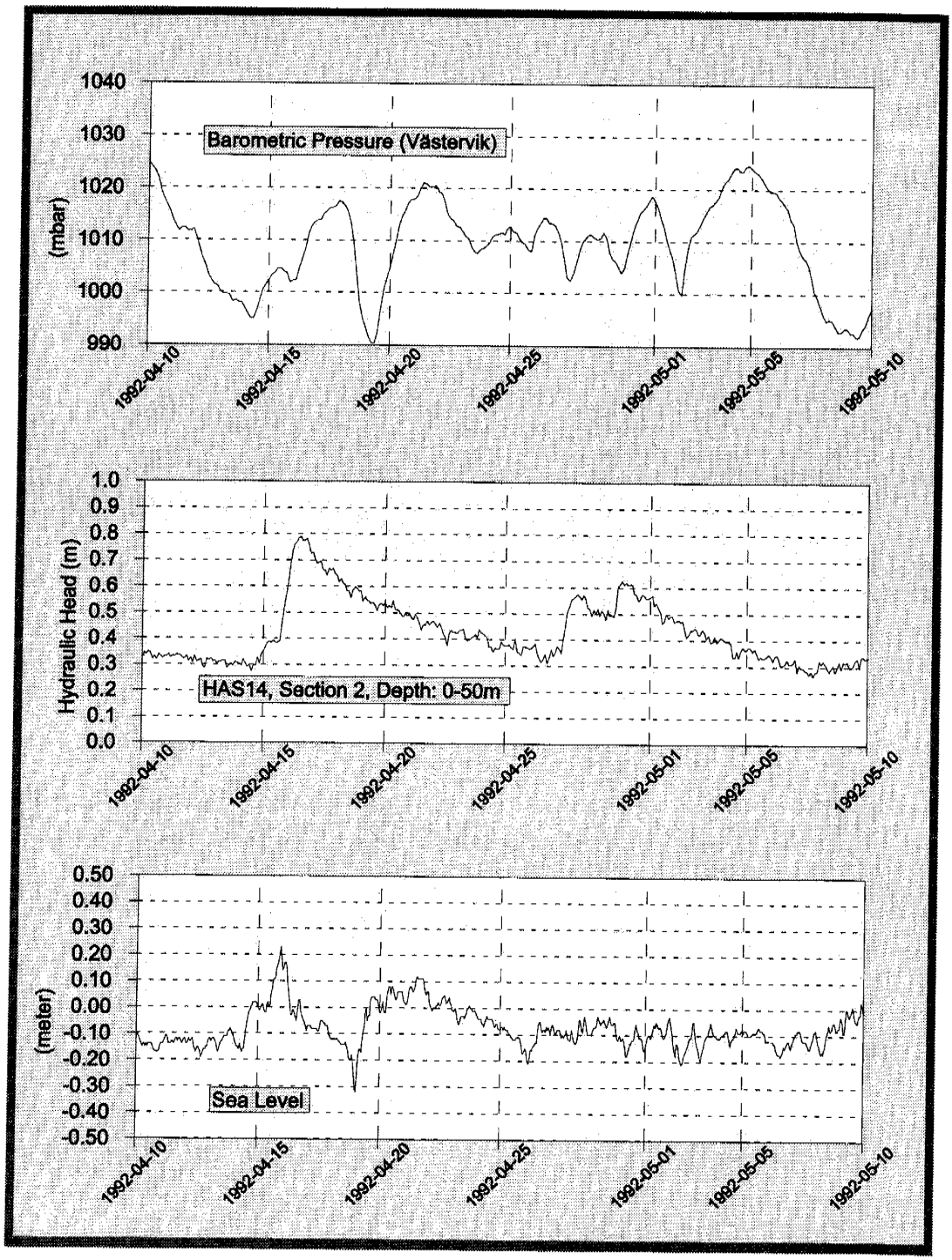

Figure 6-11. *Measured piezometric level in HAS14 (measurement section 2), measure barometric pressure (Västervik) and measured sea level (Oskarshamn).*

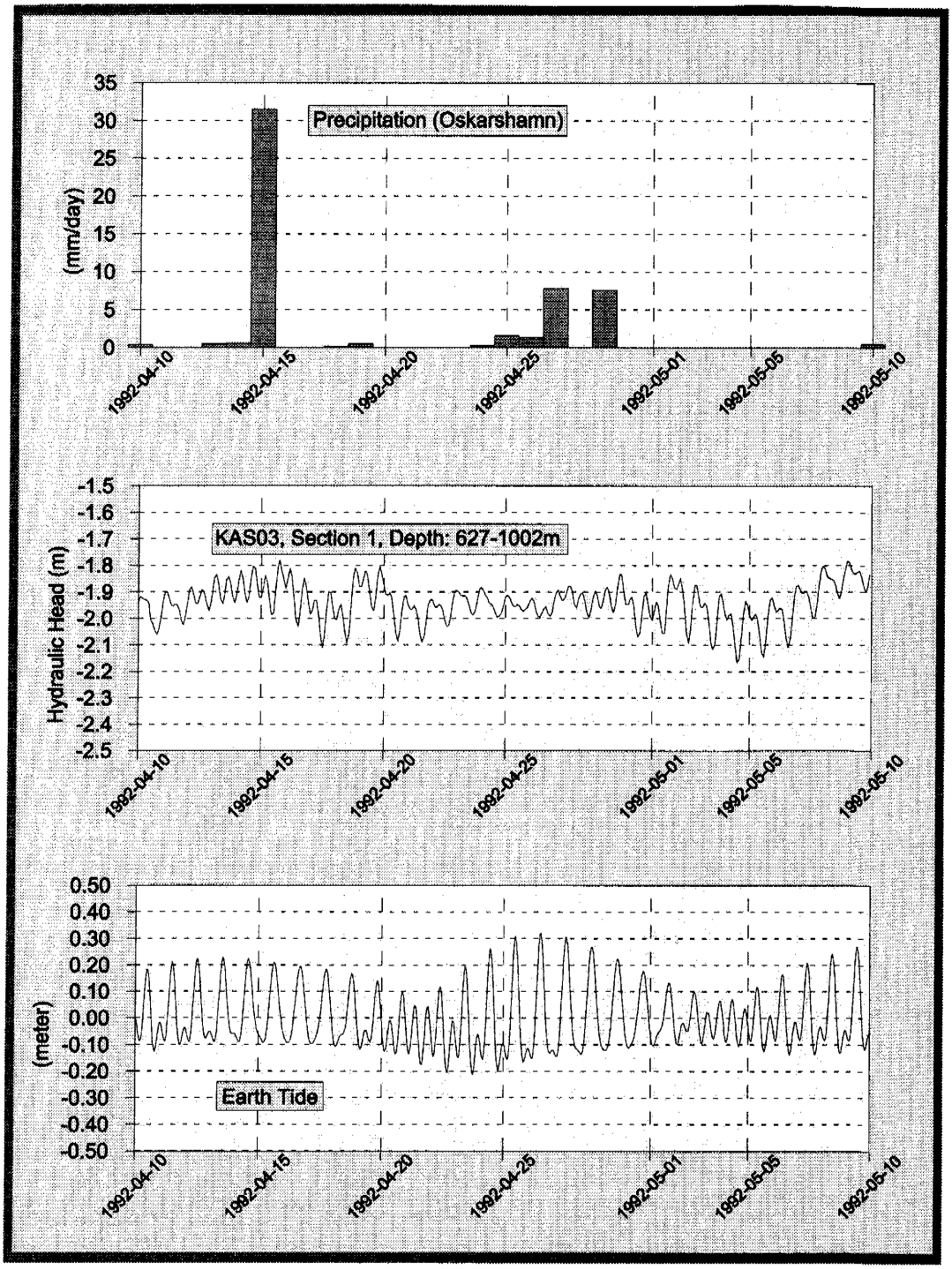

Figure 6-12. *Measure piezometric level in KAS03 (measurement section 1), measured precipitation (Oskarshamn) and calculated earth tide.*

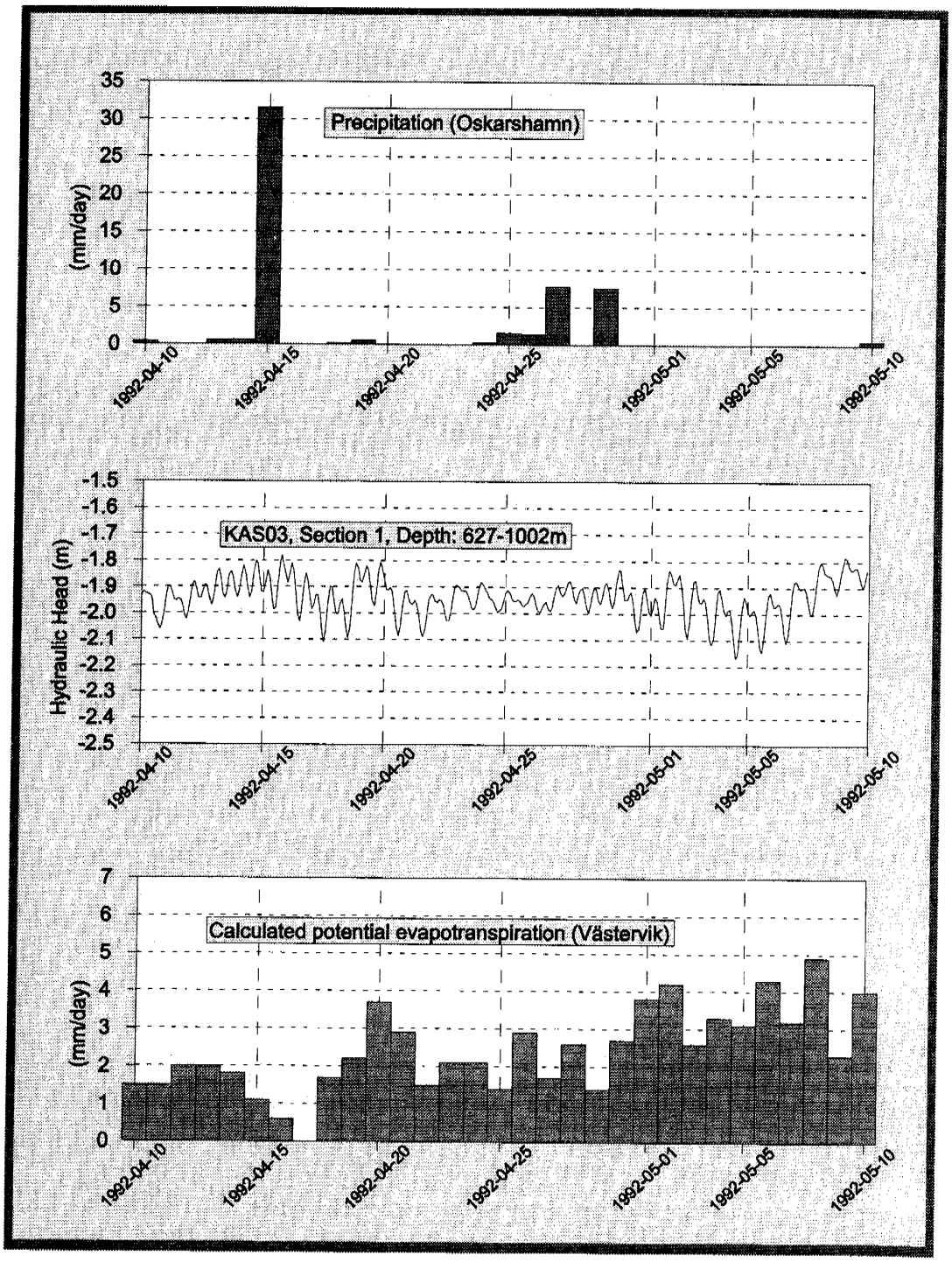

Figure 6-13. *Measure piezometric level in KAS03 (measurement section 1), measured precipitation (Oskarshamn) and calculated potential evapotranspiration (Västervik).*

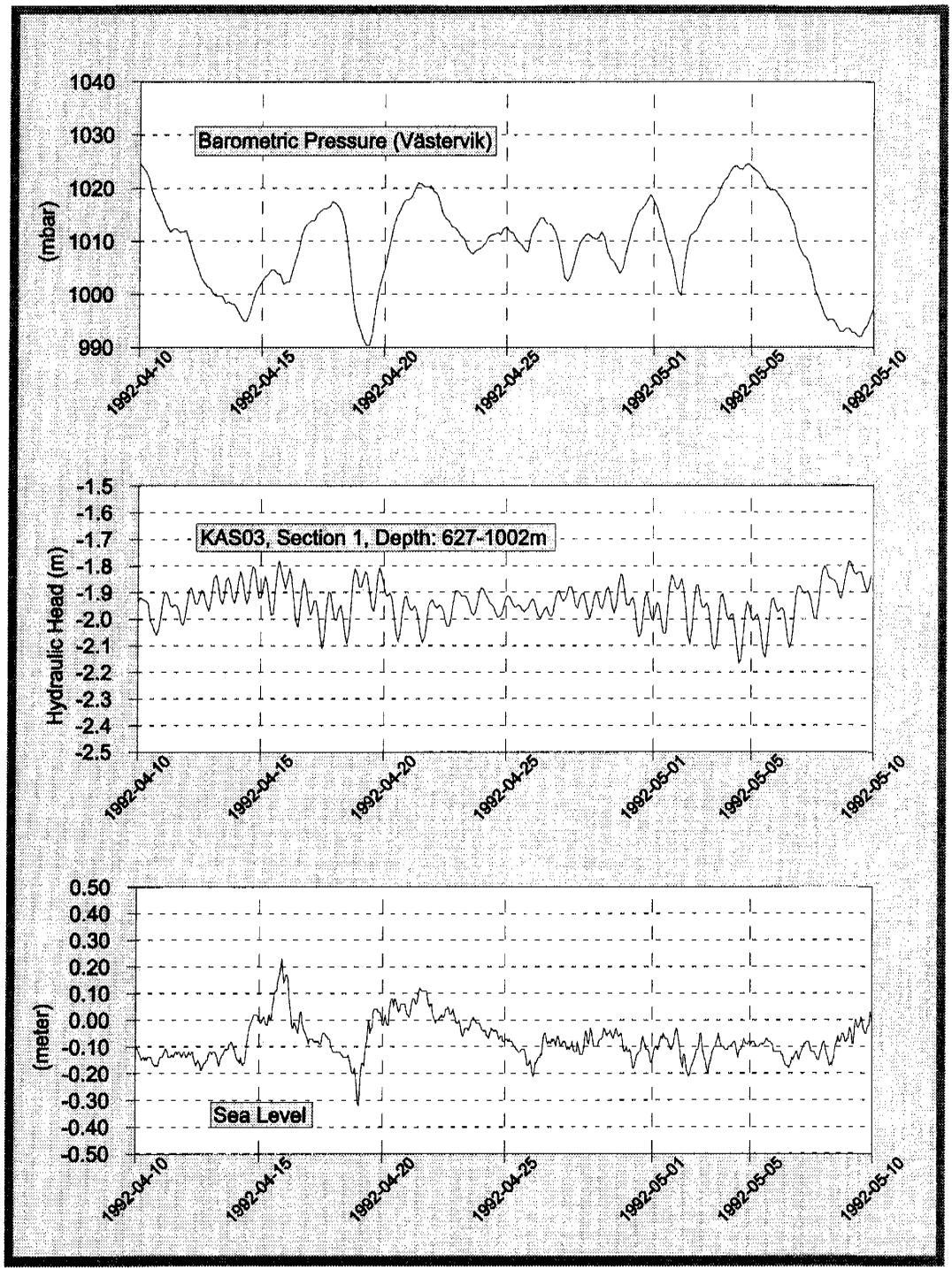

Figure 6-14. *Measure piezometric level in KAS03 (measurement section 1), measure barometric pressure (Västervik) and measured sea level (Oskarshamn).*

Level data for the Baltic Sea – present day conditions

The sea level is recorded at the city of Oskarshamn by SMHI on an hourly basis. The influence of oscillations with short frequency (waves) is filtered, both by the gauge well and when digitizing data. Sea levels are adjusted to the

national datum system (RH70), which gives approximately 6 centimetres higher values than the local system at Äspö.

The errors in the data presented in the diagrams are, according to SMHI, less than one hour in time and less than a few centimetres in elevation. For shorter periods, during quickly changing weather conditions, the difference in sea level between Oskarshamn and the Äspö area can be a few centimetres, but is normally much less. In *Figure 6-15* the 30-day means and daily values are presented for a period of approximately two years.

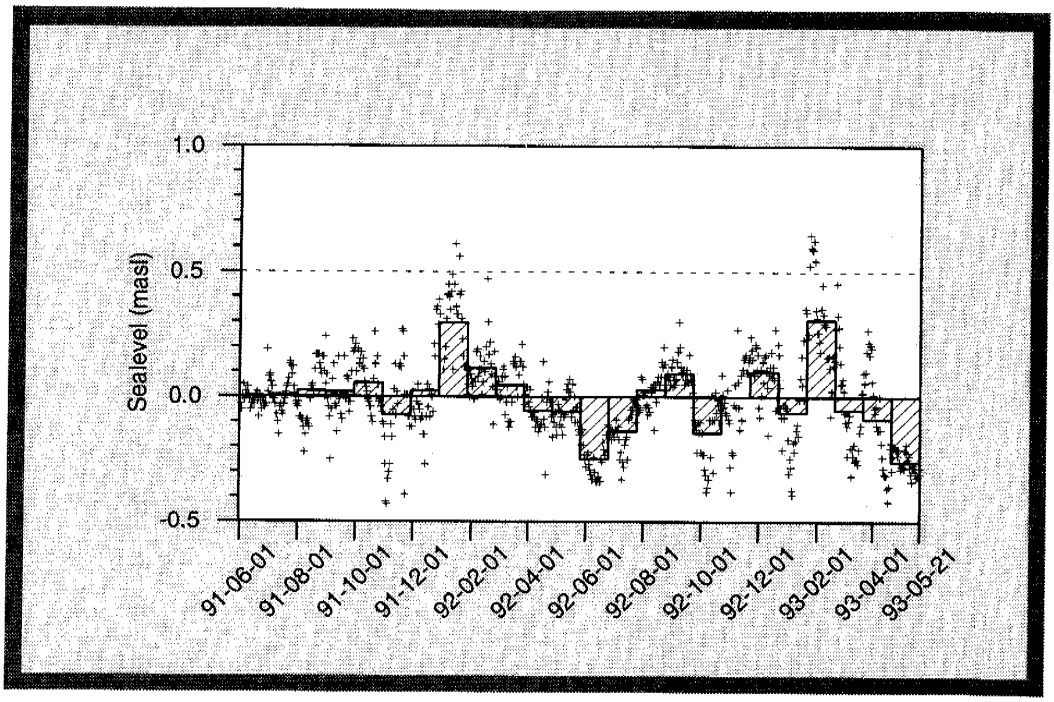

Figure 6-15. *Graphs showing the daily values and the 30-day mean value of the sea level at Oskarshamn. (masl = metres above mean sea level).*

Shore level displacement after the last glaciation

The boundary conditions for the upper boundary have changed since the last glaciation. One of these dynamic conditions is the sea level change, which is due to several reasons. In *Björk and Svensson /1992/* the sea level changes are described and several shore-displacement curves for Sweden are presented. *Figure 6-16* and *Appendix 2* show the shore-displacement curve for Oskarshamn. The shore-displacement in the model area, based on equation shown in *Figure 6-16* is illustrated in *Figures 6-17* to *6-19* for a few points of time. Shore level displacement is also presented in *Påsse /1996/*. The estimates in that report of the future shore level displacement for Oskarshamn is nearly twice the values given by equation in *Figure 6-16*. The future shore level

displacement shown in *Figures 6-17* to *6-19* should be seen as an example of how the drainage pattern may change by time.

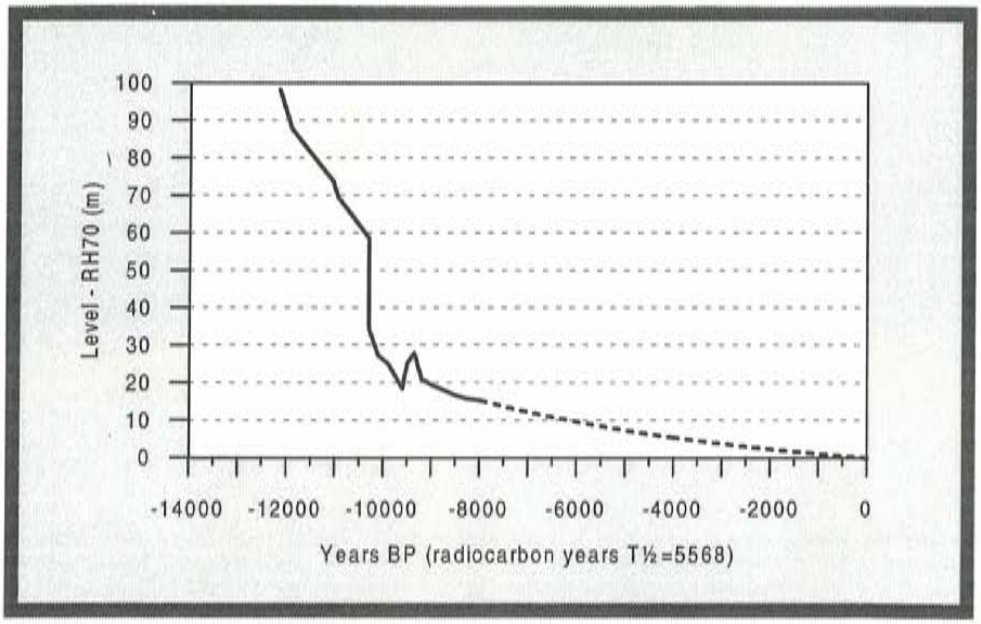

Level equation for the years - 8000 - 0 BP

$Z = 6.763 \cdot (\exp(-0.00014786 \cdot t - 1))$ (m, RH70)

Figure 6-16. *Shore-displacement curve for Oskarshamn /Björk and Svensson, 1992/. Shore-displacement in the past 8000 years is based on the fact that the present shore-displacement is 1 mm/year, the level 8000 year ago and that the displacement decreases exponentially. (Dating based on C-14, BP = Before Present).*

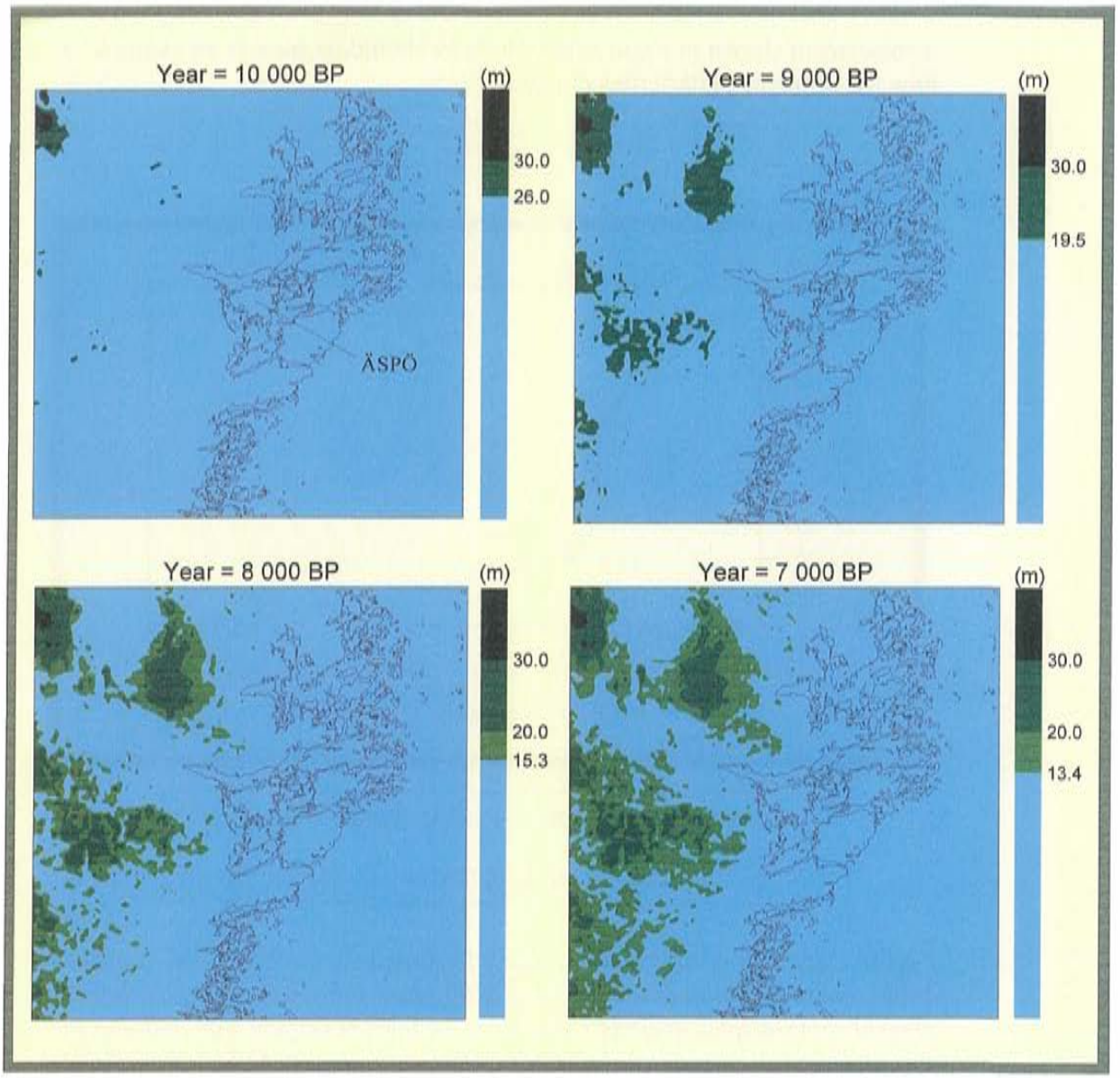

Level : RH70 (m)
Modelarea : (1545,6362)(1557,6374) RAK (km)
BP : Before Present

Figure 6-17. *Development of the shore position in the model area, 10 000 - 7000 BP. (Coordinate system: RAK).*

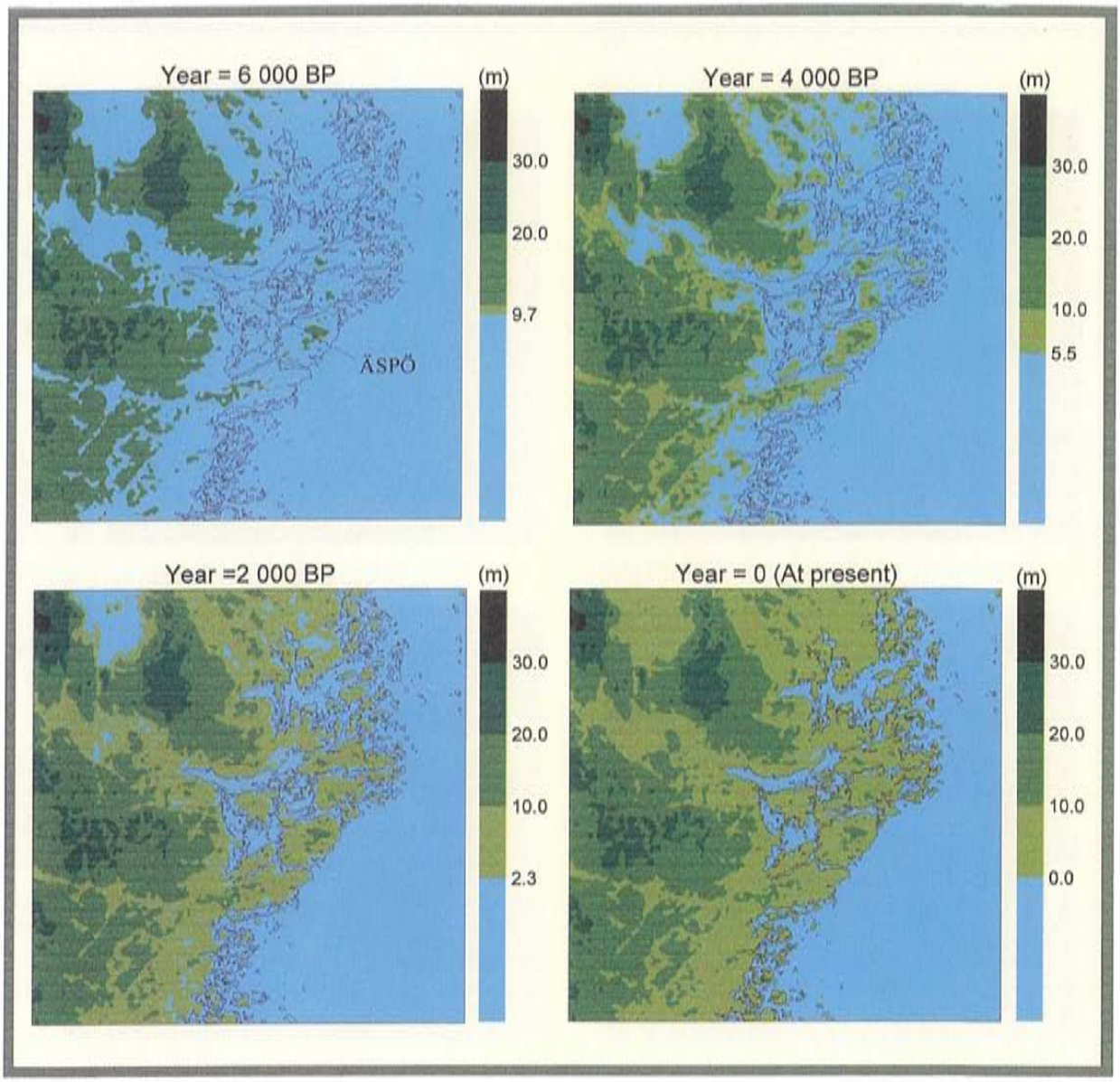

Level : RH70 (m)
Modelarea : (1545,6362)(1557,6374) RAK (km)
BP : Before Present

Figure 6-18. *Development of the shore position in the model area, 6000 BP - Present. (Coordinate system: RAK).*

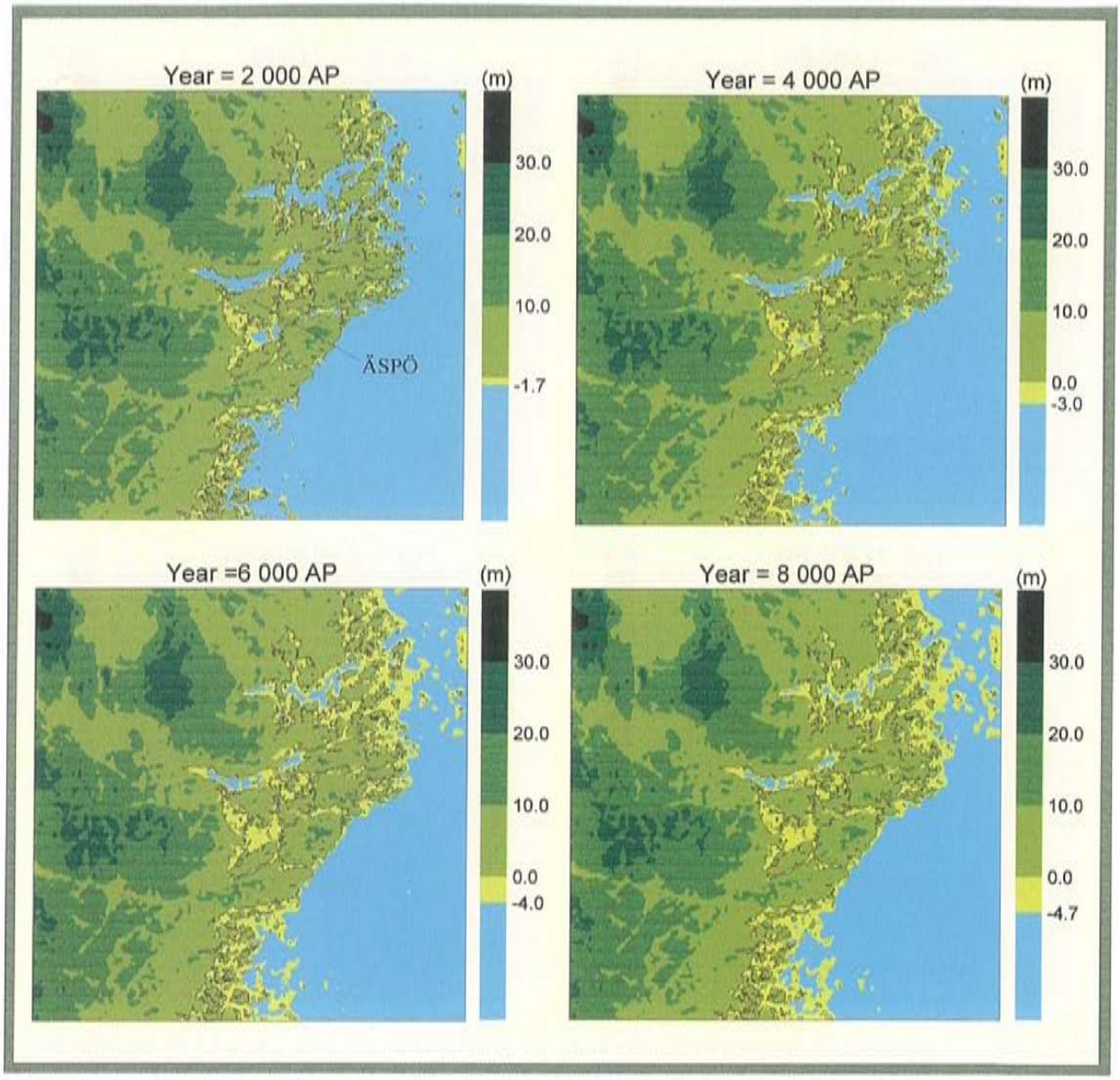

Level : RH70 (m)
Modelarea : (1545,6362)(1557,6374) RAK (km)
AP : After Present

Figure 6-19. *Development of the shore position in the model area, Present - 8000 AP (Coordinate system: RAK).*

Salinity of the Baltic Sea – present day conditions

The salinity of the Baltic Sea around Äspö is approximately 6 g/l, but varies by location and time for sampling. One sample showed 4 g/l and a few others 5-6 g/l.

Salinity and density of the ground water – present day conditions

The salinity or electrical conductivity of the ground water have been measured on several occasions during the pre-investigation and construction of the Äspö HRL.

The undisturbed conditions are presented in *Figure 6-20* for three sites, KLX01, KLX02 and Äspö. The salinity data for each borehole section is presented in *Appendix A2*. The temperature at 500 m depth is 14.6±0.3 °C and the temperature gradient is 15.0±0.3 °C/km at Äspö and approximately the same at Laxemar */Ahlbom et al, 1995* and *Sundberg, 1991/*. The relationship between the water density and electrical conductivity at 25 °C was estimated for waters sampled during the pre-investigation phase */Nilsson, 1989/*. This relationship was later slightly modified */Rhén et al, 1994b/*, and the relationship between the electrical conductivity (C), salinity (S) and the density of pure water (ρ_0) and the density of saline water (ρ) can be estimated using *Equation 6-1*.

$$\rho = \rho_0(T) + 0.00467 \cdot C = \rho_0(T) + 0.741 \cdot S \qquad (6\text{-}1)$$

ρ	=	Density of saline water	(kg/m^3)
ρ_0	=	Density of pure water	(kg/m^3)
C	=	Electrical conductivity of water	(mS/m)
S	=	Salinity	(g/L)
T	=	Temperature	(°C)

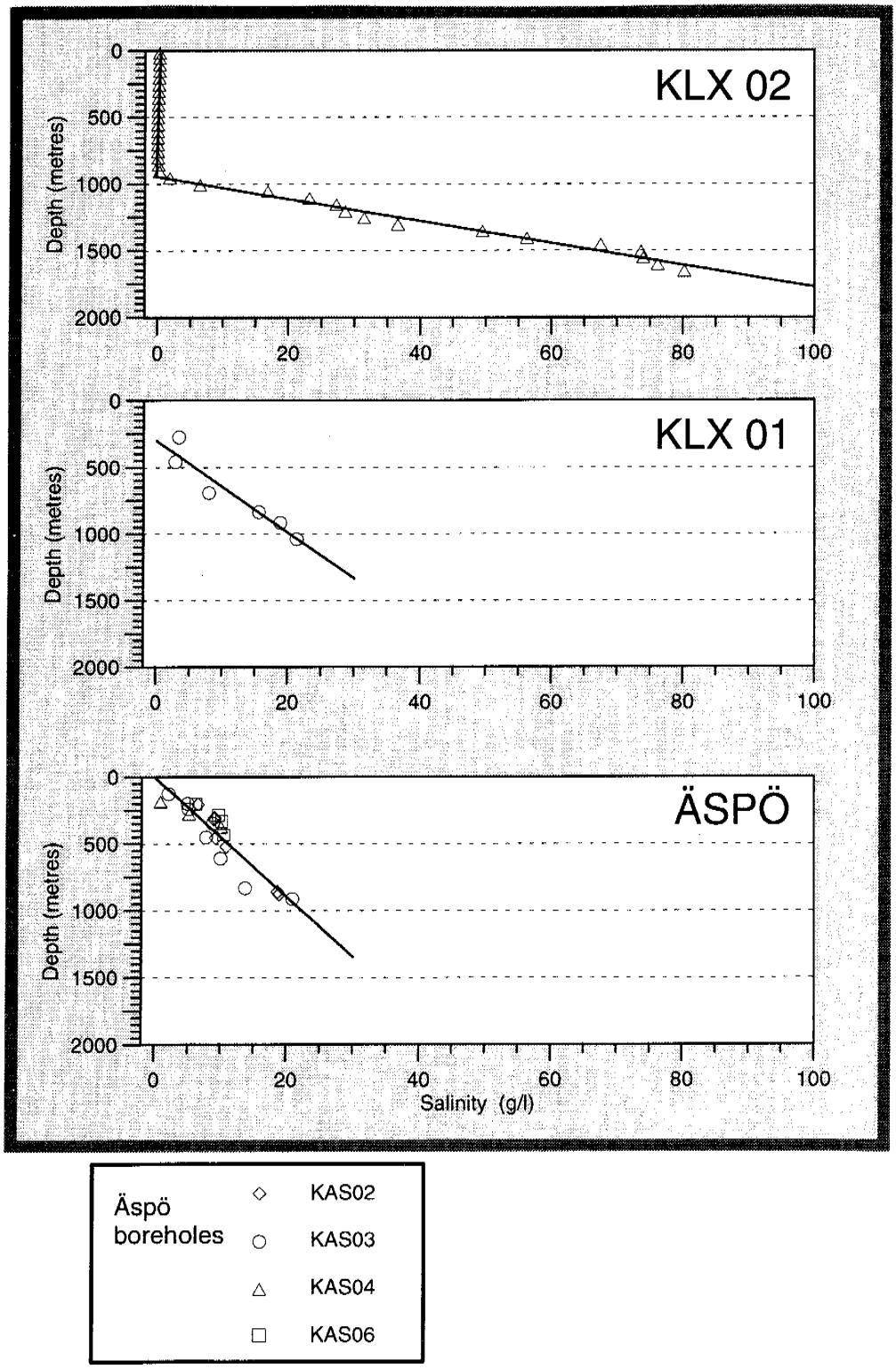

Figure 6-20. *Undisturbed salinity distribution in the ground water near the Äspö HRL. The location of the boreholes is shown in Figure 2-3. The boreholes KLX01 and KLX02 are located on the main land and KLX02 is furthest away from the present shore line.*

6.2.3 Hydraulic conductor domains

Geometric framework

The geometries of the hydraulic conductor domains are defined (in *Section 4.1.3*) by the major discontinuities, which also are shown in *Figure 6-21*. Co-ordinates for the features at the surface are given in *Appendix A2*. Dips are according to *Figure 6-21*. Besides features shown in *Figure 6-21* NW structures are present in the region, see *Figure 2-1*. Possibly conductive features, striking approximately NW-NNW, are also present in the area. These should be of the same kind as the ones discussed in the site model, *Section 6.3.3*.

The fracture zone width in the area is only known very approximately. In the verified positions according to *Figure 6-21* Ground geohysical profiling over some major lineaments indicated width of 100-200 m of low magnetic zones. However, VLF and refraction seismic anomalies were generally less than 10 m wide. It is assumed that the width can be approximated to 20 m for all hydraulic conductors in the regional scale shown in *Appendix A2*.

Material properties

It has not been possible to conduct individual hydraulic tests of the major discontinuities identified, so the geological division of the discontinuities into water-bearing and less-water-bearing was on the basis of expert judgement for assigning parameter values. Estimates of parameters and assignment were made as follows.

The transmissivities of the identified hydraulic discontinuities at Äspö are lognormally distributed with sample characteristics according to *Table 6-2*.

The water-bearing discontinuities (ww) on the regional scale are assumed to have the same characteristics as the more transmissive conductors at Äspö. The less-water-bearing discontinuities (w) are assumed to be somewhat less transmissive than the mean value for the Äspö conductors. The assumed parameters for the model are shown in *Table 6-3* and are based on the lower and upper quartiles shown in *Table 6-2*.

Other parameters for the conductors are outlined in the site scale *(Section 6.3)*.

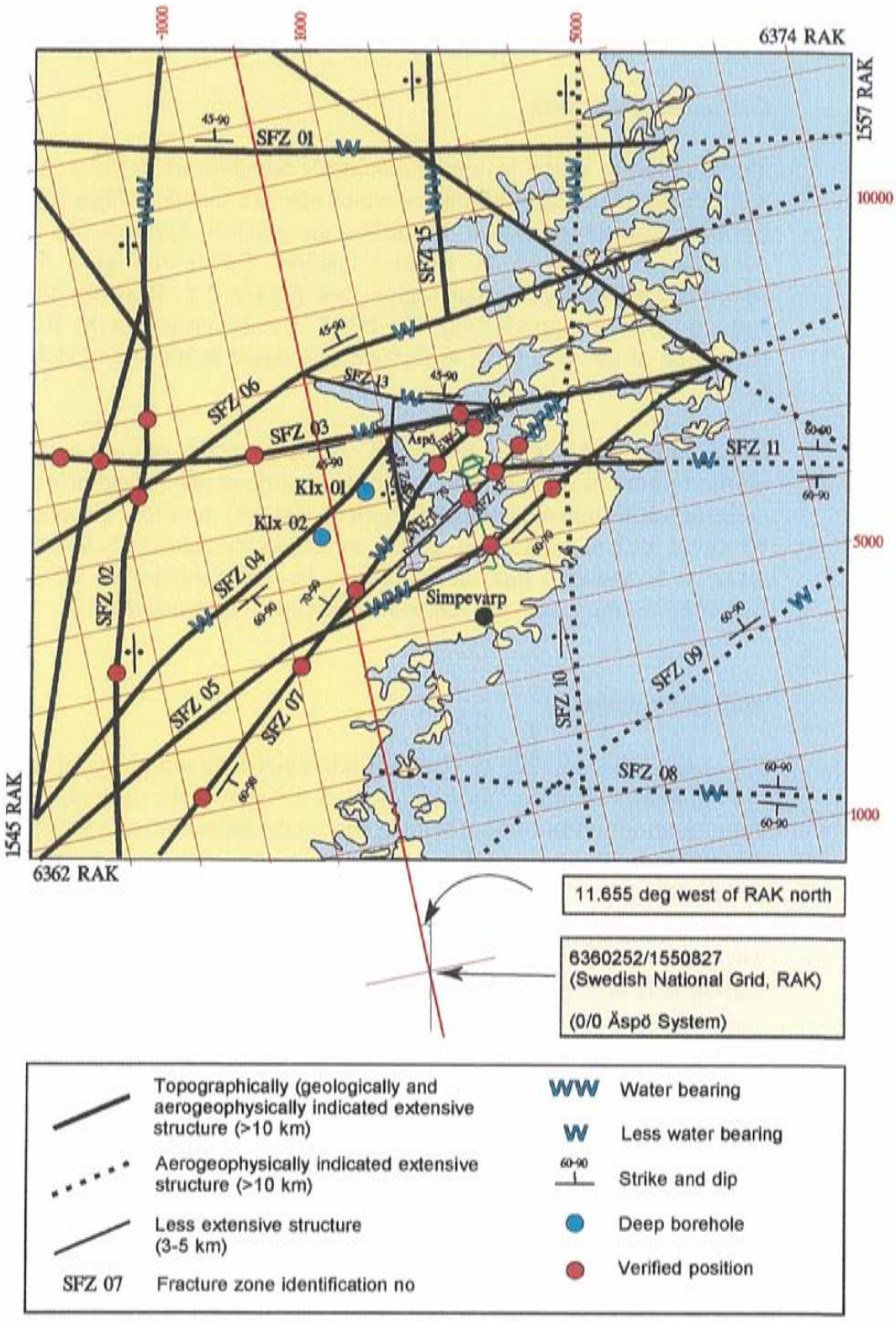

Figure 6-21. Structural model- regional scale (Coordinate systems: RAK and Äspö).

Table 6-2. Sample statistics for $Log_{10}(T)$ for identified hydraulic conductors at Äspö (see Appendix A2). (m = arithmetic mean, s = standard deviation, n = sample size).

Sample	m($Log_{10}(T)$)	s($Log_{10}(T)$)	$Log_{10}(T)$ Lower and upper quartile	$Log_{10}(T)$ 95 % confidence range for mean	n
	$Log_{10}(m^2/s)$	(-)	$Log_{10}(m^2/s)$	$Log_{10}(m^2/s)$	
Äspö HRL	-4.9	1.55	-5.5 to -3.8	-5.2 to -4.5	91

Table 6-3. Hydraulic conductor domains - Regional scale - Transmissivity.

Hydraulic conductor, water-bearing nature	Transmissivity Mean(T) (m^2/s)
w	$0.3 \cdot 10^{-5}$
ww	$10 \cdot 10^{-5}$

Spatial assignment method

Several investigations in Sweden and Finland indicate that the rock becomes less permeable with depth */Ahlbom et al, 1991a, 1991b, 1992a, 1992b, Rhén and Gustafson, 1990* and *Öhberg et al, 1994/*. Rock down to a depth of 100 or 200 m has an effective hydraulic conductivity (K) 100-1000 times greater than the effective K for the depth 500-1500 m according to the regression lines in the reports.

At the four SKB study sites there are hardly any low-conductivity borehole sections down to 100-200 m depth, but below this depth a large number were recorded as being at the lower measurement limit */Ahlbom et al, 1991a, 1991b, 1992a, 1992b/*. The hydraulic conductivity is definitely lower below 100 to 200 m compared with above, but the suggested decrease based on a power function can be discussed. From an examination of the plots it is not obvious that there is a clear decrease below 100-200 m. A similar conclusion is drawn in *Winberg /1989/*. In that report it is concluded that there is mainly a variation with depth

around a constant mean value for the hydraulic conductivity below 200 m depth at the sites Gideå, Fjällveden and Kamlunge.

For three of the sites (Gideå, Fjällveden and Kamlunge) the fracture frequency is 4-5.5/m down to 100 to 200 m and 2-2.5/m below 200 m at two sites and below 500 m at one site (Gideå). The fracture frequency is fairly constant below the depths mentioned above. The rock types at these three sites are mainly sedimentary gneiss (Fjällveden and Gideå) or a mixture of sedimentary gneiss and granite (Kamlunge). The fourth site is dominated by Småland granite (Klipperås).

One can conclude that at the Äspö HRL the decrease in K with depth is not so clear (see *Figures 5-10--5-12 in Rhén et al /1997a/).* On Äspö K is fairly constant down to 600 m, and below that, data were only obtained from only one subvertical corehole (KAS02). Within the Äspö and surrounding areas and below 600 m there are relatively few measurements but the tests indicate that the effective K is around 20% of the effective K within the depth range of 0-600 m. (All boreholes within the Äspö and in surrounding areas with test scales of approximately 100 m are included, (see *Section 6.2.4* and *Appendix A2*). Taking into account the fact that the test scale below 600 m is around 300 m and above about 100 m and also the relations between K and different test scales shown in *Rhén et al/ 1997a/*, the effective K value below 600 m should rather be 10% of the effective K within depth range 0-600 m for test scale 100 m. The base for the conclusion that K does not decrease down to a depth of 600 m is the injection tests with 3 m packer spacing and the hydraulic tests at the 100 m test scale performed at Äspö */Rhén et al, 1997a/.*

In summary, the hydraulic conductivity is fairly constant down to a depth of 500 m at Äspö and below that level there is possibly a decrease according to the pre-investigations. (Exclusion of borehole sections interpreted to be intersected by the deterministic hydraulic conductor domains in the 3 m test scale does not change the conclusion */Rhén et al, 1997a/*).

Tests in probe holes along the tunnel indicate that the hydraulic conductivity is lower for the last tunnel spiral compared to the first (depth intervall for the spiral is about 200-450 m). However, due to large-scale heterogeneity and anisotropic conditions it is not considered possible to draw the conclusion that the hydraulic conductivity decreases down to a depth of 400-500 m based on the data presented above.

Two methods are proposed here for spatial assignment based on zonation (applying the same properties within a depth range) (see *Table 6-4*). In one spatial assignment method, RCD1, it is assumed that the transmissivity of the hydraulic conductors may decrease as much as the effective hydraulic conductivity.

Table 6-4. Regional scale - hydraulic Conductor Domains (RCD) - Spatial assignment method. d_b=depth to bottom level of numerical model. Transmissivity according to Table 6-3.

Spatial assignment method	Depth range (m)	Transmissivity (m^2/s)
RCD1	0-600	T
	600-d_b	0.1*T
RCD2	0-d_b	T

6.2.4 Hydraulic rock mass domain

Geometrical framework

Two concepts are suggested. The first concept (RRD1) is based on the assumption that all lithological domains have the same properties. The other concept (RRD2) is based on the assumption that all hydraulic mass domains are based on the lithological domains defined in *Chapter 4*.

Material properties

Generally, only the specific capacity (Q/s) of the water in wells is available in the SGU Well Archive which means that some concept has to be chosen for transforming Q/s to transmissivity (T). The concept chosen is linear regression of $Log_{10}(T)$ versus $Log_{10}(Q/s)$ for superficial boreholes at the Äspö HRL. The rationale for this is that Q/s is roughly proportional to T */Carlsson and Gustafson, 1984, Domenico and Schwartz, 1990/*. *Figure 6-22* shows the relationship between $Log_{10}(T)$ and $Log_{10}(Q/s)$ for different test scales, where the test scale is defined as the length of the tested section in a borehole. The test times for pumping or injection were generally approximately the same for each test scale. These relationships have been used when estimating the transmissivity when only the specific capacity has been available, due to the fact that the test could not be evaluated using transient evaluation methods. As the water wells available in the SGU Well Archive are generally less than 100 m deep only superficial boreholes at the Äspö HRL were used to estimate the relationship between $Log_{10}(T)$ and $Log_{10}(Q/s)$ when estimating T for the SGU wells. The equations and correlation coefficients for the relations in *Figure 6-22* and the superficial boreholes at the Äspö HRL are shown in *Table 6-5*.

Figure 6-22 is based on all data available for a test scale. No data was excluded from the analysis due to an assumption that they possibly represented hydraulic conductor domains.

Table 6-5. The linear relationship between $Log_{10}(T)$ and $Log_{10}(Q/s)$ for different test scales. $Log_{10}(T)= a+b \cdot Log_{10}(Q/s)$. ρ=Correlation coefficient, n=sample size.

Scale (m)	a	b	ρ	n	Comment
3	1.52	1.18	0.89	654	Injection tests
3-25	1.75	1.13	0.90	210	Mainly pressure build-up tests in the tunnel
25-50	1.17	1.13	0.94	102	Mainly injection tests
50-200	0.16	0.93	0.74	79	Airlift and pumping tests
200-	-0.16	0.89	0.88	27	Mainly pumping tests
≈100	0.35	0.98	0.85	21	Superficial boreholes at Äspö, Ävrö, Bockholmen and Laxemar

An interesting property of the curves in *Figure 6-22* is that the slope of the curves decreases by increasing test scale. For test scales 3 m, 25-50 m, 50-200 m and 200 m- (all of these scales dominated by subvertical boreholes) $Log_{10}Q/dh = -5$ (correspond to $Log_{10}T \approx -5$, and below $Log_{10}Q/dh \approx -5$ the ratio T/(Q/dh) increases by increasing test scale. This can be interpreted to be increasing hydraulic resistance close to the borehole by increasing test scale. The reason is that longer test scales also have involved longer test times and the evaluation period for T has generally also been for relative late time. This means that in a heterogenous system it is likely that low transmissive sections close to the borehole decreases Q but the evaluated T represents some effective value for a larger volume some distance from the borehole.

The data based on the SGU Well Archive may be biased to some extent due to the following reasons:

1 Probably the water-well drillers stop drilling when they judge the well could supply the requested amount of water. This leads to an overestimation of mean T.

2 During capacity tests of very transmissive wells the drawdown probably is less than the well depth. This leads to an underestimation of the high T values.

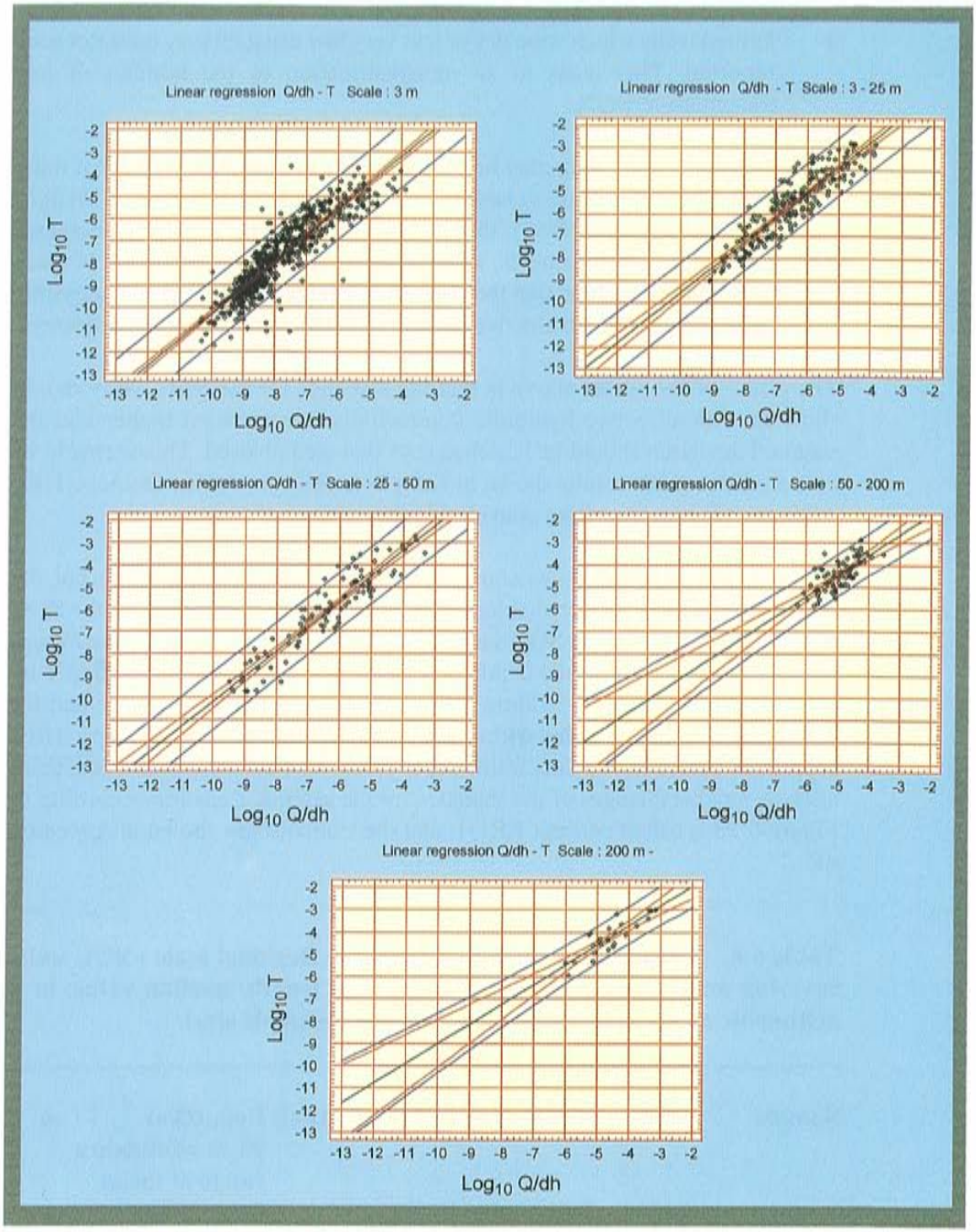

Figure 6-22. *Regression of $Log_{10}(T)$ versus $Log_{10}(Q/s)$.*
Middle line: Mean $Log_{10}(T)$.
Inner lines: 95 % confidence band on mean $Log_{10}(T)$.
Outermost lines: 95 % prediction band on $Log_{10}(T)$ as a function of $Log_{10}(Q/s)$.

3 Drilled wells which were dry or had very low capacity may have not been reported. This leads to an underestimation of the number of low transmissive wells.

4 To some extent data may be biased due to the fact that somewhat more wells are drilled close to larger lineaments. In *Sander /1996/* and *Wladis /1995/* it has been shown that the specific capacity generally decreases out from larger lineaments, which may lead to an overestimation of mean T. Studies also show that the core of very large lineaments may possibly be somewhat less conductive compared to the outer part of the lineament.

The effect of the points above is that the statistics for the SGU wells should show that the effective hydraulic conductivity is somewhat higher and the standard deviation should be less than tests that are unbiased. This seems to be in accordance to the results shown in *Table 6-6*, as we know that the Äspö HRL wells are not biased at least considering the points 1-3.

The sample statistics of Q/s show that the mean is about the same but the standard deviation is somewhat larger for the Äspö HRL data than for the SGU wells (see *Table 6-6*). The SGU sample covers an area of 25x25 km (see *Figure 6-1*). The effective hydraulic conductivity (K) was estimated by dividing T by the test length. *Figure 6-23* shows the statistics for the entire sample and for depth ranges (SGU wells within the regional model area + Äspö HRL superficial boreholes). If data from deeper levels than 200 m are included, there are only smaller changes of the statistics for the sample. Zonation according to *Figure 6-23* is called concept RRD1, and the statistics are shown in *Appendix A2*.

Table 6-6. Sample statistics for $Log_{10}(Q/s)$ - Regional scale - SGU wells covering an area of 25x25 km. (Scale = test length- median value, m = arithmetic mean, s = standard deviation, n = sample size).

Sample	Scale	m($Log_{10}(Q/s)$)	s($Log_{10}(Q/s)$)	$Log_{10}(Q/s)$ 95 % confidence range of mean	n
	(m)	$Log_{10}(m^2/s)$	(-)	$Log_{10}(m^2/s)$	
Äspö HRL	100	-5.8	1.34	-6.15 to -5.42	54
SGU wells	64	-5.51	0.75	-5.61 to -5.40	193

The hydraulic conductivity of different lithological units has been investigated in several studies but as they cover different areas all lithological units defined

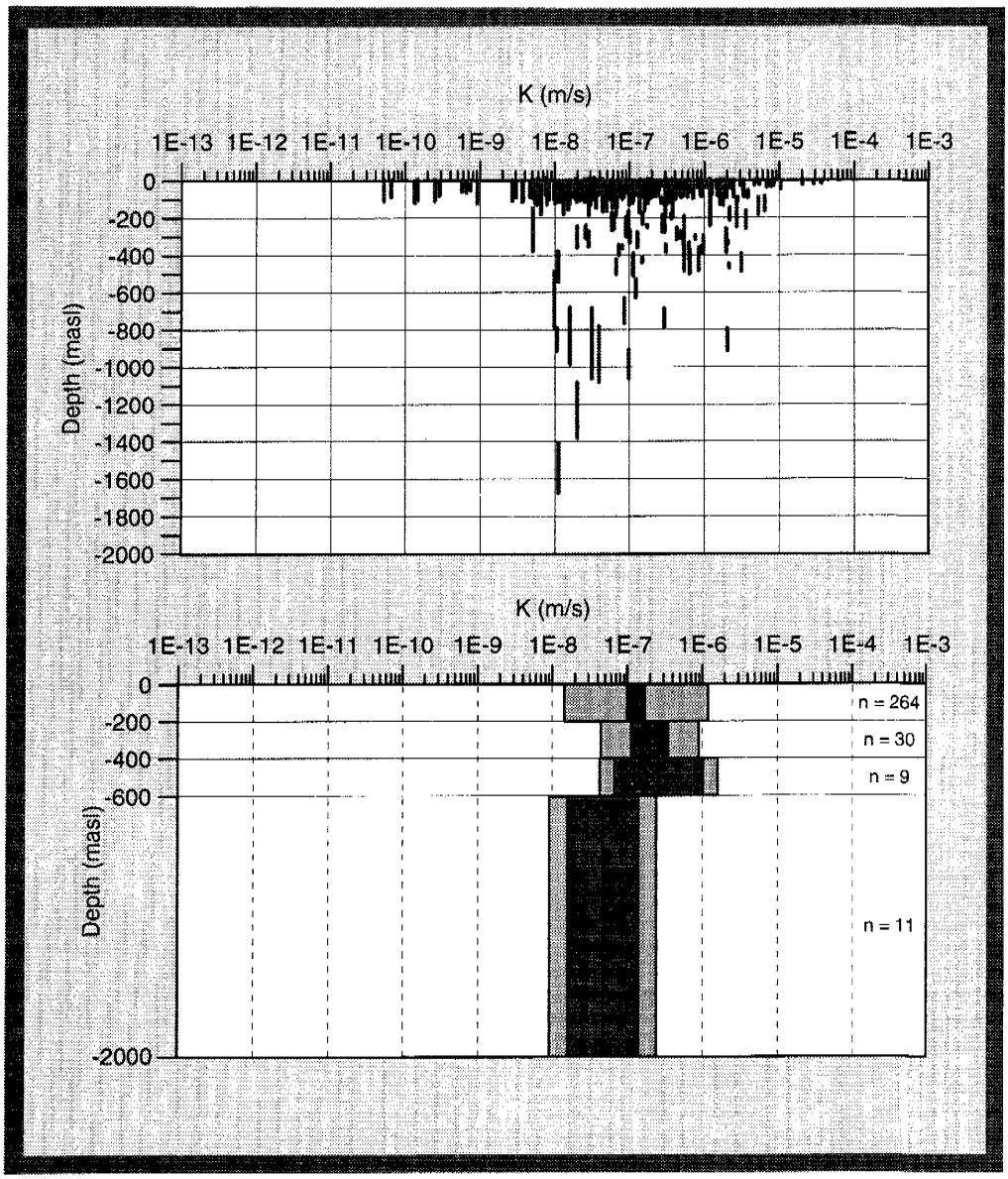

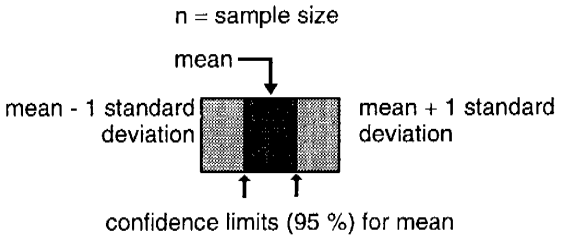

Figure 6-23. *Regional scale-hydraulic conductivity distribution. Test scale 50- ≈300 m. Spatial distribution case: RRD1.*
Top: Distribution of individual measurements at actual test scale.
Bottom: Statistics. (mean = arithmetic mean of $Log_{10}(K)$, standard deviation = Standard deviation of $Log_{10}(K)$, n = sample size).

in the regional model (*Chapter 4*) are not included in each presentation of the statistics. However, the relationships between the estimated hydraulic properties can established by compiling the results (see *Table 6-7*). As Småland granite dominates the regional area, the estimated properties shown in *Figure 6-23* mainly represent the properties of Småland granite. It is suggested for concept RRD2 that the geometric mean hydraulic conductivity (K), be taken as equal to $K=10^a$, where a=arithmetic mean of $Log_{10}(K)$, for each depth range in *Figure 6-23* (or in *Appendix A2*) is multiplied by the values in *Table 6-7* in order to get the geometric mean values for each lithological unit. It is also suggested that the standard deviation shown in *Figure 6-23* (or in *Appendix A2*) for each depth range be used for all lithological units.

Table 6-7. Relationship between hydraulic properties for different hydraulic units and sampling scales to Småland granite. Relationships in the first two columns are based on geometric mean specific capacity (Q/s) and the others on geometric mean hydraulic conductivity (K). (Y = K or Q/s: Geometric mean $Y = 10^a$, where a = arithmetic mean of $Log_{10}(Y)$. Test scale = test length).

Lithological unit	Relationships Q/s or K			
	Kalmar[1] County	Oskarshamn[1] Community	Äspö[3] tunnel	Äspö[4] boreholes
Test scale:	100 m	100 m	14 m	3 m
Anorogenic granite (Götemar, Uthammar and Virbo granites)	-	3[2]	-	-
Fine-grained granite	-	-	6.1	9.1
(Gothic rocks)	-	1.8	-	-
Småland granite	1	1	1	1
Diorite	-	-	0.45	0.45
(Gabbro/Diorite)	0.6	0.53	-	-
Greenstone	-	0.42[2]	0.69	0.45
(Diabase)	-	(0.95)	-	-

[1] */Liedholm , 1992 (Appendix 7.1)/*
[2] */Liedholm , 1987a (Table 5:1 and 5:2)/*
[3] */Rhén et al , 1994a (Table 5-1)/*
[4] */Liedholm , 1991b (TN29 , Table 4-1)/*

Table 6-8. Regional scale - hydraulic Rock mass Domain (RRD) - Material properties - concept RRD2 - Suggested relationships between the geometric mean value of the hydraulic conductivity (K) for different lithological units. (Geometric mean K = 10^a, where a = arithmetic mean of $Log_{10}(K)$. Scale = test length ≈ 100 m.)

Lithological unit	Relationship (-)
Anorogenic granite	3
Fine-grained granite	1.8
Småland granite	1
Äspö diorite	0.5
Greenstone	0.4

Spatial assignment method

The correlation between estimated hydraulic conductivities from the SGU data for the 25x25 km area indicated a correlation length of about 800 m, see *Figure 6-24*. (Two wells with the lowest hydraulic conductivity were excluded as they had a very strong impact on the correlation range). The hydraulic conductivity shown in *Figure 6-25* was estimated by kriging. As indicated in *Figure 6-25* generally the distance between wells exceeds 800 m and as also the confidence band for predicted T (see *Figure 6-22*) indicates that it is reasonable to assume that no spatial correlation exist between the available data points within the regional model area. It is therefore suggested that a stochastic continuum approach without any correlation to the measured data points to be used, assuming a log-normal distribution of K, with population characteristics according to the bottom figure in *Figure 6-23* (or in *Appendix A2*) with zonation (see *Table 6-9*).

As mentioned in *Section 6.2.3* there may possibly be conductive features striking NW-NNW, similar to those discussed in *Section 6.3*, causing anisotropic conditions.

Table 6-9. Regional scale - hydraulic Rock mass Domains (RRD) - Hydraulic conductivity - Spatial assignment method. d_b = depth to bottom level of numerical model. Test scale below 600 m depth is approximately 300 m and above 600 m depth about 100 m. For modelling purposes the statistics of $Log_{10}K$ (arithmetic mean and standard deviation) should be corrected according to discretization of the model and suggestions for scaling in *Section 6.3.*

Spatial assignment method	Depth range (m)	Hydraulic conductivity (m/s)
RRD1	0-d_b	Statistics according to zonation in *Figure 6-22* and *Appendix 2*
RRD2	0-d_b	Statistics according to zonation in *Figure 6-22* and *Table 6-8*. Lithology according to *Chapter 4*.

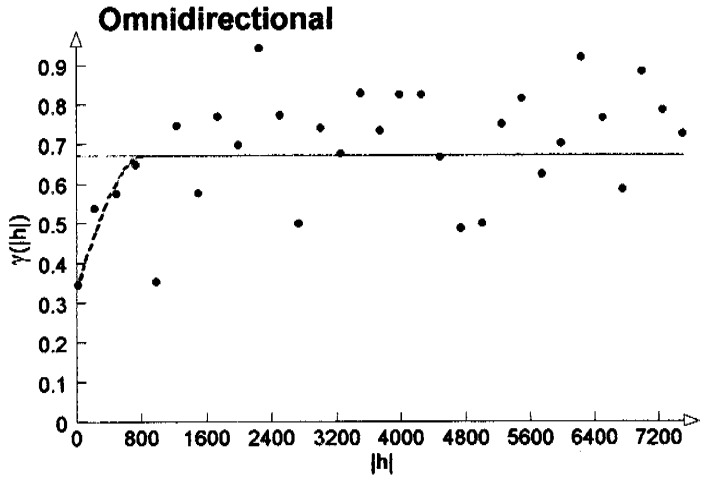

Figure 6-24. *Omnidirectional variogram based on $Log_{10}(K)$, K: Effective hydraulic conductivity (m/s). Data: SGU wells. H = "lag", distance between two points in space. (Two data points excluded in the analysis. Each point in the figure is based on approximately 100-500 data pairs.)*

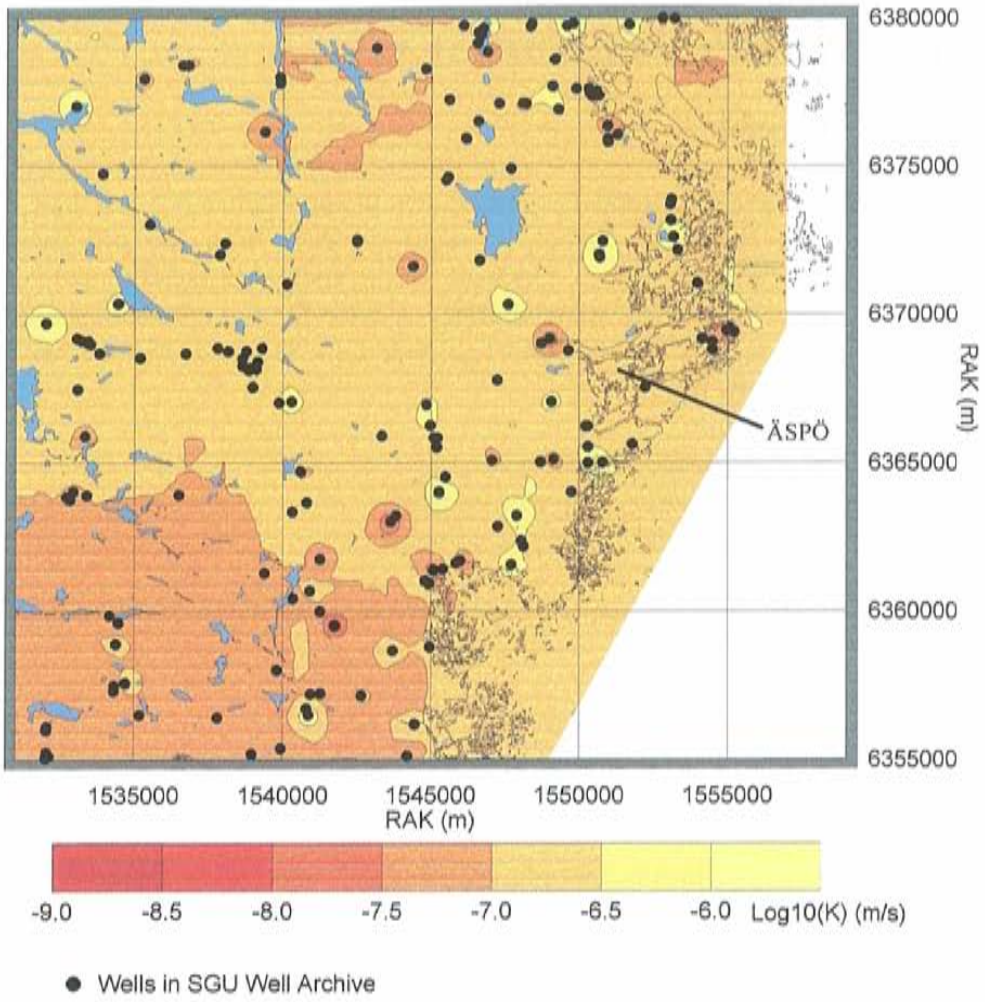

Figure 6-25. *Estimated mean $Log_{10}(K)$ by kriging for depth 0-100 m. Model area in the Regional model area. Filled circles : location of SGU well. Variogram model : gamma(h) = 0.3423+0.33007·(1.5·(h/825)-0.5·(h/825)^3), Data: SGU wells. h = "lag", distance between two points in space. (All data included in the kriging).*

6.3 MODELS ON A SITE SCALE

6.3.1 General

The site scale model covers an area of approximately 1 km^2 (see *Figure 6-26*). The site scale model is based on data from the pre-investigation and construction phases. The base for the geohydrological model is the hydraulic tests performed at Äspö HRL. A base for the site scale model is also the geological-structural model presented in *Chapter 4*. The site model comprises concepts for:

- boundary conditions
- hydraulic conductor domains
- hydraulic rock mass domains

Data for these concepts for the Äspö region are presented below.

6.3.2 Boundary conditions

Hydrological setting of the Äspö area

Drainage basins, topography, peatlands and sediments for Äspö are shown in *Figure 6-26*. The land surface of Äspö is slightly undulating, with a maximum height of about 14 m. There are no perennial streams on the island. The surface water is drained to the sea by the peatlands, sediments or directly to the sea.

The precipitation, temperature and potential evaporation of the area are described in *Section 6.2.2*.

Quaternary deposits

The valleys are filled with peat and sediments and the hills consist mainly of bare rock and some till. The soil cover, mainly till, is usually thin (0 - 5 m) and the till is of a type that contains boulders. In the low areas the till is covered by fluvial deposits mainly consisting of clay, sand and gravel. Fine-grained fluvial deposits are found were the organic deposits are present. Two soil profiles on Äspö containing organic deposits were investigated */Sundblad et al, 1991/*. The top layer was peat and in one of the places a thin layer of unsorted material, gravel and pebbles was found below the peat. The bottom layer was a clay layer, at least about 1 m thick at the sampling points. A number of samples were also taken in the strait between Äspö and Hålö. The top layer was gyttja, 2-4 metres thick. In some of the samples there was a thin layer of gravel below the layer of gyttja. The bottom layer was in most cases clay 1-2 m thick.

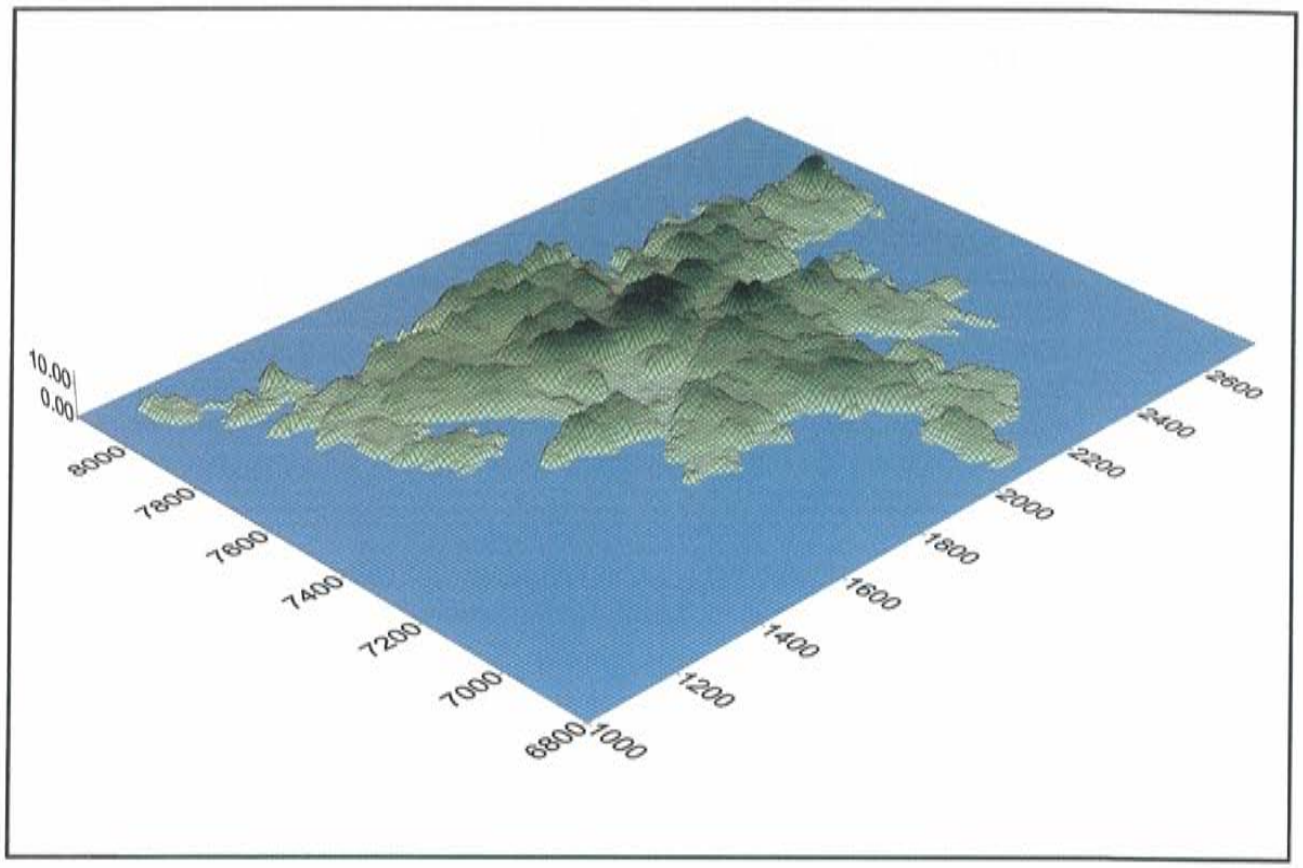

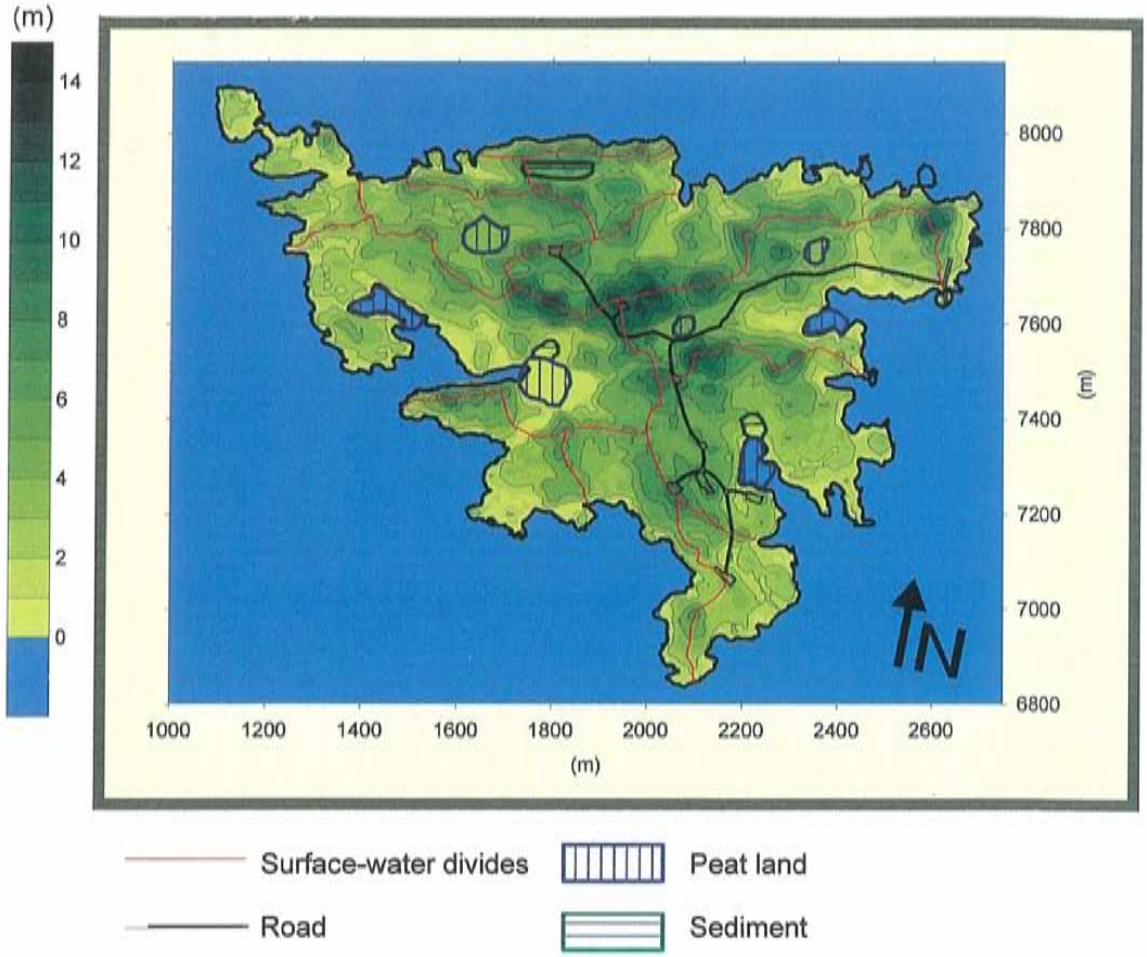

Figure 6-26. *Top: Topography of Äspö. Max level ≈ +14 m. (Vertical scale is magnified). Bottom: Hydrology and topography of Äspö.(Äspö coordinate system).*

Ground water level

The Ground water levels under undisturbed conditions (before the construction of the tunnel) and when the tunnel face was at chainage 2875 m are shown in *Figure 6-27*. The maximum water table is about 4 metres above mean sea level (masl) under undisturbed conditions and after the tunnel was constructed. The probable reason for this is that a few of the boreholes in the upper part of the bedrock on northern Äspö are not well connected to fracture systems deeper in the rock and also because the fracture zone EW-1 acts as a semi-permeable barrier, see *Section 6.3.3*. Deeper levels in borehole KAS03 on northern Äspö indicate a drawdown of a few metres. The minimum measured Ground water level on southern Äspö was found to be about -85 masl when the tunnel face was at chainage 2875 m.

The water table in *Figure 6-27* may be compared with the water table predicted by the Ground water flow model shown in *Chapter 8*.

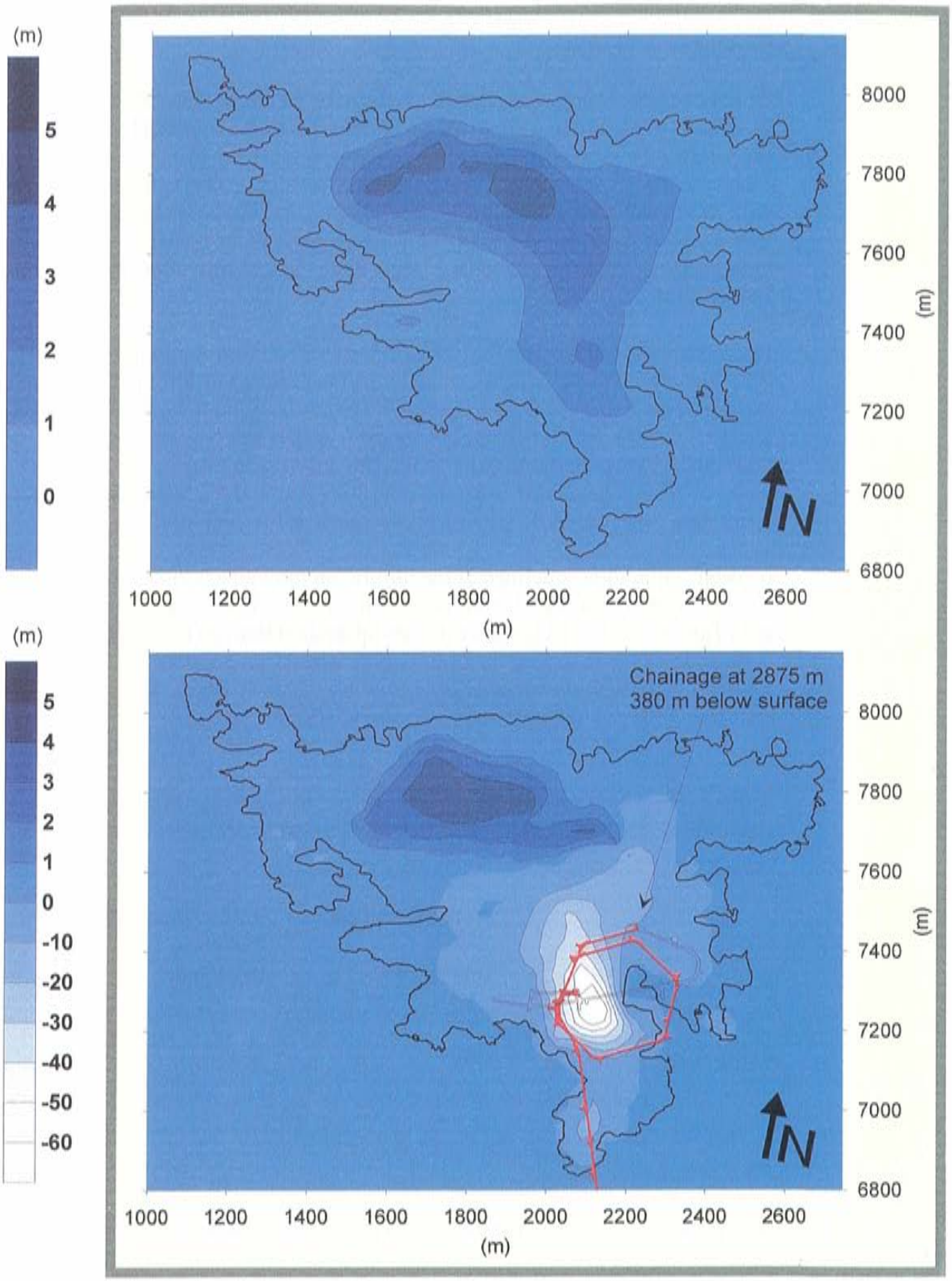

Figure 6-27. *Water table under undisturbed conditions (before the construction of the tunnel) and during construction when the tunnel face was at chainage 2875 m. The water tables shown in the figure are based on interpolation between measured values from measured section located down to a depth of 50 to 100 m. The real water table is most likely more irregular. (Äspö coordinate system).*

Ground water recharge

Ground water recharge was studied by means of a Ground water flow model */Svensson, 1997/*. In *Figure 6-28* the water table is shown for natural conditions (undisturbed by the tunnel) and with tunnel face at tunnel chainage 3600 m. In *Chapter 8* figures show the vertical infiltration rates for natural conditions and with the tunnel face at tunnel chainage 3600 m. In the model the potential recharge is set to 100 mm/year and the actual recharge in the model depends on the local level of the water table, (see *Chapter 8* and *Svensson /1995/* for further details).

In *Chapter 8* it can be seen that the horizontal flow close to ground surface decreases on southern Äspö when the tunnel is present but still much of the flow goes out to the sea via the peatlands. On northern Äspö the flow pattern does not change. The infiltration of water to deeper levels in the rock mass takes mainly place in the fracture zones. The infiltration rates in the fracture zones increase a great deal when the tunnel is present and a large part of the infiltrating water comes from the fracture zones below the Baltic Sea.

If "deep" infiltration is defined as the infiltration through a horizontal surface 5 m below ground surface the average infiltration on Äspö is calculated to be as in *Table 6-10*. The table shows the net-infiltration through the surface. The vertical downwards flow in the centre of the island is larger than the value in *Table 6-10* and the downwards flow also decreases by depth. More details concerning the groundwater flow is shown in *Chapter 8*.

Table 6-10. Average net-infiltration through a surface (limited by the coastline of Äspö) at a depth of 5 m below ground */Svensson, 1997/*.

	Natural conditions (mm/year)	**Tunnel face at chainage 3600 m (mm/year)**
Entire Äspö	0.4	134

Flow into the tunnel

During the construction of the tunnel water flow into the tunnel was measured.

The total inflow and outflow of water were measured at tunnel chainage 700 m. At tunnel chainage 682 m there was a dam and a weir for measuring the flow (Q_{wl}) of water into the tunnel chainage 0 - 682 m. After tunnel chainage 683 m approximately every 150 m along the tunnel a concrete dam was built in the tunnel floor, and connected to a weir downstream (see *Appendix A2*). In

this way the flow (Q_{wi}) into a number of tunnel sections could be measured more or less continuously. The total flow into the tunnel ($\sum Q_{wi}$) is shown in *Figure 6-29* and the monthly flow into each tunnel section is shown in *Figure 6-30* and *Appendix A2*. Details about the flow measurements are presented in *Rhén (ed) /1995/*. The total flow into the tunnel was about 1750 l/min ($29.2 \cdot 10^{-3}$ m^3/s) in December 1995. The decrease in flow rate during spring 1995 is probably due to the permanent reinforcements of the tunnels performed from January to late May 1995.

During the construction of the tunnel the air-velocity, humidity and temperature were also measured for the air flowing in and out at tunnel chainage 710 m. The flow of vapour in (Q_{ai}) and out (Q_{ao}) of the tunnel were estimated from these values (see *Rhén et al /1994a/*). The net inflow of water in the air was approximately 0 - 2.1 l/min ($0\text{-}0.035 \cdot 10^{-3}$ m^3/s), in May to August and the net outflow of water in the air was approximately 0 - 3.6 l/min ($0\text{-}0.06 \cdot 10^{-3}$ m^3/s) from September to April.

Salinity of the water measured at the weirs was measured a few times. The results are presented in *Appendix A2*.

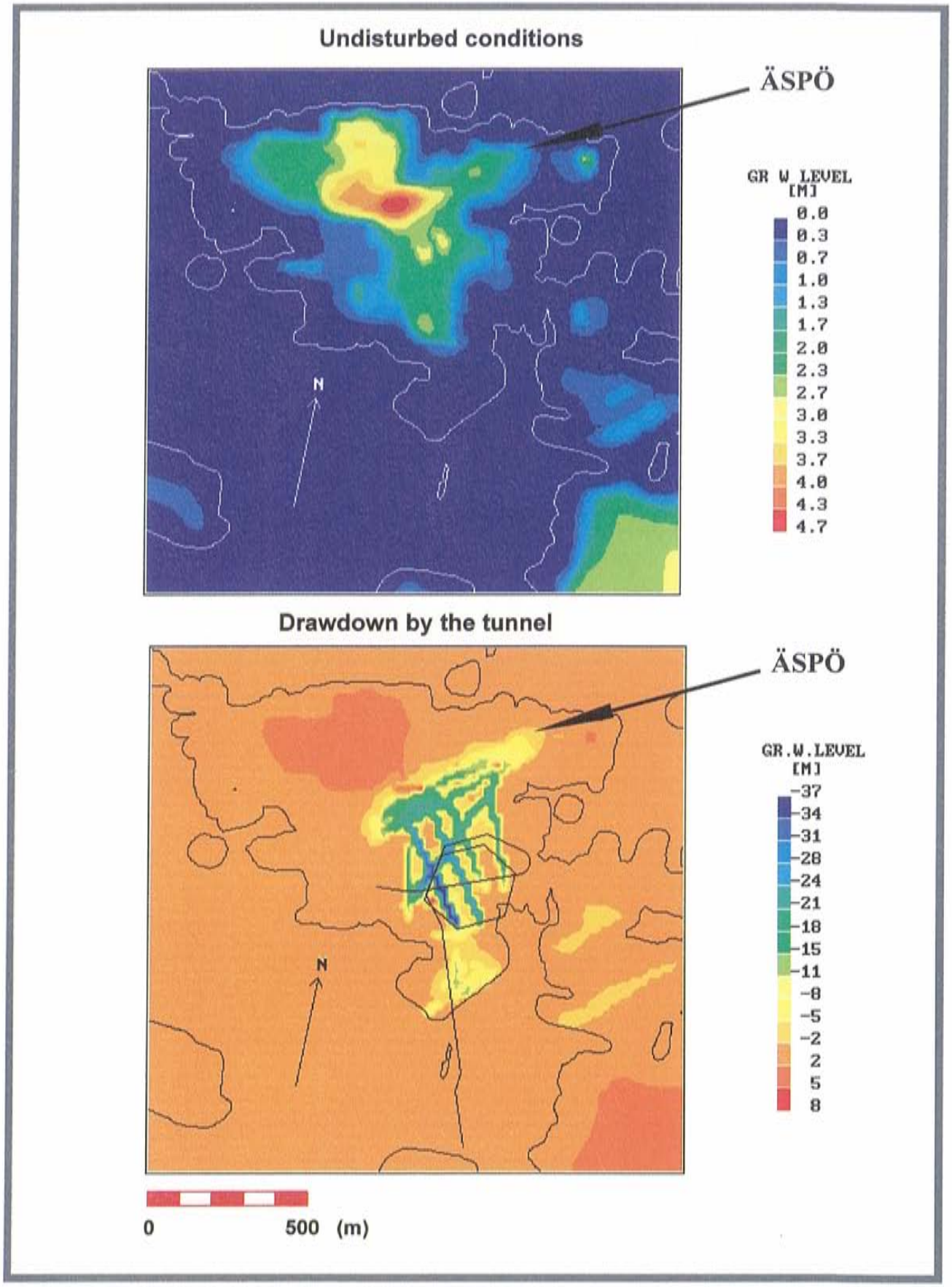

Figure 6-28. *Top: The water table under natural conditions (undisturbed by the tunnel). Bottom: The water table with the tunnel face at tunnel chainage 3600 m. Steady state simulations /Svensson, 1997/.*

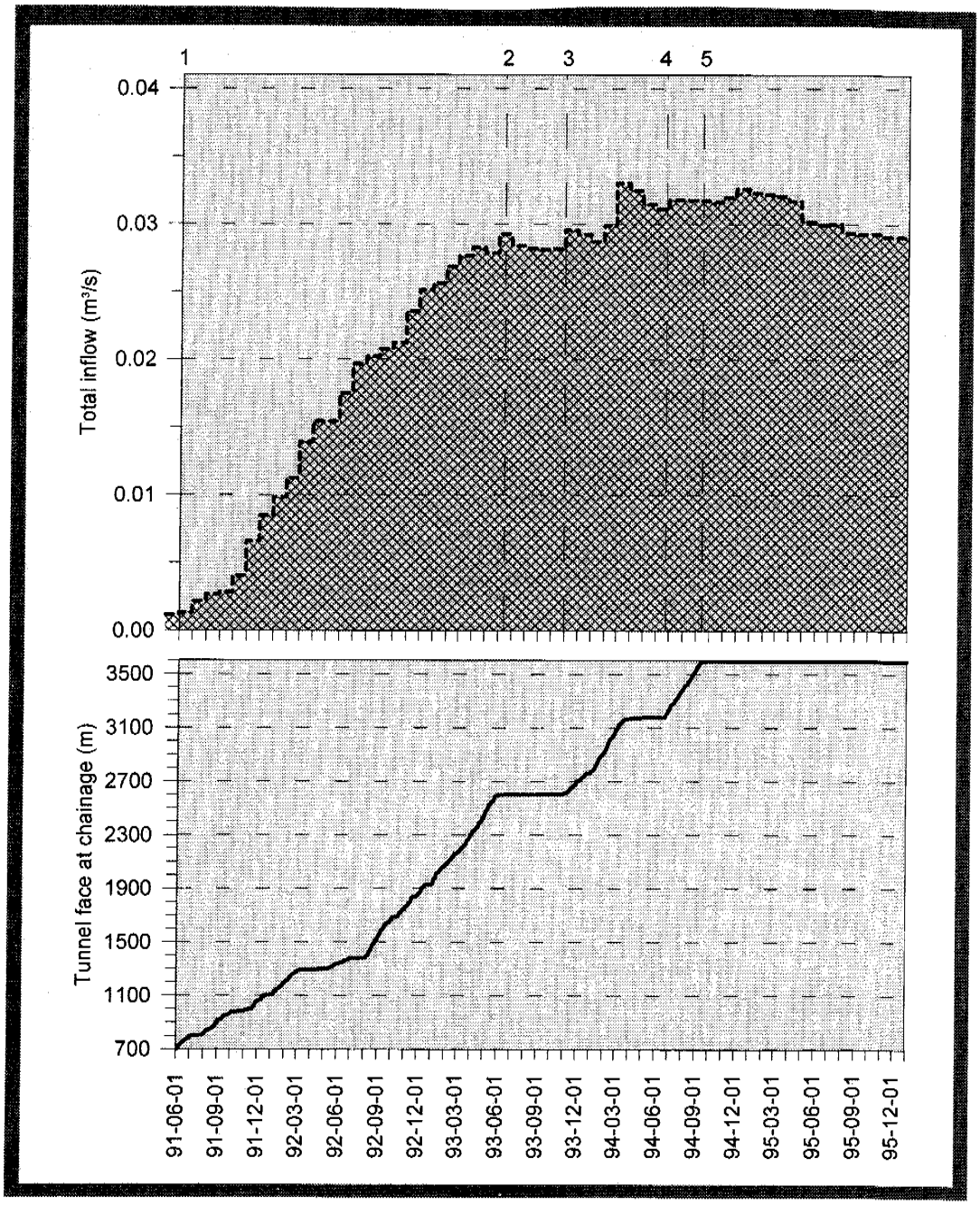

1 Passage of tunnelsection 700 m
2 Stop of excavation at 2600 m
3 Start of excavation at 2600 m
4 Start of TBM drilling
5 End of TBM drilling

Figure 6-29. *Flow into tunnel chainage 0-3600 m. The monthly inflow to the tunnel is the sum of the estimated monthly mean inflows measured at each weir.*

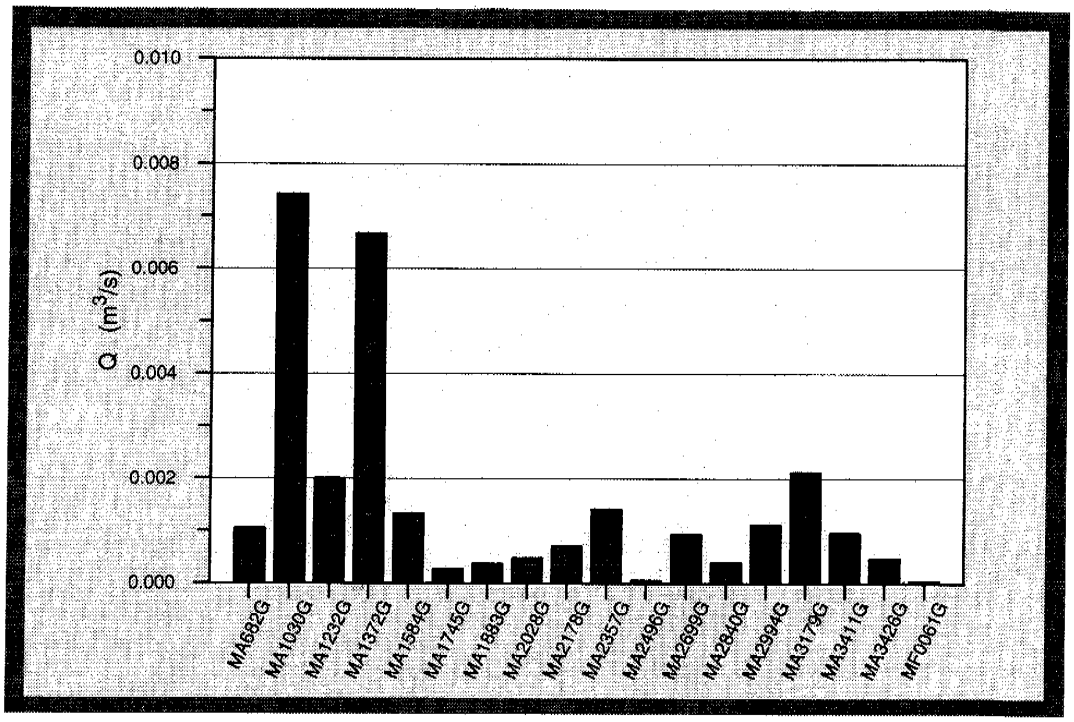

Figure 6-30. *Water flows into tunnel sections. Monthly average values for October 1995. (MYXXXXZ: Measurement point in the tunnel for tunnel section xxxx, see Appendix 2).*

6.3.3 Hydraulic conductor domains

Geometrical framework

The geometries of the hydraulic conductor domains are defined by the major discontinuities described in *Chapter 4*. A simplified discontinuity model was made by fitting a plane to the observations at ground level and in the boreholes. This model is shown in *Figure 6-31*. In *Figure 6-32* a schematic figure shows the fracture sets that are interpreted to dominate the hydraulic conductor- and rock mass domains. Two coordinates for the trace of the discontinuity on the surface (or rather for level= 0 metres above mean sea level (masl)) and one coordinate at a deeper level are given in *Appendix A2*. The interpreted extension of the discontinuities are also presented in *Appendix A2*.

One deterministic hydraulic conductor, NNW-8, is not shown in *Figure 6-31*. The reason is that it is assumed that this structure never reaches the surface. Three interference tests in borehole KAS03 at depths between 350 and 620 m indicated good hydraulic communication with the northern part of EW-1 */Rhén, 1988/*, but as EW-1 does not intersect KAS03 there may be a subvertical structure of limited extent close to the borehole. All three tests indicated about the same transmissivity, similar flow regimes and similar responses in observation boreholes. A vertical structure with the same strike as, for example, NNW-1, here called NNW-8, can explain the responses. The conductor should be considered possible.

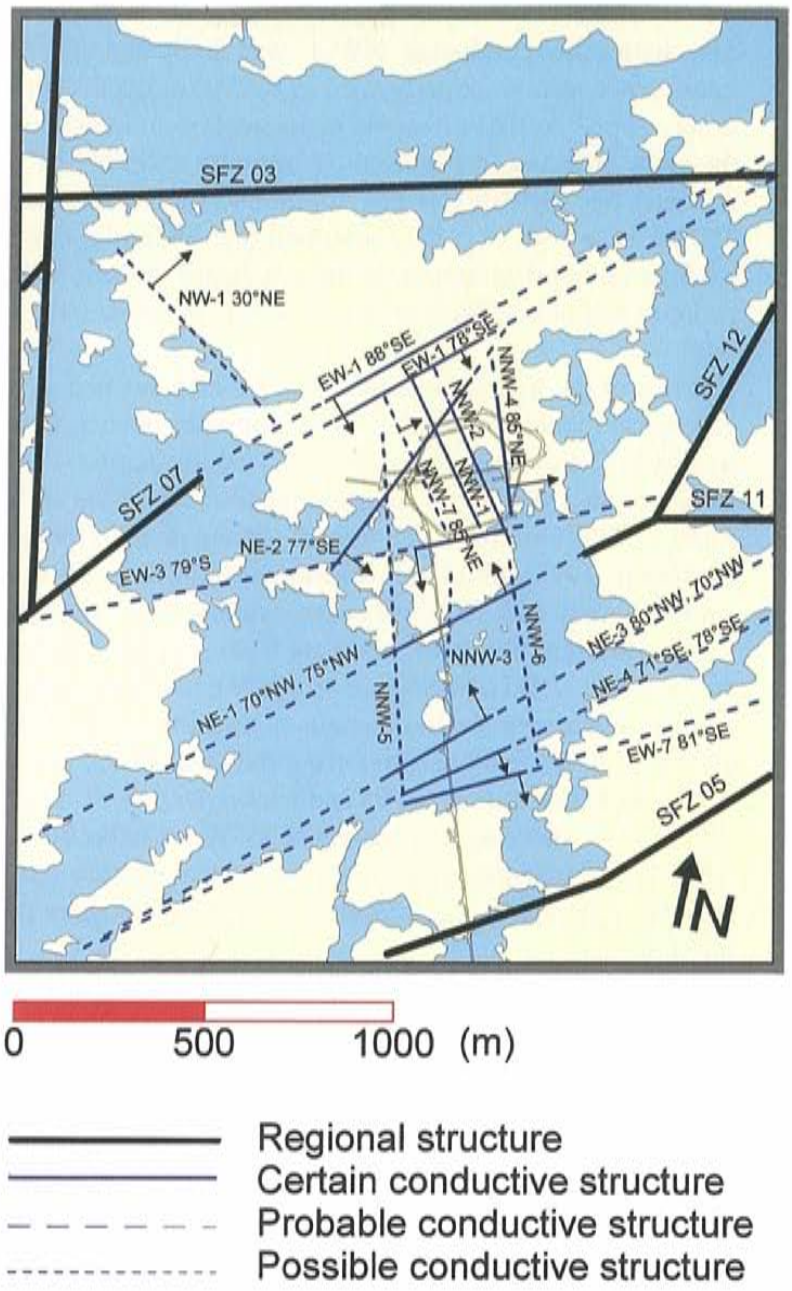

Figure 6-31. *Model of hydraulic conductors on the site scale. (Äspö coordinate system).*

The hydraulic conductor NW-1 was indicated by responses when two interference tests were performed in KAS03 at depths between 200 and 250 m */Rhén, 1988/*. At the surface there are geological indications of a structure with the same strike as in *Figure 6-31* but with a dip 65-70° to the east. This dip indicates that the structure can not intersect KAS03 at depth between 200 and 250 m. However, it is here assumed that hydraulic conductor NW-1 can be used as an approximation of the conductor system in the upper part of the bedrock responses. The conductor should be considered possible.

The rest of the hydraulic conductors are also defined as discontinuities in the geological model. Some of the discontinuities have a clear increase of fracture density but some are rather diffuse and are in *Chapter 4* called fracture swarms. However, in a number of interference tests, from the surface */Rhén, 1988* and *Rhén, 1990/* and from the tunnel */Rhén et al, 1994a* and *Forsmark and Stenberg, 1993/* elliptical drawdown-ellipsoids with main axis trending approximately NW to NNW, were evaluated. By combining the results from tests in different boreholes and data from supplementary investigations */Rhén and Stanfors, 1995 and Rhén et al, 1995/* it was indicated that a few subvertical features could explain the responses seen in the interference tests. There are also other investigations supporting the idea behind fracture swarms trending NW to N-S */Hermanson, 1995* and *Kickmaier, 1993/*. The hydraulic conductors called NNW strike approximately N 35°W are believed to be a fracture swarm which mainly consists of the main subvertical fracture sets with strikes NW and N-S. See *Chapter 4* and *Sections 6.3.4* and *6.4* for more details concerning the fracture sets.

The hydraulic conductor EW-1 is a complex structure (see *Chapter 4*) which is geologically considered to have a more intense fracturing in the northern and southern part of discontinuity EW-1. According to injection tests and flowmeter logging in cored borehole KAS04 there are a number of rather conductive sections through EW-1. However, a number of interference tests showed that the core of EW-1 acts as a semi-permeable barrier */Rhén, 1989, Rhén, 1990, Rhén et al, 1991, Forsmark, 1992, Rhén et al, 1992/*. Due to the evaluated results from the interference tests and the geological nature of EW-1 it is judged that the core of EW-1 has parts whose conductivity is low, giving an average hydraulic conductivity that is less in the N-S direction than in the E-W direction. Some tests indicate relatively good hydraulic communication in the southern part of EW-1 in the E-W direction. */Stanfors et al, 1994/*.

Hydraulic tests give at hand that the hydraulic conductor EW-3 has a transmissivity as the geometric mean of the transmissivities for the deterministic structures (see *Figure 6-33*). However, the interpretation is that the conductivity of core of EW-3 on average is low, for several reasons. The geological nature is that the core of the discontinuity is clay-rich (see *Chapter 4*). The mapping of water conducting features and documentation of pre-grouting in the tunnel */Rhén and Stanfors, 1995/* shows that the tunnel is fairly wet and pre-grouted south of EW-3 but dry and with no pre-grouting some hundred metres north of EW-3. The interpretation is therefore that the core of EW-3 is of fairly

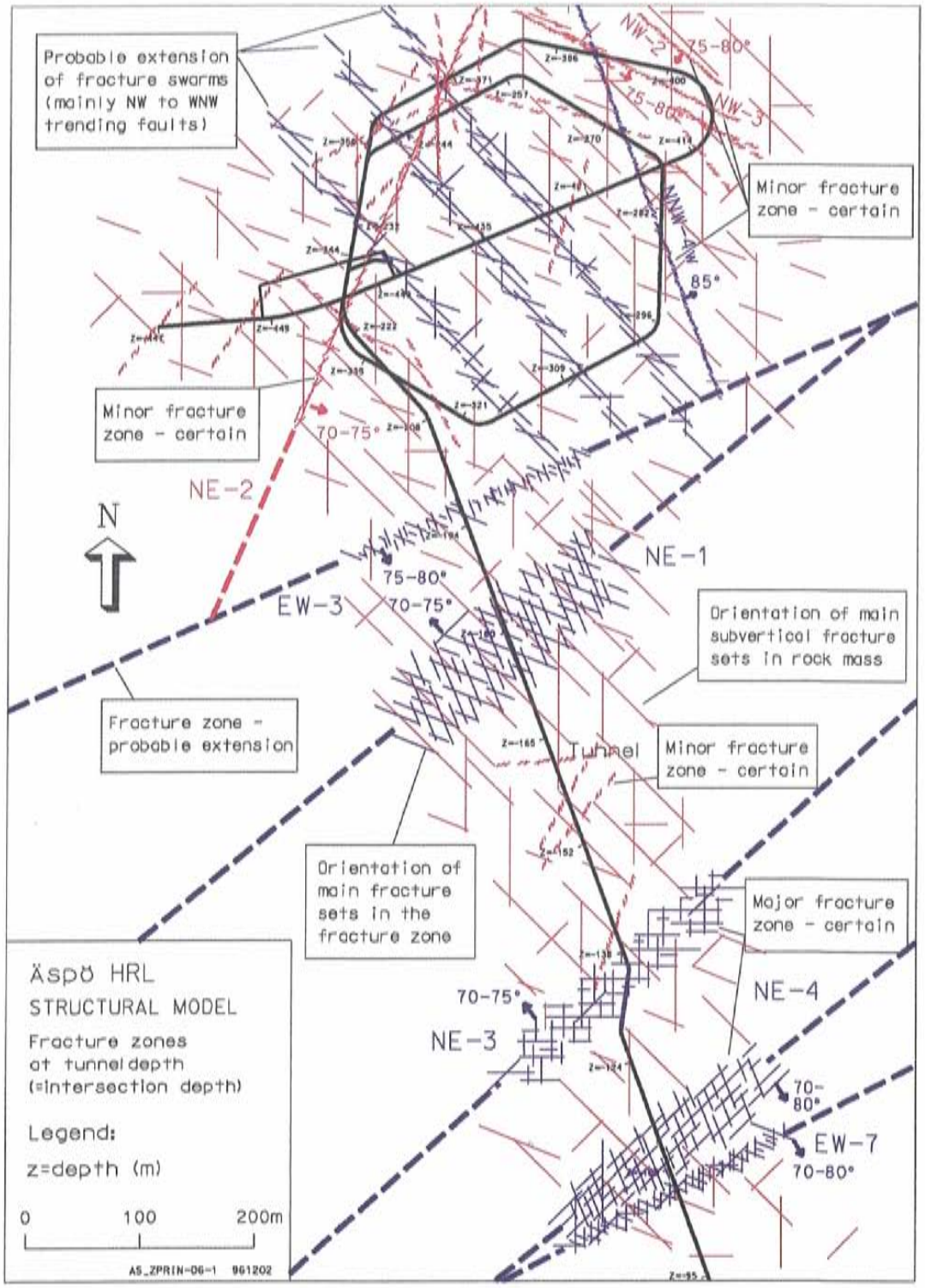

Figure 6-32. *1996 model of hydraulic conductors on southern Äspö - site scale. A schematic figure of the fracture sets present at Äspö and how these sets are interpreted to form some of the hydraulic conductor domains. The NNW-domains ('Fracture swarms' in the figure above) are interpreted to be formed by interconnected, steeply dipping fractures mainly with strikes N-S and WNW to NW. The frequency of the WNW to NW fractures dominates (see Chapter 4). NNW-4W in the figure is called NNW-4 in this Chapter, and Appendix 2. NNW-1, 2 and 7 indicated as NW to WNW trending faults. (Fracture lengths not to scale).*

low conductivity but the outer part of EW-3 is rather conductive and that the evaluated transmissivity represents the outer part of EW-3.

There are several tests which show that NE-1 is in good hydraulic contact with NNW-2 and NNW-4 */Rhén, 1990, Rhén et al, 1991, Forsmark, 1992, Rhén et al, 1992/*. On a few occasions there were large flows of water into the tunnel during the construction of the tunnel south of Äspö. The measured drawdown responses clearly indicated that there was a good hydraulic communication northward from NE-1, where NNW-4 and NNW-2 are supposed to be but not west of these two structures */Rhén and Stanfors, 1995/*. It is therefore assumed that NE-1 cuts through EW-3 in a way that does not significantly reduces the transmissivity of NE-1.

The position and extent of NNW-3, NNW-5 and NNW-6 must be considered uncertain. The features were only indicated by geophysical measurements from the surface in the pre-investigation phase. Cored boreholes were drilled from the tunnel towards the west, and there are some indications that can be interpreted as being at the intersection with NNW-5 */Olsson et al, 1994, Olsson (ed), 1994/*. The conductors should be considered possible.

It can also be noted that interference tests indicate that there is good hydraulic communication between the uppermost measurement sections in KAS02 and KAS05. It is also good hydraulic communication between two of the upper measurement sections in KAS06 and KAS07, which was seen in the LPT2 test. No hydraulic features have been included in the *Model 96* as there are no clear indications of fracture zones or fracture swarms that could explain these responses.

Material properties

Transmissivity

Most of the hydraulic conductors have been penetrated by boreholes and different hydraulic tests were performed, such as air-lift tests and pump tests of the entire borehole in combination with flow metre logging. Interference tests, where selected conductors were pumped, and hydraulic injection tests were also made. Generally, tests were performed in one or a few parts of the zone. In a few cases several tests from different parts of the discontinuities are available and make it possible to assign the variability within the zone. In some cases discontinuities, that have been identified by geological and/or geophysical investigations, have not been tested hydraulically. NNW-6 was not tested and the test assumed to be representative of NNW-5 must be considered uncertain. In cases where no tests are available the interpreted geological nature is the basis for assigning the material properties.

Figure 6-33 and *Figure 6-34* show the statistics for all deterministic hydraulic conductors. As can be seen in *Figure 6-33* the geometric mean transmissivity (T) is $1.4 \cdot 10^{-5}$ m^2/s with a standard deviation of 1.55 for $Log_{10}(T)$. *Figure 6-34* shows the statistics for each deterministic hydraulic conductor. As can be seen the confidence limits for T are quite wide for some conductors. The reason is that in some cases the sample is very small but in other cases the evaluated transmissivities are widely spread for the conductor at the positions where the conductor is interpreted to intersect the borehole, for example NE-2. If the sample size was less than 7 the confidence limits for mean have not been plotted. The detailed statistics are presented in *Appendix A2*.

Tests in the probeholes (test scale 15 m) were also classified as belonging to deterministic fracture zones or rock mass outside these zones. The mean (arithmetic mean of $Log_{10}K$) hydraulic conductivity (K) of tunnel sections intersected by deterministic fracture zones is about $8 \cdot 10^{-8}$ m/s and for the rock mass outside these zones mean K is about $1.5 \cdot 10^{-9}$ m/s for tunnel section 1400-3600 m, see *Appendix 2*. If also tests in the parts of the tunnel which were mapped as "fracture zone" (according to the definition used during the excavation of the tunnel) are added to the tests assigned as representing deterministic fracture zones mean K becomes about $2 \cdot 10^{-8}$ m/s and for the rock mass outside "zones" mean K becomes $1.4 \cdot 10^{-9}$ m/s. This is expected as it is assumed that the deterministic conductors defined should be the most transmissive conductors.

As can be seen in *Figure 6-33* all conductors in *Figure 6-31* are not represented. The reason is that no reliable test was performed in the structure. For the NNW-6, the statistics for the entire sample in *Figure 6-33* is assumed to be a relevant approximation (see *Appendix A2* for statistics).

The data has been used for groundwater flow modelling. Due to calibration some transmissivities were changed, see *Chapter 8* and *Svensson /1997/*.

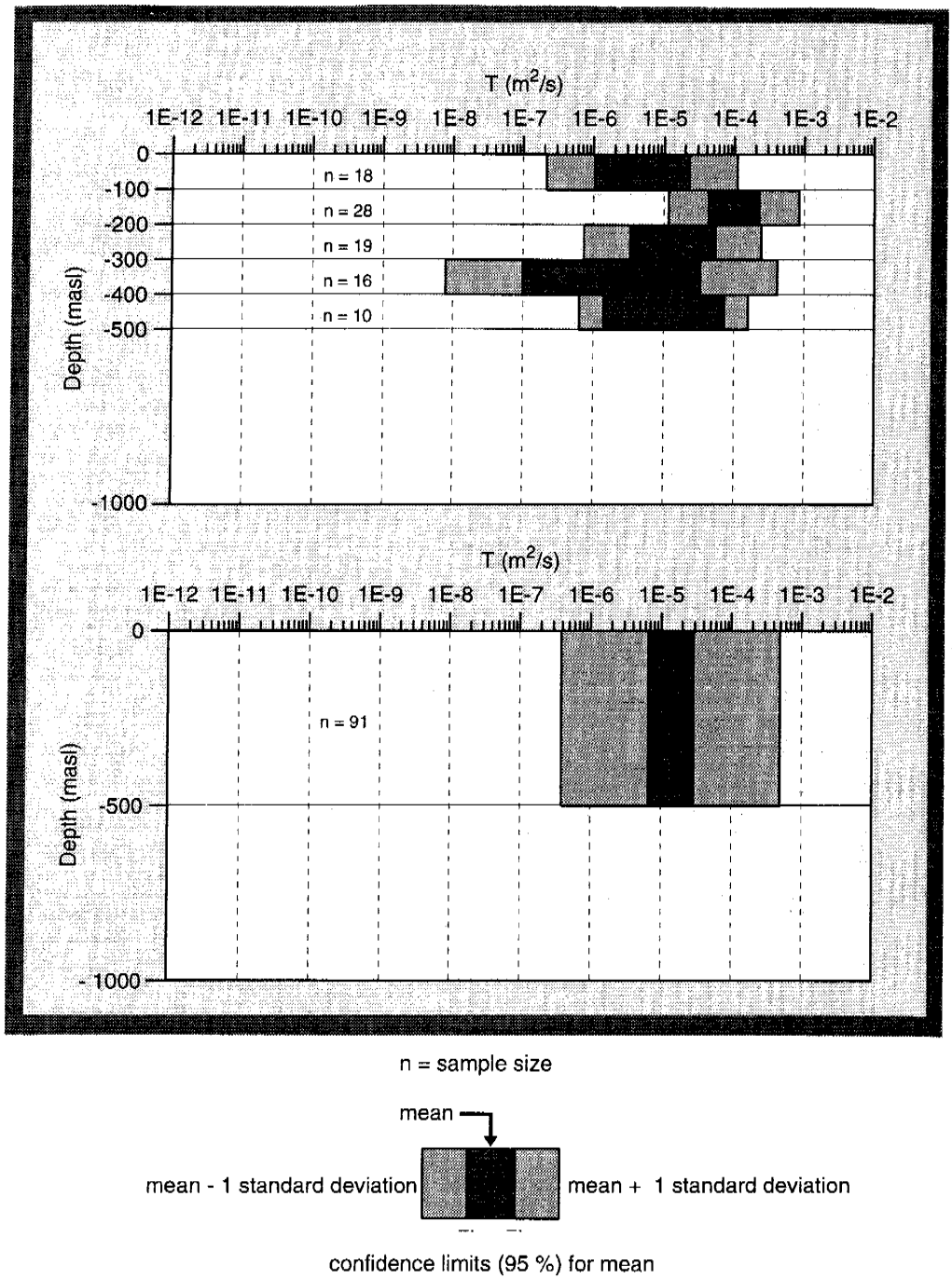

Figure 6-33. *Transmissivity (T) for deterministically determined hydraulic conductors in site scale (mean= arithmetic mean of $Log_{10}(T)$, standard deviation=Standard deviation of $Log_{10}(T)$, n=sample size).*

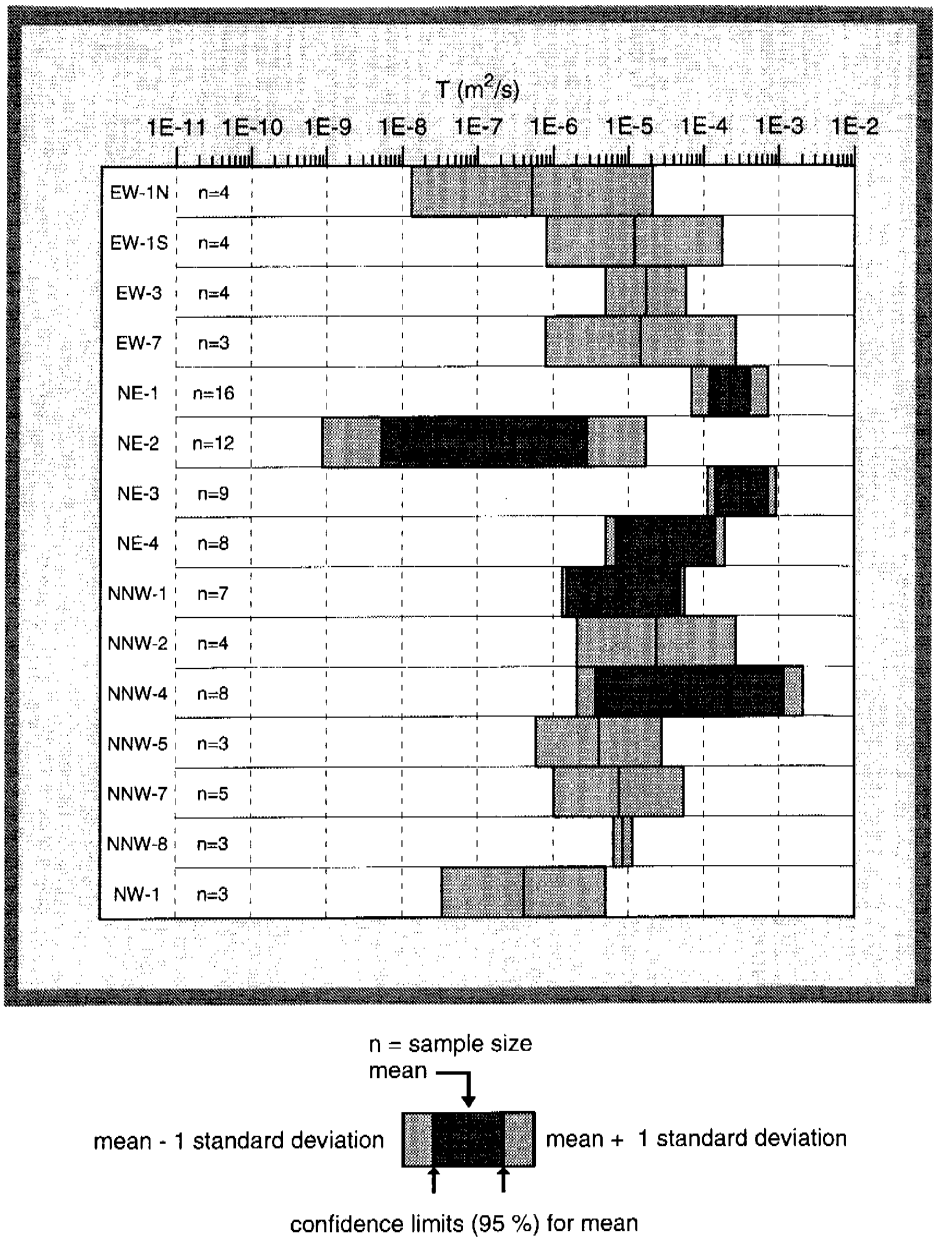

Figure 6-34. *Transmissivity (T) for deterministically determined hydraulic conductors on and south of Äspö in site scale (mean = arithmetic mean of $Log_{10}(T)$, standard deviation = Standard deviation of $Log_{10}(T)$, n = sample size).*

Storage coefficient

There are very few interference tests at Äspö HRL that are judged to be useful for direct evaluation of the storage coefficient (S) of a hydraulic conductor, where the radial flow assumption can be interpreted to be valid. The reason is that the distance between the observation sections is relatively long in comparison with the distances between hydraulic conductors with higher transmissivities (T). The evaluated T and S for tests, where it was judged that the flow regime was radial flow and the flow was mainly within a defined sub-planar feature with a higher conductivity compared with the surroundings, is shown in *Figure 6-35*. The relationship between T and S is shown in *Figure 6-35*, approximated to a power law relationship, which is also presented in *Table 6-11*.

Table 6-11. The linear relationship between $Log_{10}(T)$ and $Log_{10}(S)$ in *Figure 6-35*. Test scale approximately 100 m. $S = a \cdot T^b$. ρ =Correlation coefficient. n = sample size.

Scale (m)	a	b	ρ	n
100	0.00922	0.785	0.71	5

However, the relation in *Figure 6-35* and *Table 6-11* seems to give unrealistic low S values for very low T values. There are few points for the regression which makes the relation uncertain. Probably the slope should be less than shown. The variability of S is however probably relatively large, which *Figure 6-35* indicates.

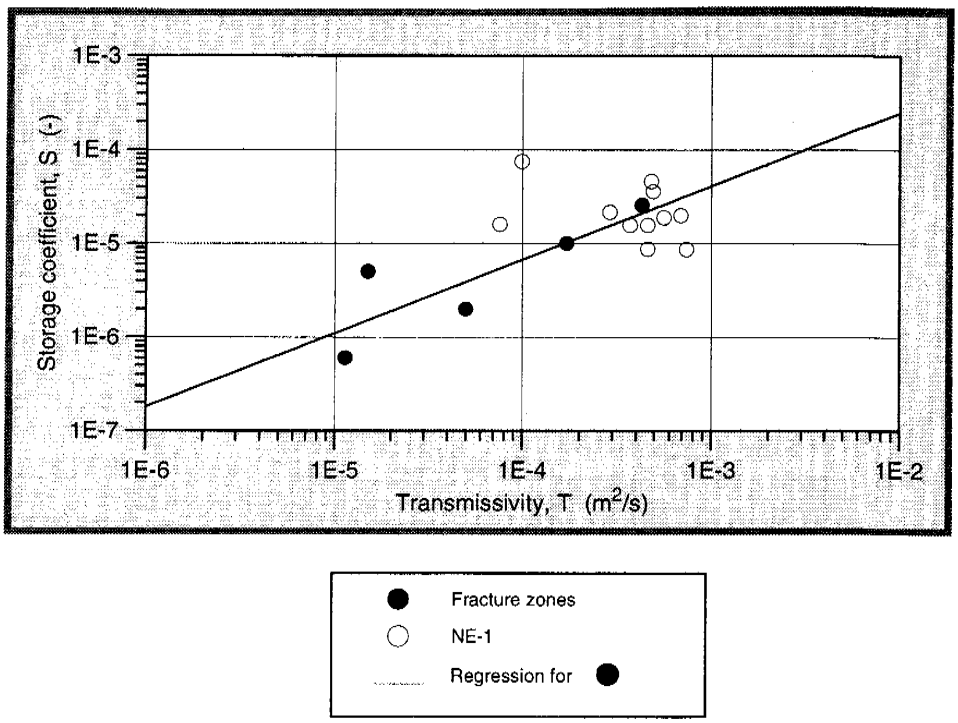

Figure 6-35. *The relationship between $Log_{10}(T)$ and $Log_{10}(S)$ evaluated from interference tests in hydraulic conductor doms. Test scale approximately 100 m. (One of the filled circles represents the arithmetic mean of the values for NE-1 shown as open circles).*

The rock mass along the tunnel was classified according to the RMR system and these values can be used to estimate approximate values of the deformation modulus (E_d) */Jibao, 1992, Johansson et al, 1995/*. Several relationships between RMR and E_d have been suggested, and here a slightly modified equation by *Serafin and Pereira /1983/* is used, *Equations 6-2* and *6-3*. Above RMR=70 a linear approximation up to Young's modulus of intact rock (E_i) is used as the equation given by *Serafin and Pereira /1983/* gives unrealistic E_d values for high RMR values. According to *Stille and Olsson, /1996/* the tests on core samples from the tunnel, mainly in the first part, showed a range for E_i of 63-96 GPa and a range for the Poisson's ratio (ν) of 0.18-0.29. Seismic tomography tests between boreholes in what can be considered as fairly good rock at about 400 m depth indicated Young`s modulus in the range of 76-83 Gpa */Olsson et al, 1996/*. E_i is therefore approximated to 80 GPa for RMR=100. *Table 6-12* shows the estimated values of E_d, compressibility of porous medium (bulk) (α_b) and specific storage (S_s). In *Appendix A2* normal probability plots for RMR and E_d is shown. As can be seen in *Table 6-12* the compressibility of the water (β_i) can more or less be neglected. (Increased salinity, pressure and temperature will decrease β_i, but only to a minor degree given the expected values at Äspö HRL.) It is also possible to see that the storage coefficient for a 10-20 m wide zone may be around 10^{-5}, which is in good accordance with *Figure 6-35*. RMR values for the tunnel below the sea are somewhat lower than shown in *Table 6-12*, giving somewhat higher S_s values. The Poisson's ratio of 0.3 gives slightly lower S_s values.

RMR≤ 70:

$$E_d = 10^{\frac{RMR - 10}{40}} \tag{6-2}$$

RMR> 70:

$$E_d = 31.6 + \frac{RMR - 70}{30} \tag{6-3}$$

$$\alpha_b = \frac{3(1 - 2\nu)}{E} \tag{6-4}$$

$$S_s = \varrho \cdot g \cdot (n\,\beta_l + \alpha_b) \tag{6-5}$$

where				
	ϱ	=	Fluid density	(kg/m^3)
	g	=	Acceleration of gravity	(m/s^2)
	α_b	=	Compressibility of porous medium (bulk)	(m^2/N)
	n	=	Porosity	(-)
	β_l	=	Coefficient of compressibility of a fluid	(m^2/N)

The storage coefficient or storativity (S) is defined as the specific storage of a feature multiplied by its thickness (b):

$$S = S_s \cdot b \tag{6-6}$$

Table 6-12. Estimate of the deformation modulus (E_d), compressibility of a porous medium (bulk)(α_b) and specific storage (S_s) based on RMR estimates for tunnel chainage 1400-3600 m. The probability distribution of RMR for zone is of more or less perfect normal distribution. (Type = characterization of tunnel walls: zone, increased fracturing and rock (= not zone or increased fracturing), Cd = Cumulative density, n = Porosity, ν = 0.2 . Temperature = 15°C for estimation of the fluid density and coefficient of compressibility of water).

Type	Cd (%)	RMR	E_d (Gpa)	α_b (Pa^{-1})	S_s n=0 (m^{-1})	S_s n=0.05 (m^{-1})
zone	5	42	6	2.9E-10	2.8E-6	3.0E-6
zone	50	58	16	1.1E-10	1.1E-6	1.3E-6
zone	95	78	45	4.0E-11	4.0E-7	6.3E-7

Spatial assignment method

Deterministic assignment was used in the numerical modelling, see *Chapter 8*, based on the mean of $Log_{10}(T)$ in *Figure 6-34* and *Appendix A2* for the transmissivity. However, the transmissivities were slightly modified due to calibration, see *Chapter 8*. The relationship between the transmissivity and storage coefficient shown in *Table 6-11* is suggested to be used for assigning the storativity.

6.3.4 Hydraulic rock mass domain

Geometric framework

The Äspö area is divided into five groups of Site hydraulic Rock mass Domains (SRD) with different hydraulic properties :

- SRD 1: Northern part of Äspö, bounded to the south by the northern part of EW-1.
- SRD 2: Volume bounded by the northern and southern parts of EW-1.
- SRD 3: Southern part of Äspö bounded to the north by the southern part of EW-1 and to the south by EW-3.
- SRD 4: South of EW-3.

- SRD 5: A Fine-grained granite domain in the middle of the tunnel spiral at about 350 m depth.

Outside Äspö SRD1-4 are assumed to be valid within an area bounded by EW-7 to the south and some 100 m outside Äspö to the west, north and east (see *Figure 6-36*). Possibly the properties can be extrapolated within the volume bounded by the hydraulic conductor domains limiting the rock mass domains to the north and to the south and the borders for the model area shown in *Figure 6-36*. The assumption is then that the geological conditions are about the same, which seems reasonable, possibly except for the Laxemar and Mjälen areas, which partly are included in SRD 4. These areas may be less conductive as they probably are less fractured.

Material properties

Hydraulic conductivity

The estimate of the material parameters is mainly based on hydraulic injection tests (with a test scale of 3 m) but, as hydraulic tests have shown themselves to be scale dependent, also hydraulic injection tests (with a test scale of 30 m), air-lift tests and pump tests of the entire borehole were used to establish an empirical relationship between the test scale and hydraulic conductivity. The scale dependency can be illustrated by *Figure 6-37*. In this figure all hydraulic tests performed at Äspö HRL during the pre-investigation and construction phases are shown. As can be seen in the figure the variability decreases and the median effective hydraulic conductivity increases as the test scale increases. However, there are generally neither all test scales in all boreholes nor all test scales along an entire borehole length. One cannot therefore draw any certain conclusions on the scale dependency based on *Figure 6-37*. Borehole sections where injection tests with 3 m packer spacing were performed have therefore been used as the basis for evaluating the scale relationships. (The injection tests with 3 m packer spacing have been re-evaluated since *Wikberg et al /1991/*. Where no transmissivities were possible to evaluate the specific capacity was used to estimate the transmissivity for the 3 m test section according to *Section 6.2.4.*)

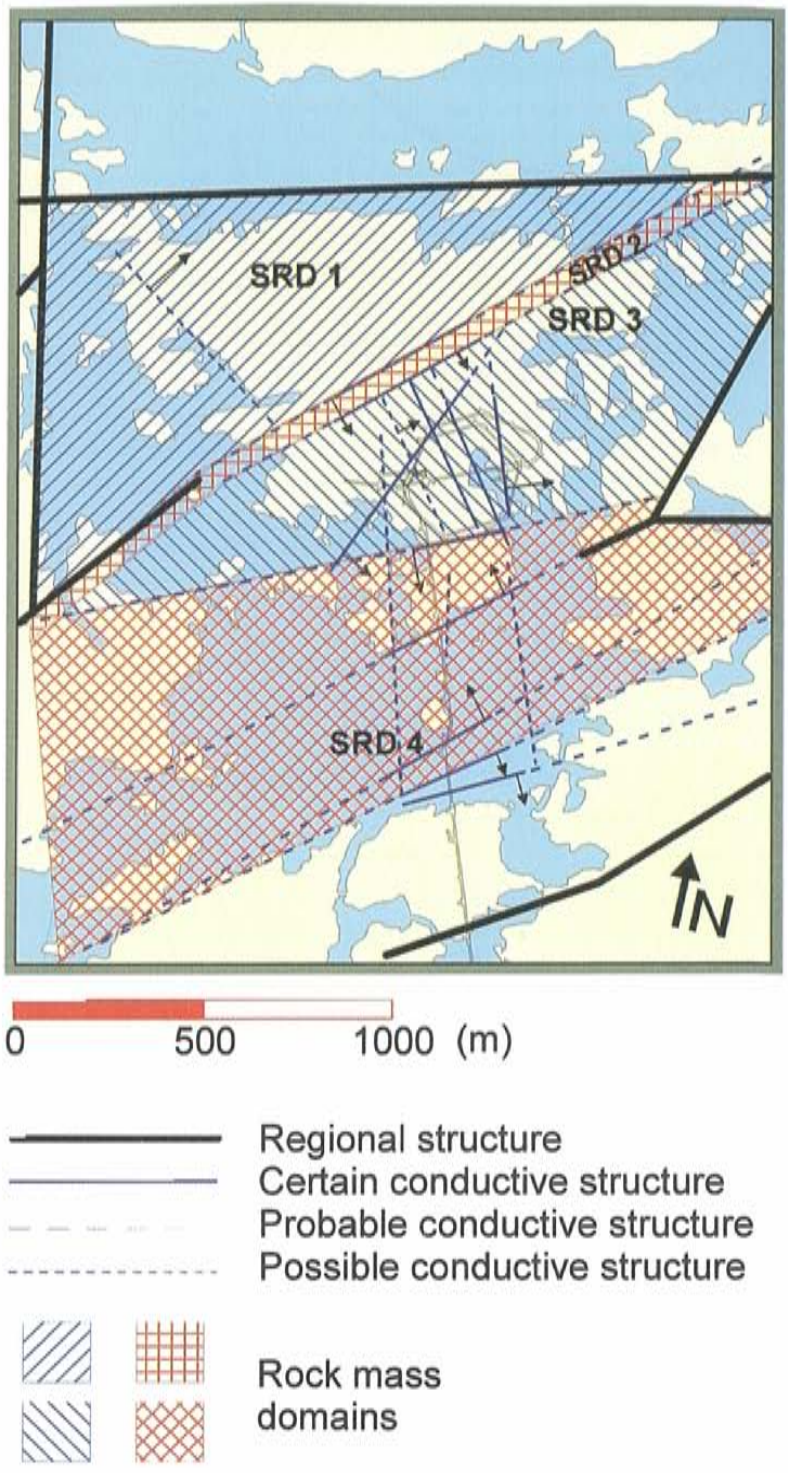

Figure 6-36. *Model of the Site scale hydraulic Rock mass Domains (SRD). (Äspö coordinate system).*

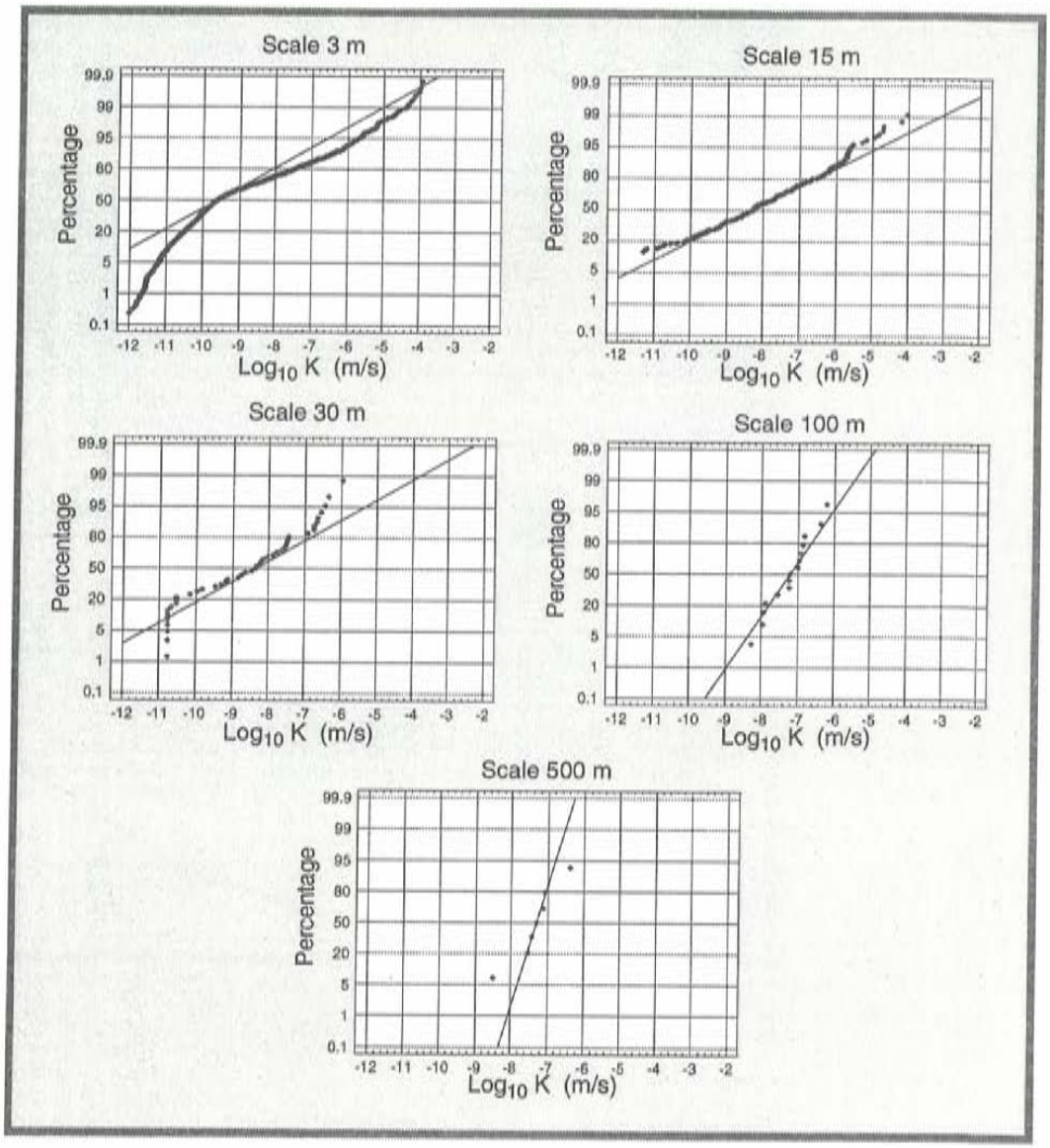

Figure 6-37. *Normal probability plot of $Log_{10}(K)$, where K=effective hydraulic conductivity in m/s, for different test scales and based on tests performed in boreholes drilled on Äspö. The 3 m tests are based on data from KAS02-08, 15 m tests from probeholes in the tunnel section 1400-3600 m, 30 m tests from KAS02-03, 100 m tests (test section length approximately 100 m) from KAS05-08 and 500 m tests from KAS02-08. Black line : Line through median value with slope according to the standard deviation.*

The empirical relationship between the test scale and hydraulic conductivity presented in *Wikberg et al /1991/* has been re-evaluated and the result is shown in *Figure 6-38* and *Table 6-13*. The arithmetic mean, geometric mean and standard deviation for each borehole are also shown in *Figure 6-38*. As injection tests with 3 and 30 m test scale were not performed in the uppermost 100 m, and in some cases the deepest part of core holes, the transmissivity for

the entire borehole was reduced with the estimated transmissivities for these sections. In a few cases the transmissivities for the tests performed on the 100 m scale was also reduced. The estimated transmissivities for the sections outside the range of interest were based on results from flow metre logging and tests performed on the 100 m scale. For each borehole the statistics for the effective hydraulic conductivity (K) was calculated for each test scale (effective hydraulic conductivity = transmissivity/length of tested section). The statistical measures were the mean of $Log_{10}(K)$ and the standard deviation of $Log_{10}(K)$.

Table 6-13. The linear relationship between Y and Log_{10} (scale). $Y = Log_{10}(K_a / K_{bh})$, $Log_{10}(K_g / K_{bh})$ $Log_{10}(K_a)$, $Log_{10}(K_g)$ or $s(Log_{10}(K))$. K = hydraulic conductivity (m/s), K_a = arithmetic mean, K_g = geometric mean, K_{bh} = effective hydraulic conductivity for the entire borehole, $s(Log_{10}(K))$ = standard deviation of $Log_{10}(K)$, Entire borehole length ≈ 500 m. $Y = a+b \cdot Log_{10}(scale)$. ρ = Correlation coefficient .

Y	a	b	ρ
$Log_{10}(K_a / K_{bh})$	1.184	-0.50	-0.70
$Log_{10}(K_g / K_{bh})$	-2.107	0.782	0.80
$Log_{10}(K_a)$	-6.119	-0.466	-0.59
$Log_{10}(K_g)$	-9.411	0.817	0.67
$s(Log_{10}(K))$	2.089	-0.758	-0.92

The mean of $Log_{10}(K)$ and the standard deviation of $Log_{10}(K)$ for a rock mass domain is given for a specified test scale (measurement scale) in this report. When generating the hydraulic conductivity field in a numerical Ground water flow model it is suggested that the cell size in the model should be used as the target scale to obtain the values of the statistical distribution to be used for generating the field. The following procedure for renormalisation of the hydraulic properties is suggested:

$$Log_{10} K_{it} = Log_{10}(K_{im}) + (Y_{it} - Y_{im}) \quad (6\text{-}7)$$

$$s_{st}(Log_{10}(K)) = s_{sm}(Log_{10}(K) \bullet (Y_{it}/Y_{im}) \quad (6\text{-}8)$$

index i: **g** (value representing **g**eometric mean of K), **a** (value representing **a**rithmetic mean of K) or **s** (standard deviation of $Log_{10}(K)$)

index m: value representing **m**easurement scale

index t: value representing target scale

Y_{im}: value according to equation for $Log_{10}(K_a/K_{bh})$, $Log_{10}(K_g/K_{bh})$ or $s(Log_{10}(K))$ in *Table 6-13* using the measurement scale.

Y_{it}: value according to equation for $Log_{10}(K_a/K_{bh})$, $Log_{10}(K_g/K_{bh})$ or $s(Log_{10}(K))$ in *Table 6-13* using the target scale

The reason for using a different formulation for the standard deviation is that the standard deviation may become negative if s_{sm} is low for a small measurement scale and the target scale is large. *Equation 6-8* is thus considered more robust. The formulation for K_g/K_{bh}should be used for the scale transformation to the target value for K_g.

The use of a linear relationship as suggested in *Figure 6-38* can be discussed. It is used because it was not considered justified to use a more complicated relationship. The linear relationship cannot be used for test scales larger than log_{10} scale ~2.7 ≈500 m, which is the maximum length of test section used in the individual boreholes. Possibly it should not be used for scales larger than about 200 m. As can be seen in the figures there is a spread of K_a and K_g values for test scale ≈500 m indicating a standard deviation that probably should be taken into account considering scaling of values for a site and not just a borehole. However, several other functions give about the same correlation coefficients as the linear fit and the functions can be made to converge asymptotically to the estimated values for the entire borehole. The difference will be larger correction for smaller test scale, (less than about 3 m) and smaller corrections for larger test scales (>3 m).

The statistics for the eight tests of the entire boreholes shown in *Figure 6-38*, with a test scale of about 500 m, are:

Median	:	K	=	$6.2 \cdot 10^{-8}$ m/s
Mean of $Log_{10}(K)$	:	K	=	$5.3 \cdot 10^{-8}$ m/s
Standard dev of $Log_{10}(K)$	:	$s(Log_{10}(K))$	=	0.60

These values are similar to the 100 m scale.

The scales effects are discussed in more detail in *Rhén et al /1997a/.*

The statistics for the rock mass domains SRD1-3 are shown in *Figures 6-39 to 6-44.* The data has been divided into two parts:

- zones - parts of the borehole where it is judged that the deterministically defined hydraulic conductors intersect the borehole.
- rock - parts of the borehole where it is judged that no deterministically defined hydraulic conductors intersect the borehole.

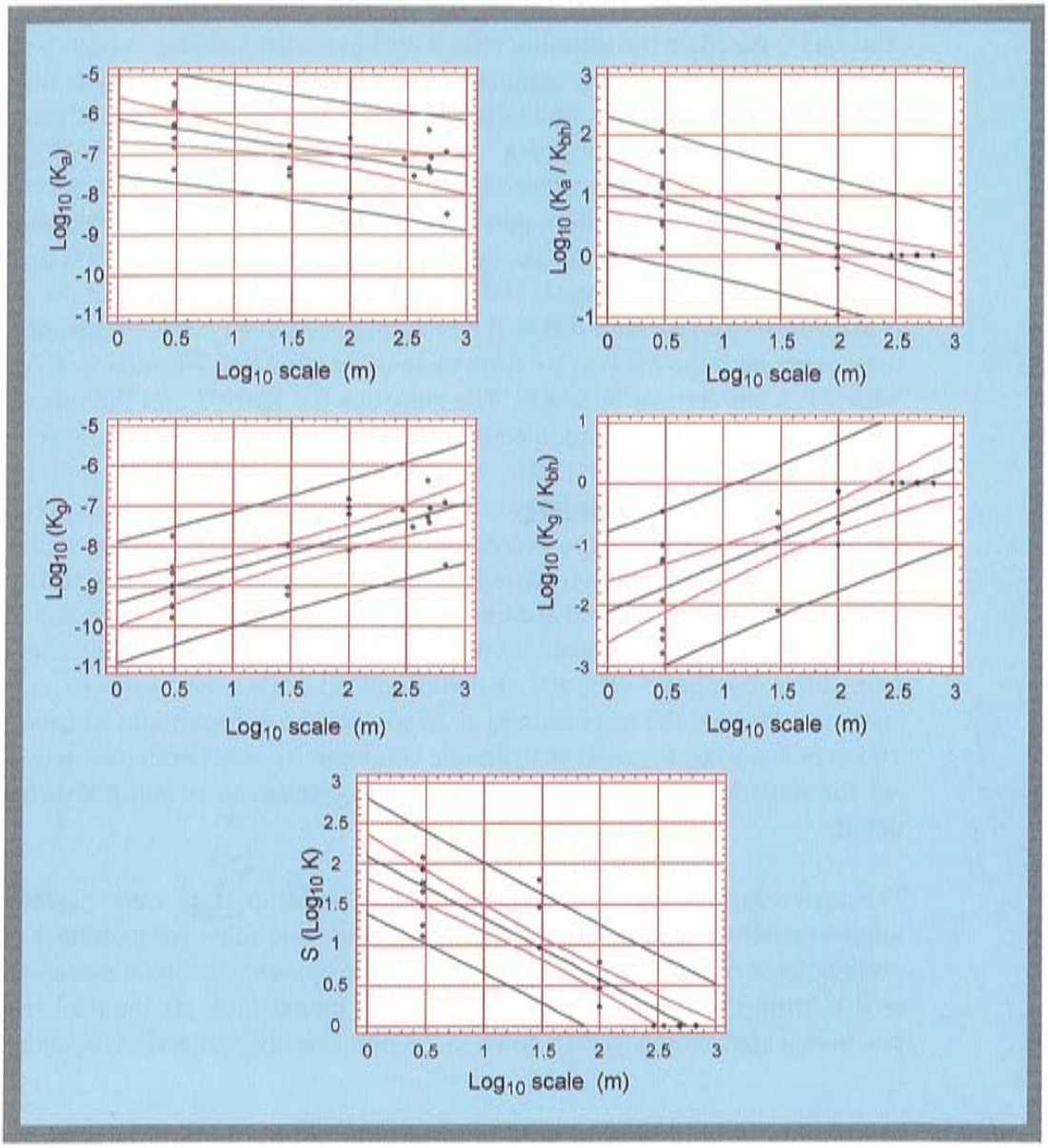

Figure 6-38. *Regression of Y versus Log_{10} (scale). Y = $Log_{10}(K_a/K_{bh})$, $Log_{10}(K_g/K_{bh})$, $Log_{10}(K_a)$, $Log_{10}(K_g)$, or s($Log_{10}(K)$). K = hydraulic conductivity (m/s), K_a = arithmetic mean K, K_g = geometric mean K. K_{bh} = mean K when entire borehole was tested, corrected according to test sections outside the range for other test scales. Scale = test section length in the borehole. The values of K_g and K_a for Log_{10} scale ≈2.5-3 are identical as they are the effective hydraulic conductivity for the entire borehole. The linear relation should not be used for test scales larger than log_{10} scale ~2.3 ≈200 m. Data are from the pre-investigation phase, including boreholes KLX01, KAS02-08. (Standard deviation was set to zero for the 'entire borehole' value as there is only one value for K_a and K_a).*

Middle line: *Mean of Y.*
Inner lines : *95 % confidence band on mean of Y.*
Outer most black lines : *95 % prediction band on Y as a function of Log_{10}(scale).*

The data is based on the injection tests with 3 m packer spacing. As can be seen in *Figures 6-39* to *6-44* the estimated mean hydraulic conductivity is highest within discontinuity EW-1 (data from KAS04) and lowest on the southern part of Äspö. The zonation for "rock" is questionable for boreholes KAS03 and KAS04 as the samples are rather small and only from a single borehole within each domain. On the southern part of Äspö the sample size for each zonation range is quite large except for the depth range 0-100 m and below 500 m. The measurements in depth range 0-100 m are from several boreholes but the depth is just somewhat less than 100 m. The estimate is probably rather relevant. The measurements below 500 m are from more or less one single borehole, KAS02, which is a subvertical borehole. The statistics for KAS02 and the other two subvertical boreholes, where injection tests with 3 m packer spacing were been performed, KAS05 and KLX01, have the lowest means for $Log_{10}(K)$ (see *Appendix A2*). The probable reason for this will be outlined below, but already here it can be stated that the decrease in hydraulic conductivity below 500 m in *Figure 6-42* should be considered uncertain. Statistics for injection tests with 30 m packer spacing were also compiled. These tests do not indicate any clear decrease in hydraulic conductivity with depth either, but data are only available from three boreholes (KAS02, KAS03 and KLX01) (see *Appendix A2* for statistics). Nor do the tests located at Äspö with the approximate test scale of 100 m indicate any decrease in hydraulic conductivity with depth (see *Appendix A2* for statistics). In *Rhén et al /1997a/* this discussion is outlined in more detail.

During construction of the tunnel pressure build-up tests were performed approximately every 16 m in two 20 m long boreholes (probeholes). The probeholes were drilled from 4 m in front of the tunnel face directed at an angle of 20° from the tunnel line and ahead of the tunnel face. As the packer was positioned approximately 5 m down in the borehole the test scale was about 15 m.

The additional data from the construction phase from the tests in probe holes indicate that the effective hydraulic conductivity is somewhat lower for the last spiral turn (below about -310 m) compared to the first spiral turn, see *Appendix 2*. However, due to large-scale heterogeneity and anisotropic conditions it is not considered possible to draw the conclusion that the hydraulic conductivity decreases down to a depth of 400-500 m based on the data presented above.

South of NE-1 few hydraulic tests were performed during the pre-investigation phase. Due to this, data from the probeholes was used to asign the properties to the rock mass domains south of NE-1 in the following way. Based on the geological documentation in the tunnel the tests in the probeholes were classified into four groups:

1 Mapped zone deterministically defined discontinuity (for example NE-1) according to *Chapter 3*
2 Mapped zone - according to the documentation manual for the tunnel
3 Increased fracturing
4 Rock - not mapped as 1, 2 or 3 as above, representing more or less intact rock.

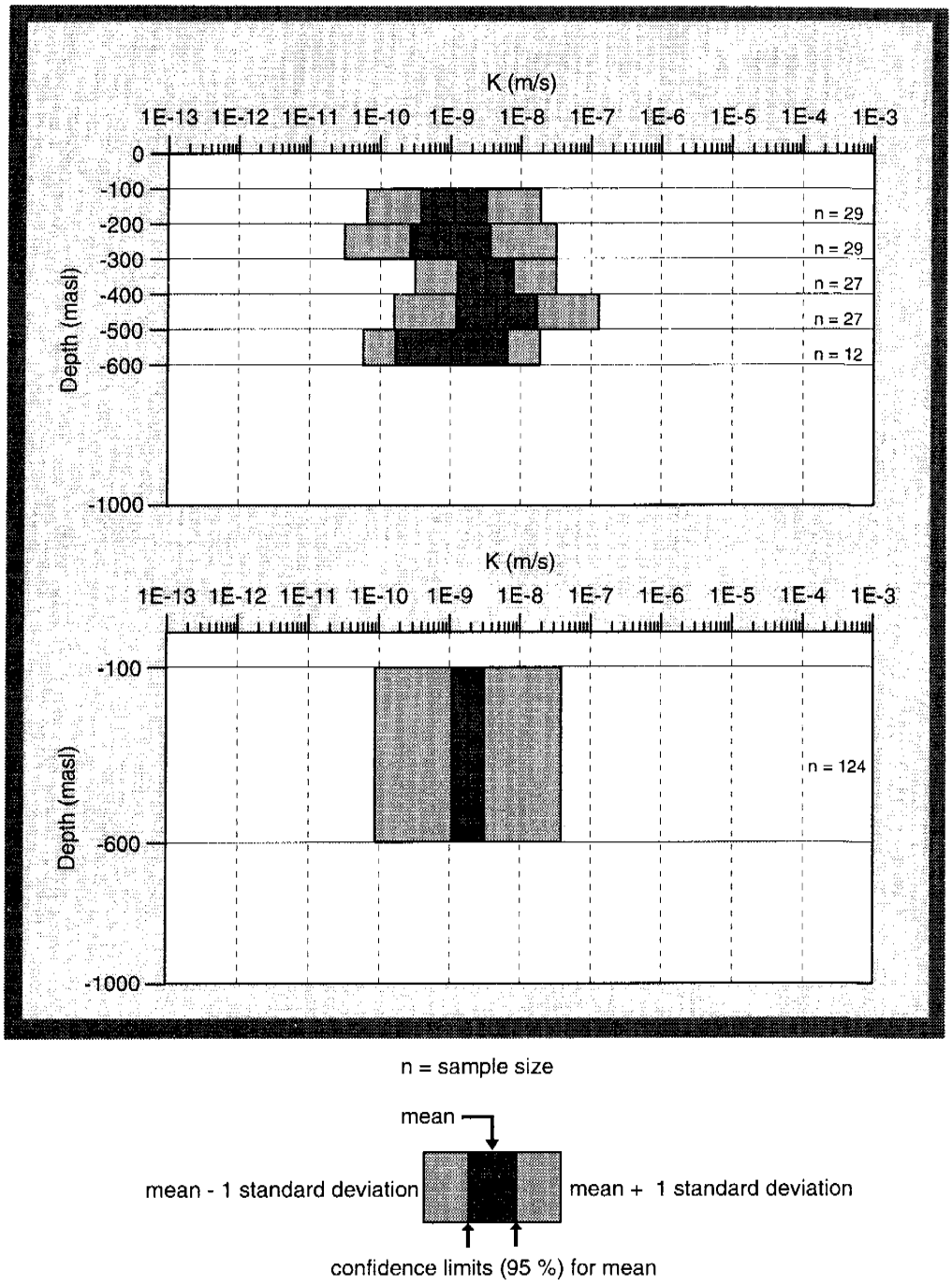

Figure 6-39. *Hydraulic conductivity (K) distribution on the site scale. Test scale 3 m. Statistics for "rock" in KAS03. (Northern part of Äspö, equal to SRD 1). (mean = arithmetic mean of $Log_{10}(K)$, standard deviation = Standard deviation of $Log_{10}(K)$, n = sample size).*
Top: Zonation, data = KAS03.
Bottom: Entire sample, data = KAS03.

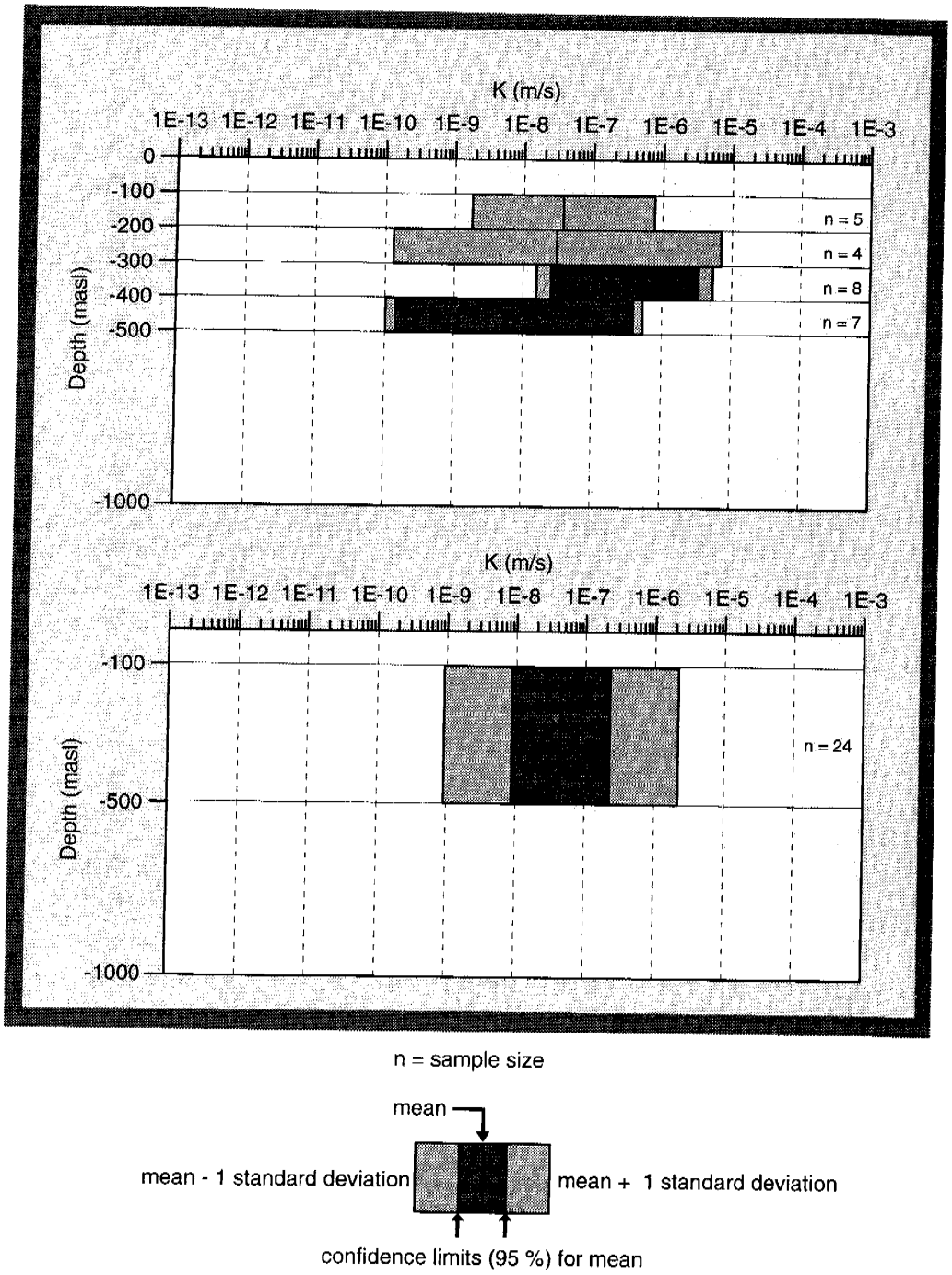

Figure 6-40. *Hydraulic conductivity (K) distribution on the site scale. Test scale 3 m. Statistics for "zone" in KAS03. (Northern part of Äspö). (mean = arithmetic mean of $Log_{10}(K)$, standard deviation = Standard deviation of $Log_{10}(K)$, n = sample size).*
Top: Zonation, data = KAS03.
Bottom: Entire sample, data = KAS03.

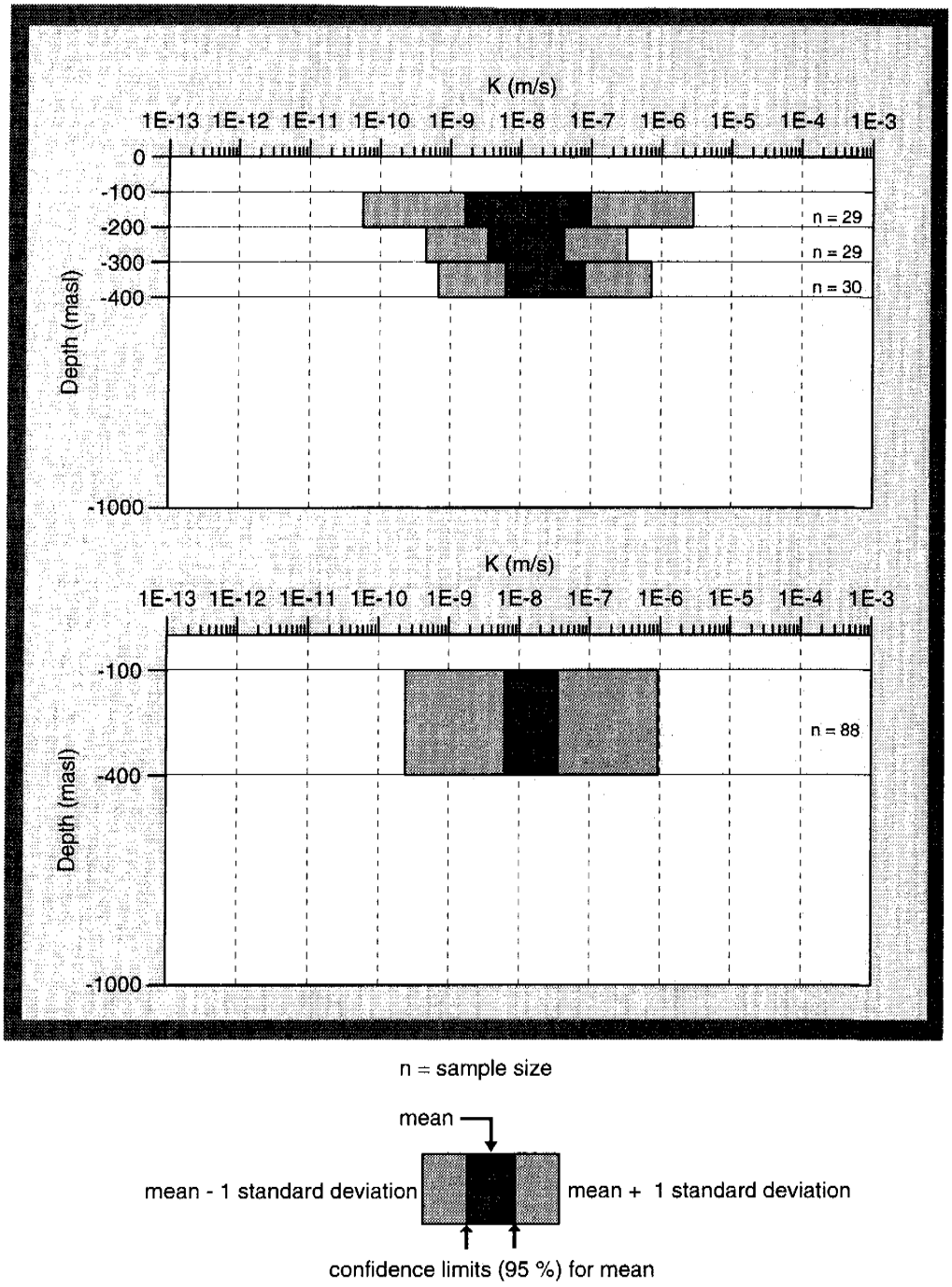

Figure 6-41. *Hydraulic conductivity (K) distribution on the site scale. Test scale 3 m. Statistics for "rock" in KAS04. (Äspö shear zone, equal to SRD 2). (mean = arithmetic mean of $Log_{10}(K)$, standard deviation = Standard deviation of $Log_{10}(K)$, n = sample size).*
Top: Zonation, data = KAS04.
Bottom: Entire sample, data = KAS04.

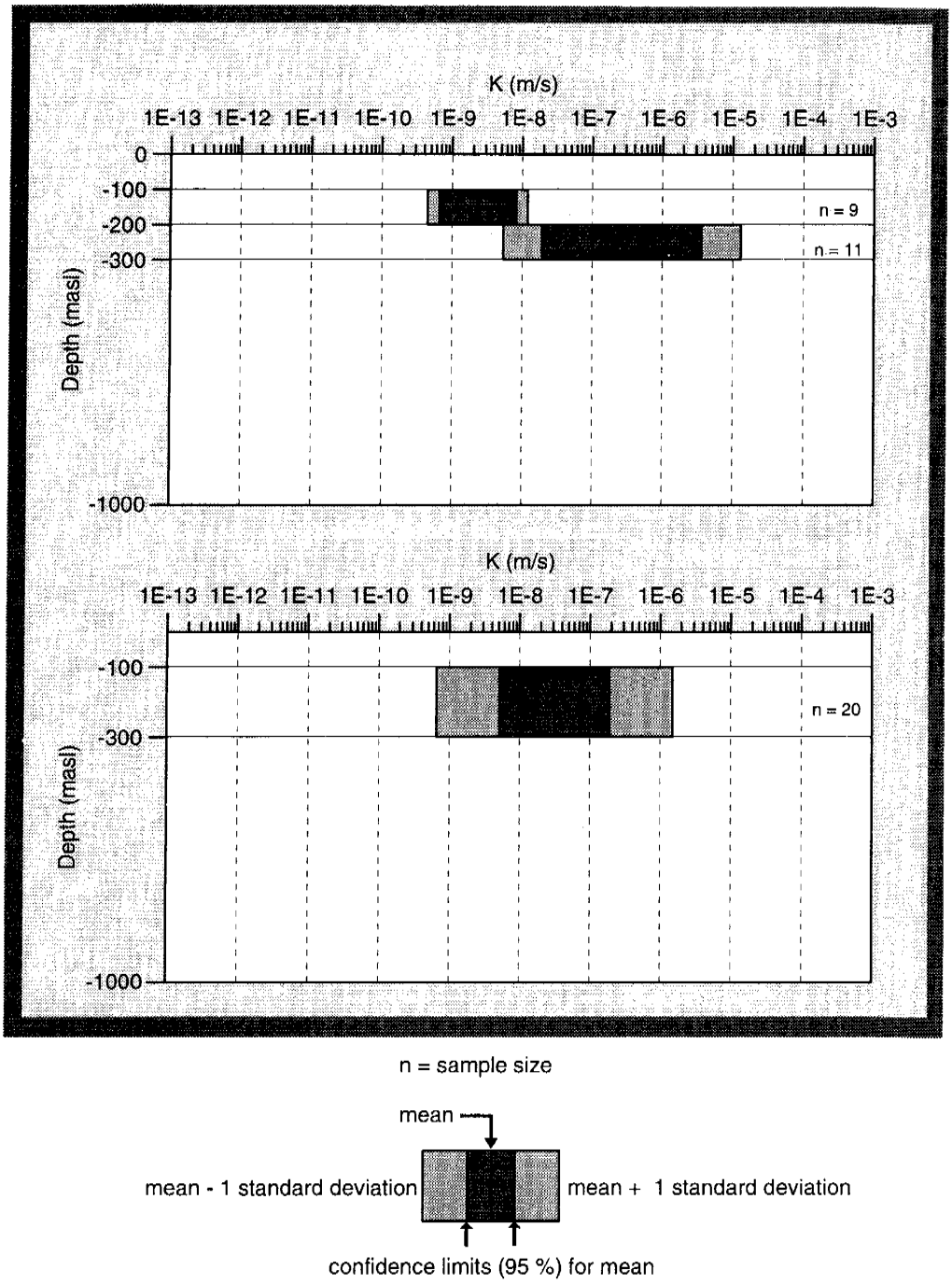

Figure 6-42. *Hydraulic conductivity (K) distribution on the site scale. Test scale 3 m. Statistics for "zone" in KAS04. (Äspö shear zone). (mean = arithmetic mean of Log_{10} (K), standard deviation = Standard deviation of Log_{10}(K) n = sample size).*
Top: Zonation, data = KAS04.
Bottom: Entire sample, data = KAS04.

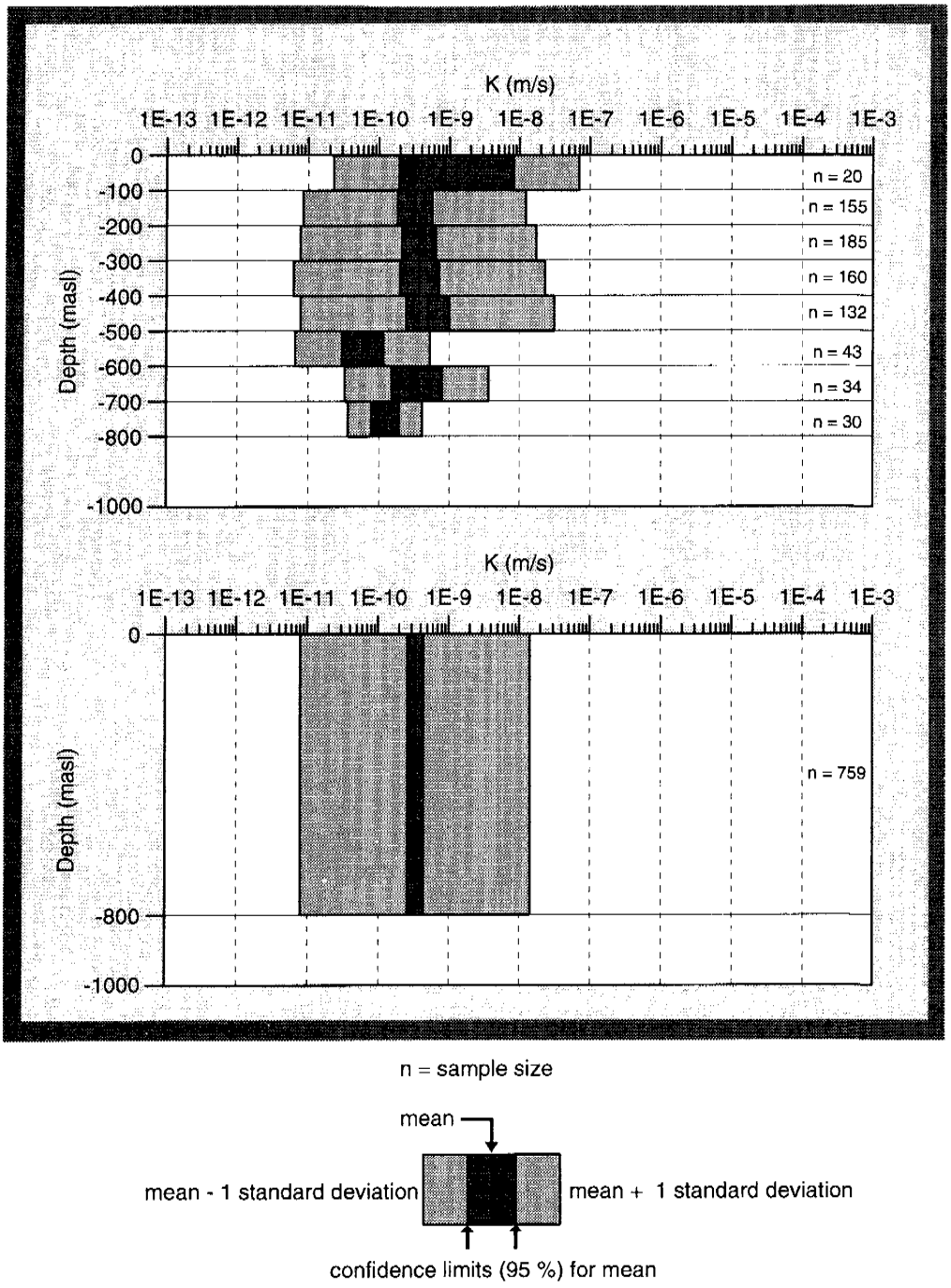

Figure 6-43. *Hydraulic conductivity (K) distribution on the site scale. Test scale 3 m. Statistics for "rock" on southern Äspö. Based on results from 5 cored boreholes. (Equal to SRD 3) (mean = arithmetic mean of $Log_{10}(K)$, standard deviation = Standard deviation of $Log_{10}(K)$, n = sample size).*
Top: Zonation, data = Southern Äspö.
Bottom: Entire sample, data = Southern Äspö.

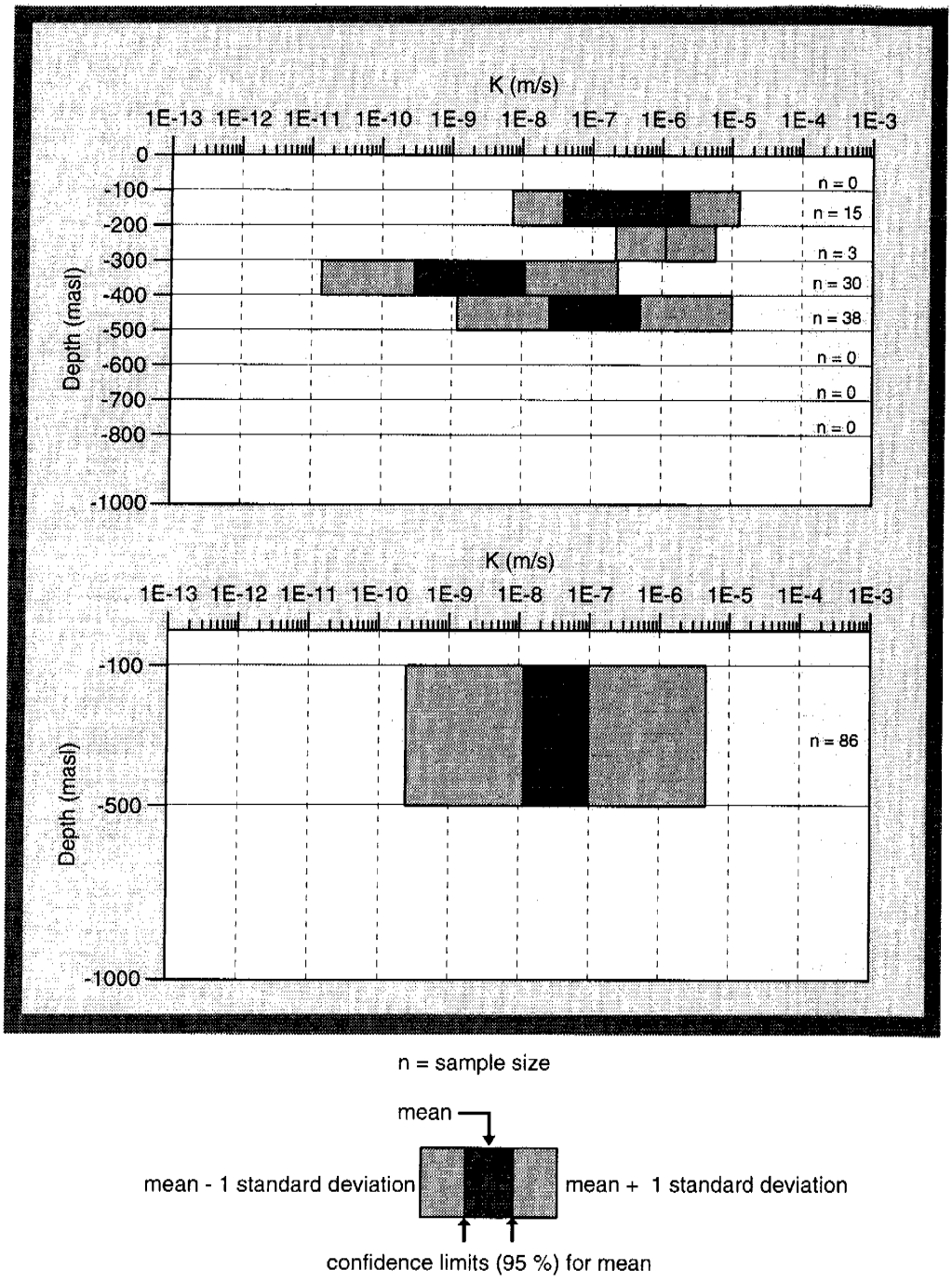

Figure 6-44. *Hydraulic conductivity (K) distribution on the site scale. Test scale 3 m. Statistics for "zone" on southern Äspö. Based on results from 5 cored boreholes. (mean = arithmetic mean of $Log_{10}(K)$, standard deviation = Standard deviation of $Log_{10}(K)$, n = sample size).*
Top: Zonation, data = Southern Äspö.
Bottom: Entire sample, data = Southern Äspö.

The test results for tunnel chainage 700-1400 m were divided into two groups:

- Mapped zone - deterministically defined discontinuity
- Other tests (groups 2, 3 and 4 above)

The statistics of "other tests" should be compared with "rock" for the injection tests with packer spacing 3 m. The statistics of "other tests" were used for the rock mass domain SRD4, see *Table 6-21*.

The tests performed in the cored boreholes from the ground surface are probably to some extent biased, at least the injection tests with the 3 m packer spacing, due to the fact that the boreholes are subvertical and that the main part of the water conducting fractures are subvertical, according to the investigation in the tunnel. An investigation of the structural geology of water-bearing fractures was made in the tunnel */Hermanson, 1995/*. It was found that the entire fracture system consists of five sets. The mapped water-bearing fractures and the fractures filled with grout (from the pre-grouting ahead of the tunnel face) are dominated by a subvertical fracture set striking WNW-NW. The N-S and NNW subvertical sets are also present but these subvertical sets are less pronounced compared with the entire fracture set (see *Figure 6-45*). *Figures 6-46, 6-47* and *6-48* show the mapped fractures, water-bearing fractures and fractures filled with grout for the first tunnel spiral. The relevance of the orientation of the mapped water-bearing fractures can be questioned as the zone closest to the tunnel wall is damaged to some extent by the excavation, giving increased fracturing and possibly a change in the hydraulic properties. However, the mapped grout-filled fractures should be a good indicator of the water conducting fractures, as the grouting was performed generally 5-15 m ahead of the tunnel face where the rock mass should be fairly undisturbed.

A mapping campaign of major larger water-bearing fractures in the spiral showed that all mapped fractures either had a substantial water inflow and/or grout and often gouge, brecciation or ductile precursors */Hermanson, 1995/*. They were not in any case classified as zones and their widths ranged from millimetres to centimetres. *Figure 6-49* shows the mapped fractures. The fractures shown were mainly subvertical. According to *Hermanson /1995/* the fault system trending NW and NNW generally appear as sub-planar fractures with a central water-bearing fault plane that often contains fault breccia and/or fault gouge as well as mineral assemblage.

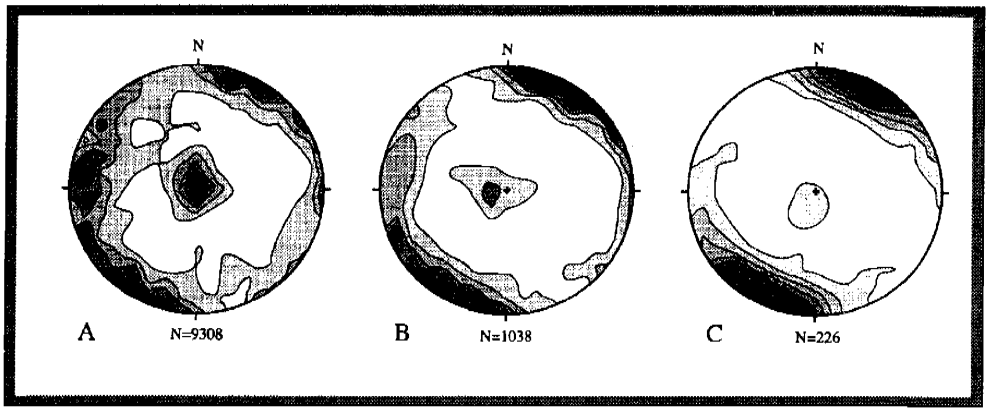

A : All fractures
B : Waterbearing fractures
C : Fractures filled with grout

Figure 6-45. *Schmidt nets with lower hemisphere projection of Kamb contoured poles to fracture planes. Contour interval 2.0 sigma. N = sample size. /Hermanson, 1995/.*

A: All fractures from 705 m to the end of the TBM tunnel, 3600 m. The plot shows five concentrations of fracture orientations, one sub-horizontal set, four steep sets striking N-S, NNW, WNW-NW and a comparatively less pronounced NE set.

B: Water-bearing fractures from the same part of the tunnel as A. The steep set striking WNW-NW is more pronounced compared with the same set in plot A. The other sets are less evident.

C: Fractures with grout from the same part of the tunnel as A. The plot is dominated by steep fractures striking WNW-NW. All other sets mentioned earlier are still visible, though not as pronounced as the WNW-NW set.

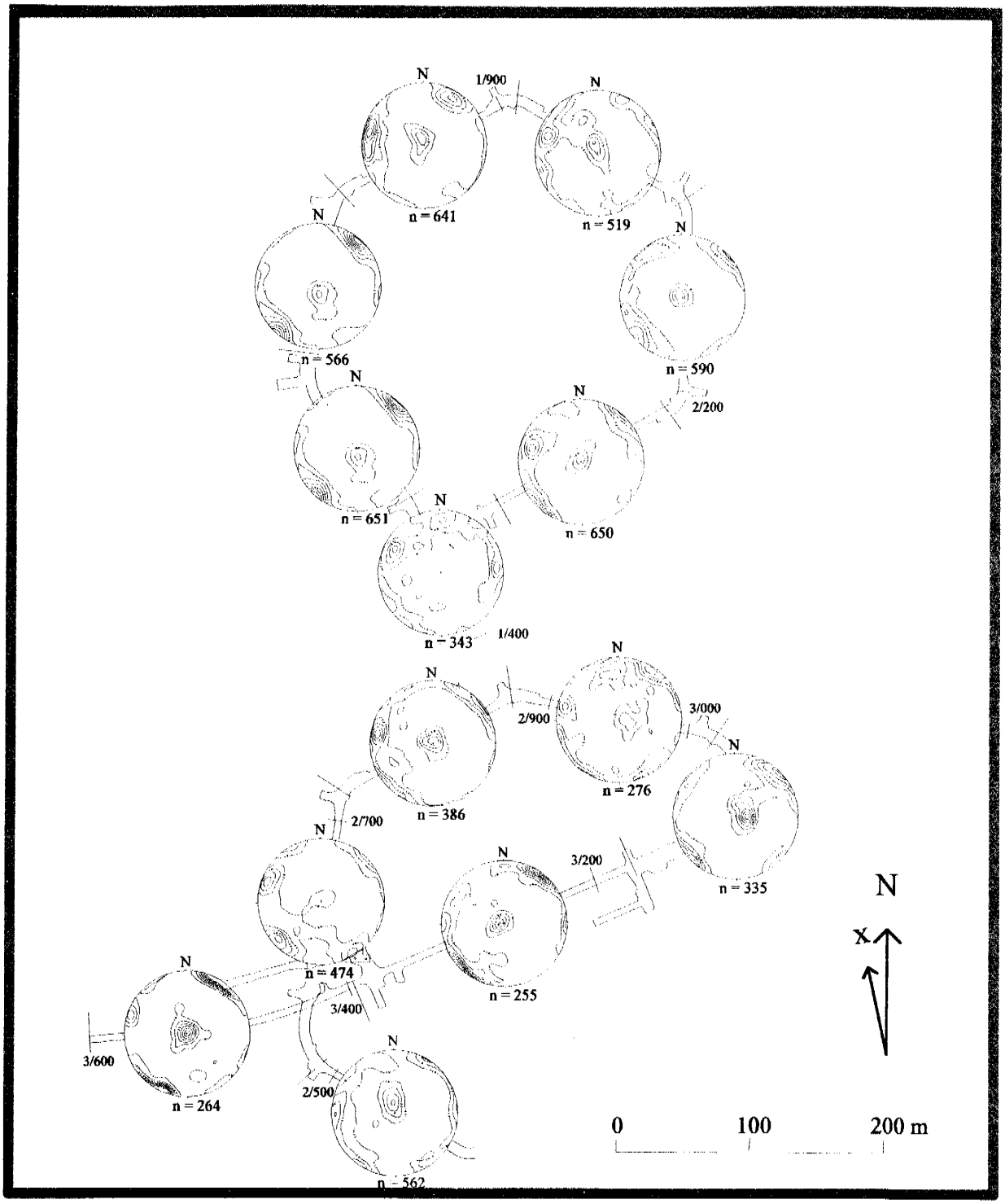

Figure 6-46. *All fractures plotted for sections of the tunnel. Stereonets have not been corrected for any orientation bias. Samples are from tunnel walls, tunnel roof and tunnel face (approximately every 4 m). n = sample size. N = Magnetic north, x = North in the Äspö coordinate system.*

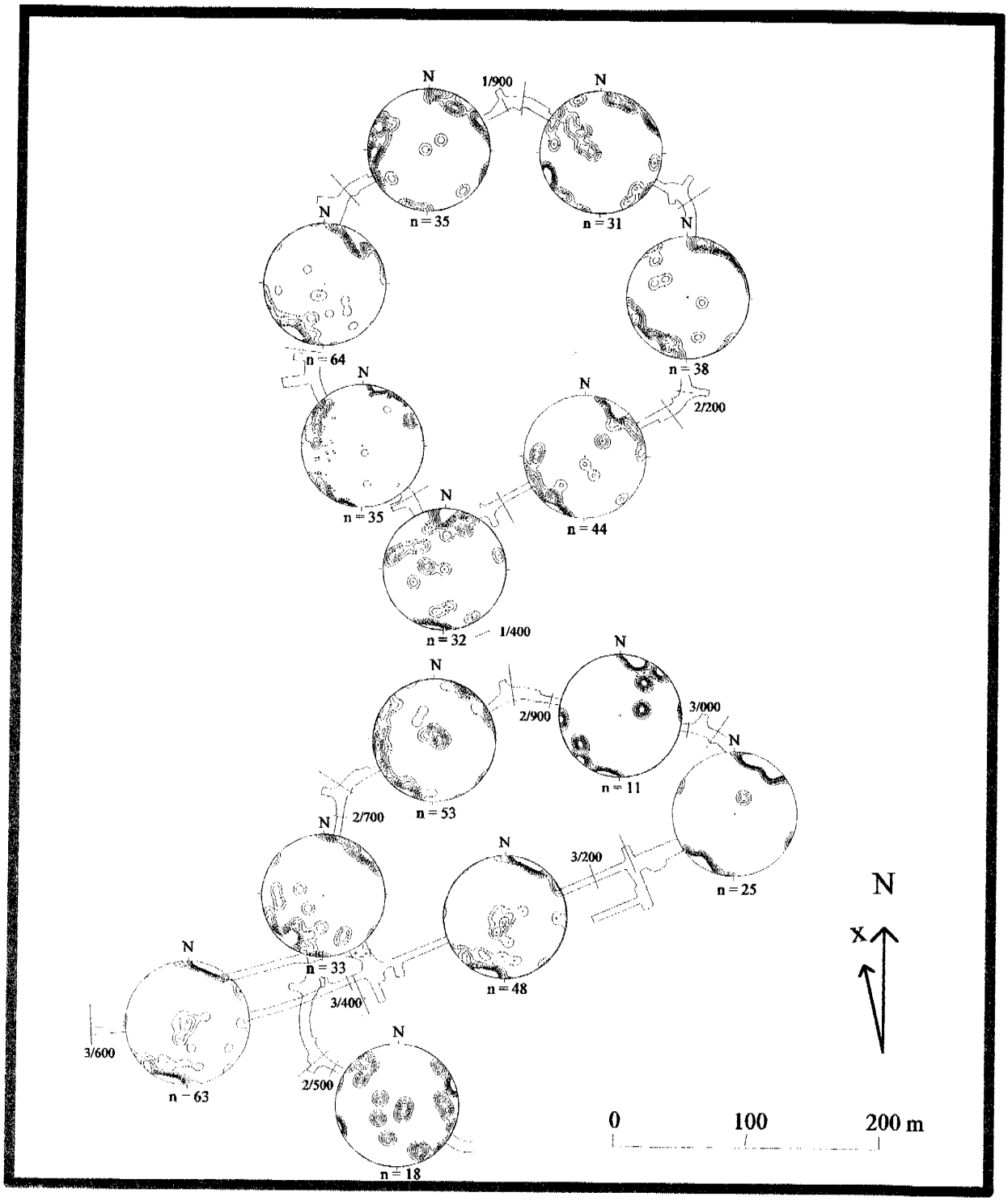

Figure 6-47. *Waterbearing fractures plotted for sections of the tunnel. Stereonets have not been corrected for any orientation bias. Samples are from tunnel walls, tunnel roof and tunnel face (approximately every 4 m). n = sample size. N = Magnetic north, x = North in the Äspö coordinate system.*

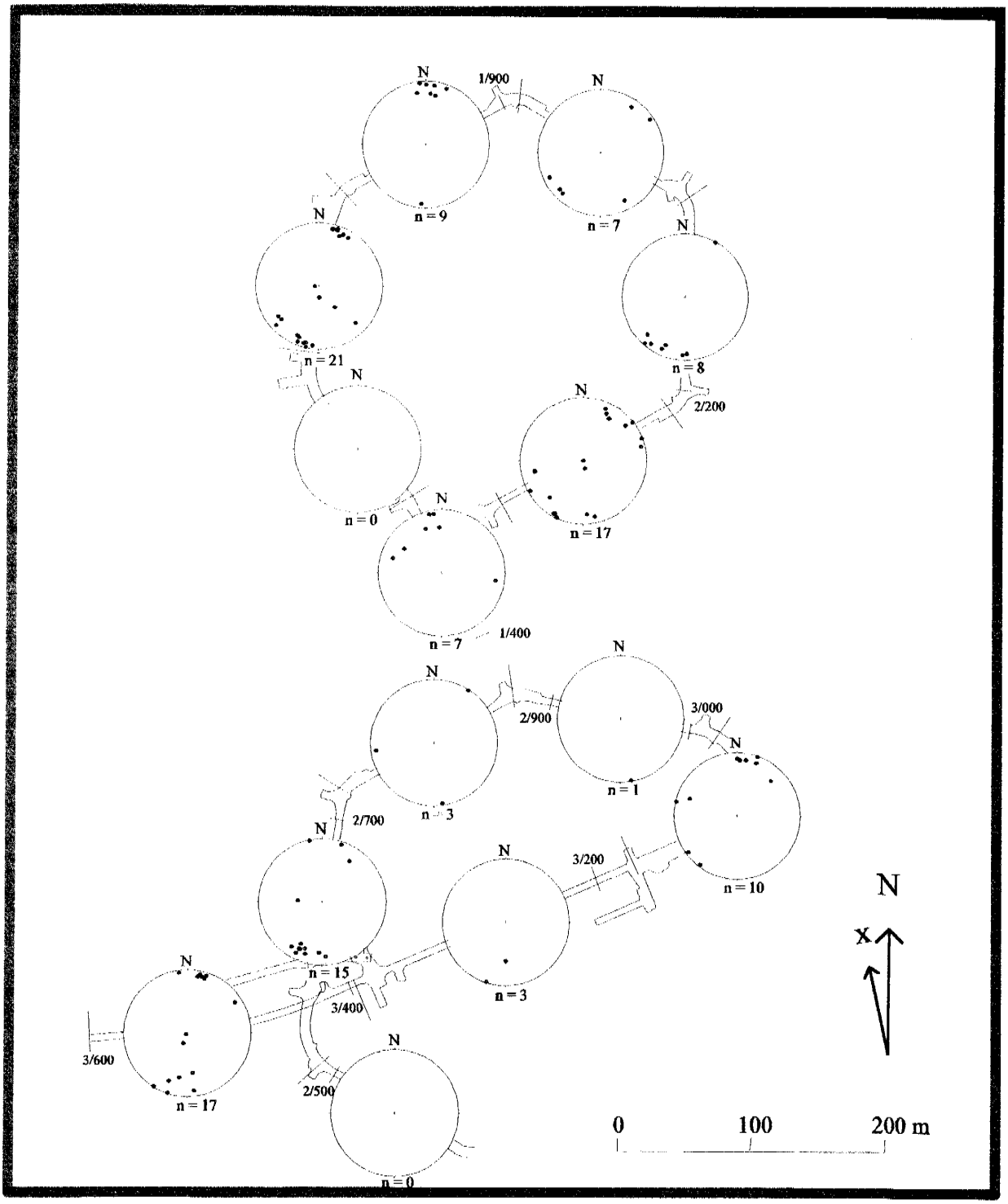

Figure 6-48. *Grouted fractures plotted for sections of the tunnel. Stereonets have not been corrected for any orientation bias. Samples are from tunnel walls, tunnel roof and tunnel face (approximately every 4 m). n = sample size. N = Magnetic north, x = North in the Äspö coordinate system.*

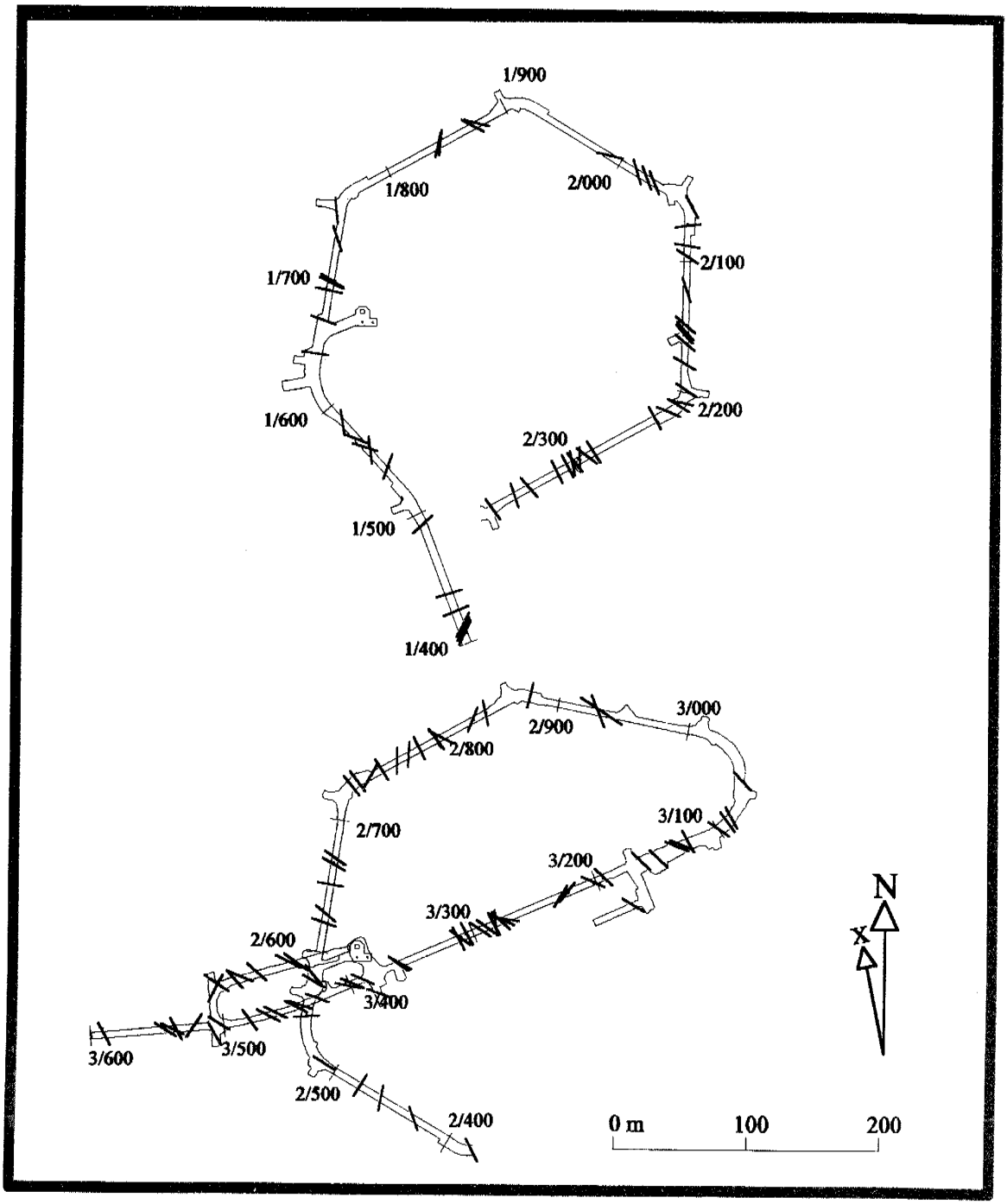

Figure 6-49. *Mapped large, single, open, water-bearing fractures in the tunnel. The fractures are mainly subvertical. N = Magnetic north, x = North in the Äspö coordinate system.*

Data from tests performed in the probeholes for tunnel Section 1400-3600 m were analysed to see if the hydraulic properties varied in different directions. The results are shown in *Figure 6-50* and in *Appendix A2*. The estimated transmissivity for each borehole is assumed to mainly represent planar features

that are more or less perpendicular to the borehole. As can be seen in *Figure 6-50* (with the above assumption) the fractures with a strike of around NW are more transmissive compared with fractures with strike of NE. This may seem contradictory to the results from the interference tests where a number of conductive features called NNW with a strike of approximately N35°W. The reason is that the number of NW fractures is greater than the number of N-S fractures, and as the test time is short compared with the interference tests, the tests in the probe holes are probably dominated by the conductive NW fractures. At longer test time the fewer, but probably greater and possibly more conductive N-S fractures and the NW fractures make a "fracture swarm" which in the interference tests is seen as a large conductive feature with strike around N35°W. However, in *Figure 6-50* the presence of possible high transmissive N-S features can also clearly be seen.

In order to see if there were any different results for a subhorizontal plane the data from the cored boreholes in the tunnel spiral area were analysed. Data from KAS 02, 05-08 depth interval -200 to -500 m were used. Most of the cored boreholes on southern Äspö are at a plunge of 60° and the average plunge of KAS02 and 05 is about 85°. However, the injection tests available were performed with a packer spacing of 3 m. In order to permit comparison with the measurements in the probe holes the transmissivities (T) were estimated as the sum of T values for 3 m sections. The sum was then slightly reduced depending on the way in which the arithmetic mean value of hydraulic conductivity is expected to decrease (see *Figure 6-38*). This was made for different scales (see *Table 6-14*).

The results indicate that the hydraulic properties in the 10-20 m scale are anisotropic. The results are summarized in *Table 6-15*. It should be remembered that the data in *Figure 6-50* and *Tables 6-14* and *6-15* are based on all data, including fracture zones. The results should also be regarded as an approximate relation as the testing methods were different.

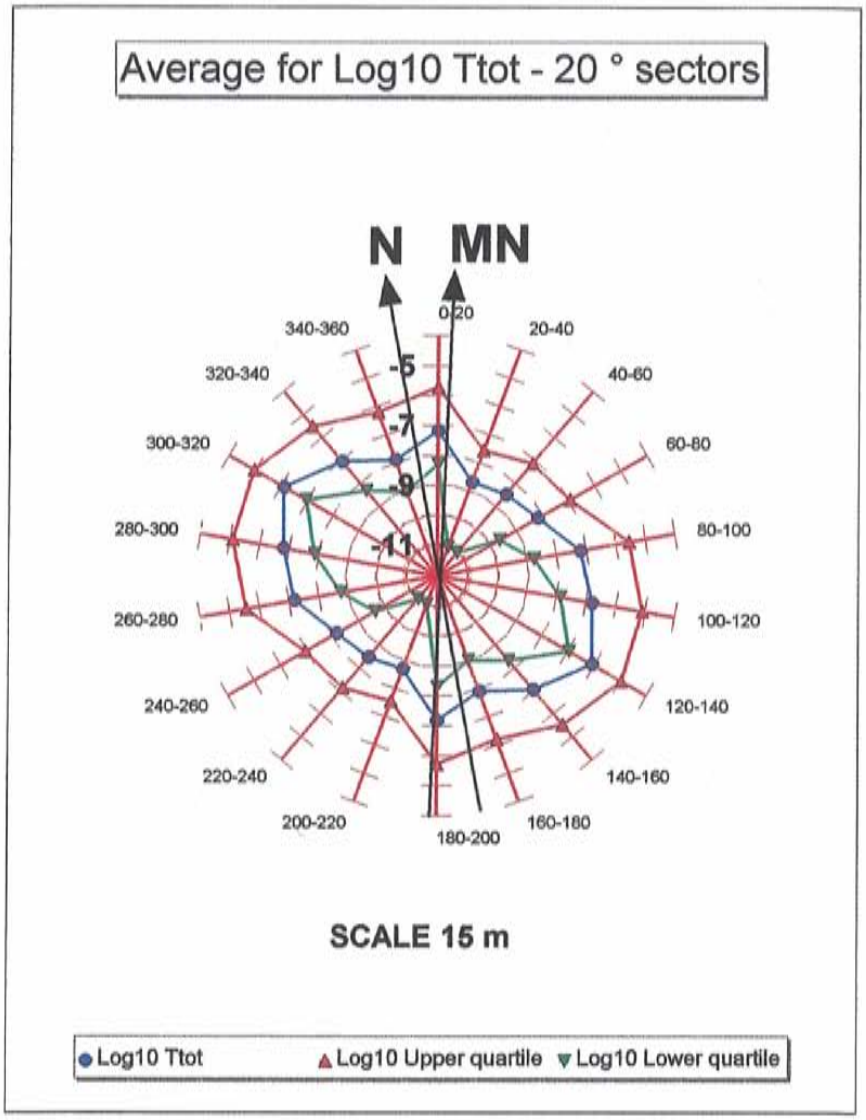

Figure 6-50. *Estimated transmissivities (T) for different directions according to the Äspö coordinate system in the spiral of the Äspö HRL. The direction is given as the strike of a plane perpendicular to the borehole. Data : probe holes in tunnel section 1400-3600 m. The points in the figure represents arithmetic mean, upper quartile and lower quartile of Log_{10} (T) for planes within a 20° sector in the horizontal plane. The points are in the middle of the sector and the directions of the sector is given for the Äspö coordinate system. N = North for the Äspö coordinate system. MN = Magnetic North. Scale 15 m = Length of test section is 15 m.*

Table 6-14. Statistic for $Log_{10}(T)$ for evaluated transmissivities (3 m scale) and estimated transmissivities (scales 9, 15, 24 and 30 m). Data: cored boreholes KAS02, 05, 06, 07, 08 for depth -200 to -500 m. (Scale = test length, m = arithmetic mean of $Log_{10}(T)$, s = standard deviation, n = sample size).

Scale (m)	n	m (m^2/s)	Median m^2/s)	s(Log10 T) (-)	Up.Quart. (m^2/s)	Low. Quart. (m^2/s)
3	548	2.0E-09	4.1E-10	1.90	5.0E-08	6.8E-11
9	181	2.0E-08	9.2E-09	1.91	1.2E-06	4.3E-10
15	108	5.3E-08	1.0E-07	1.86	2.4E-06	8.7E-10
24	66	1.6E-07	5.9E-07	1.77	4.3E-06	2.0E-09
30	53	1.8E-07	5.4E-07	1.80	4.5E-06	2.0E-09

Table 6-15. Estimates of transmissivities in different directions within the tunnel spiral at the Äspö HRL.

Probe holes **Strike of plane perpendicular to the probe hole directions** **(°) (Äspö coordinate system)**	**Scale** **(m)**	**T** **(m^2/s)**
120-140	15	$8 \cdot 10^{-7}$
20 - 80	15	$4.5 \cdot 10^{-9}$
Cored boreholes **Direction of plane perpendicular to the probe hole directions**	**Scale** **(m)**	**T** **(m^2/s)**
≈Horizontal	15	$5 \cdot 10^{-8}$

Laboratory tests of the permeability (k) of rock cores and also hydraulic tests in boreholes on the 5 cm scale indicate that more or less unfractured rock at Äspö has a k value of about $10^{-20} - 10^{-19}$ m^2 */Olsson et al, 1996/*. Some of the tests were re-evaluated spring 1997 and the evaluation indicated that the permeability should be about 10 times higher than reported in *Olsson et al*

/1996/. Equation 6-9 expresses the relationship between the hydraulic conductivity and permeability:

$$K = \frac{k \cdot \varrho \cdot g}{\mu} \qquad (6\text{-}9)$$

K	=	Hydraulic conductivity	(m/s)
k	=	Permeability	(m^2)
μ	=	Dynamic viscosity	(Pa s)
ϱ	=	Density	(kg/m^3)
g	=	Gravitational force	(m/s^2)

ϱ and μ are dependent on the temperature, and an example is given below in *Table 6-16*. Considering the values in *Table 6-16* a lower limit of the hydraulic conductivity at small scales – metre or so – should be around $K = 10^{-11}$ - 10^{-12} m/s.

Table 6-16. Example of how temperature affects the relationship between the hydraulic conductivity (K) and permeability (k).

T (°C)	$\frac{\varrho \cdot g}{\mu}$ (1/(ms))
10	$0.75 \cdot 10^7$
20	$0.98 \cdot 10^7$
30	$1.22 \cdot 10^7$
40	$1.49 \cdot 10^7$

The temperature has only a minor influence on the evaluated hydraulic properties if the natural temperature gradient (about 15°C per km, */Sundberg, 1991/)* and a depth down to around 1000 m are considered. The salinity has even less influence on the viscosity, at least down to a depth of 1000 m at Äspö, as the salinity is less than 2% down to that depth, */Earlougher, 1977/.*

Specific storage

There are very few interference tests at Äspö HRL that are judged to be useful for direct evaluation of the specific storage (S_s) of a hydraulic rock mass domain. The reason is that the distance between the observation sections are comparatively long. However, a reasonable lower limit can be estimated from the measurements of the Young's modulus of intact rock (E_i). As can be seen

in *Table 6-18* an approximate value of S_s with E_l =80 Gpa and a Poisson's ratio of 0.2 and a porosity = 0-0.05 is around 10^{-7} m^{-1}. This value, and the lower limit of the hydraulic conductivity (K) =10^{-12} m/s discussed above in the text, are supposed to be representative of the more or less intact rock.

In order to obtain an approximate estimate of S_s the interference tests performed on southern Äspö, excluding tests where NE-1 was intersected by the pumped borehole, were evaluated. The observation sections were both in the defined hydraulic conductor domains and in the rock mass outside the conductor domains. The greatest number of observations were in the rock mass outside the conductor domains. Up to about 80 observation sections were used in the evaluated tests. The test scale (length of the pumped borehole section) was approximately 500 m and the distances to the observation sections were in most cases less than the test scale. Due to this one should expect that the flow field around the borehole should be more or less radial some 100 metres from the pumped borehole. The evaluation of the distance-drawdown plots at the end of the pumping, after approximately 3 days, assuming radial or spherical flow field gives a range for S_s for the evaluated effective hydraulic conductivity (K). K was estimated as the evaluated transmissivity divided by the length of the borehole for the radial flow assumption. The evaluation made should give reasonable, but of course approximative, estimates of the relation between K and S_s in 500 metres test scale . The mean of the evaluated S_s and K are shown in *Figure 6-51.* The points in the figure represent the entire rock mass including the hydraulic conductor domains. (The maximum values of S_s are about 10 times greater than the minimum estimates.)

The relationship between Log_{10} (K) and Log_{10} (S_s) is in *Figure 6-51* approximated to a power law relationship, which is also presented in *Table 6-17.*

Table 6-17. The linear relationship between $Log_{10}(K)$ and $Log_{10}(S_s)$ in *Figure 6-50*. $S_s = a \cdot K^b$. n = sample size.

a	b	n
$6.037 \cdot 10^{-5}$	0.2312	3

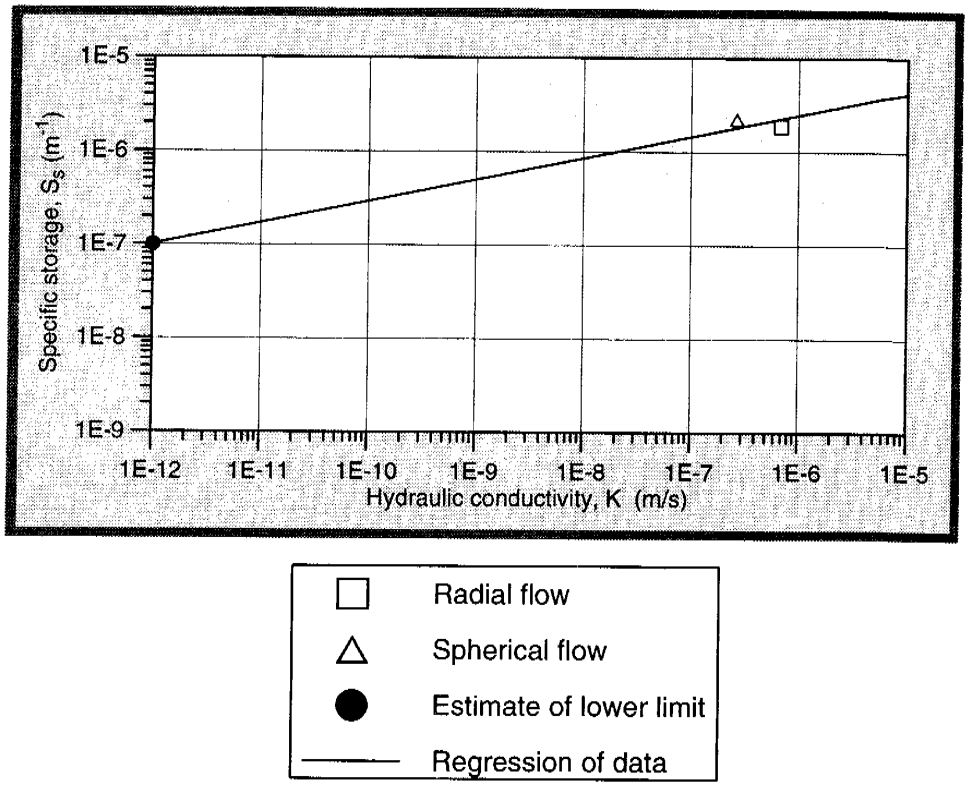

Figure 6-51. *The relationship between $Log_{10}(K)$ and $Log_{10}(S_s)$ evaluated from interference tests in hydraulic conductors. Test scale approximately 100 m.*

Based on *Equations 6-2* to *6-6* the RMR values along the tunnel were used to estimate S_s (see *Table 6-18*). *Table 6-18* shows that the specific storage for the entire rock mass should be in the range 10^{-6} m^{-1}, which compares rather well with *Figure 6-51*. RMR values for the tunnel below the sea are somewhat lower than shown in *Table 6-18*, giving somewhat higher S_s values.

Table 6-18. Estimate of the deformation modulus (E_d), compressibility of porous medium (bulk)(α_b) and specific storage (S_s) based on RMR estimates for tunnel chainage 1400-3600 m. The probability distribution of RMR for each "Type"is of more or less perfectly normal distribution. Type = characterization of tunnel walls: zone, increased fracturing and rock (= not zone or increased fracturing), tot. samp. = total sample including zones, Cd = Cumulative density, n = Porosity, ν = 0.2. (Temperature = 15°C for estimating the fluid density and coefficient of compressibility of water.)

Type	Cd (%)	RMR	E_d (Gpa)	α_b (Pa^{-1})	S_s n=0 (m^{-1})	S_s n=0.05 (m^{-1})
incr.fr	5	36	4	4.0E-10	4.0E-6	4.2E-6
incr.fr	50	55	13	1.4E-10	1.3E-6	1.6E-6
incr.fr	95	75	40	4.5E-11	4.5E-7	6.7E-7
rock	5	58	16	1.1E-10	1.1E-6	1.3E-6
rock	50	70	32	5.7E-11	5.6E-7	7.9E-7
rock	95	84	54	3.3E-11	3.3E-7	5.6E-7
tot.samp	5	48	9	2.0E-10	2.0E-6	2.2E-6
tot.samp	50	68	28	6.4E-11	6.3E-7	8.6E-7
tot.samp	95	83	53	3.4E-11	3.4E-7	5.7E-7
		100	80	2.3E-11	2.2E-7	4.5E-7

Spatial assignment method

Hydraulic conductivity

The spatial correlation between the available data points within the site model area has been evaluated in several studies. *Liedholm /1991a/* evaluated the auto correlation structure of the injection data in KAS02-08, based on tests with 3 m packer spacing. He concluded that the significant ranges at which the data were correlated along the boreholes were less than 6 m in boreholes KAS03-06 and 18 m to 30 m in KAS02, 07 and 08. Trend corrections did not usually have any effect.

Niemi /1995/ analysed the same data from the pre-investigation phase as in *Liedholm /1991a/*. She fitted variogram models to find the correlation structure along the boreholes. The result is shown in *Table 6-19*. As can be seen in *Table 6-19* the range is greater than was found by *Liedholm /1991a/*. The difference is, however, an artifact as *Liedholm /1991a/* defined the range where there was a statistically significant correlation, while in *Niemi /1995/* the range was defined as the range used in the variograms.

The spatial correlation was evaluated in *La Point /1994/*. The conclusion from the evaluation of injection tests with 3 m packer spacing was that the sample could be described as a single population and that no greater significant trends were present. The spatial correlation in 3-D indicated a nugget effect of about 60% of the observed variance. The model considered to perform most accurately was a model with Nugget + Spherical model (short range) + Exponential model (long range), data according to *Table 6-20*. The difference, however, was considered to be small between the different models.

Table 6-19. Models and model parameters for variograms of $Log_{10}(K)$, (K: (m/s)). /Niemi, 1995/.

Borehole	Model	Nugget C_0	Sill C_1	Range a_1 (m)
KAS02	Gaussian[1]	1.9	3.0	50
KAS03	Exponential[2]	2.0	3.2	20
KAS04	Exponential[2]	4.0	5.6	20
KAS05	Exponential[2]	1.8	2.9	17
KAS06	Exponential[2]	2.7	4.7	14
KAS07	Gaussian[1]	1.7	2.6	56
KAS08	Gaussian[1]	1.5	2.6	65
KLX01	Exponential[2]	1.2	1.9	20

[1] $\gamma(h)=C_0+ C_1\cdot(1-\exp(-(h/a))$
[2] $\gamma(h)=C_0+ C_1\cdot(1-\exp(-(h/a)^2)$
Gaussian model: $a^1=a\cdot(3)^{0.5}$
Exponential model: $a^1=a\cdot3$
h= length of lag vector **h**

Table 6-20. Models and model parameters for variograms of $Log_{10}(K)$, (K: (m/s)). Data below the measurement limits defined in the evaluation shown in the original report for the injection tests, was excluded in the analysis and thus reducing the total variance compared to the total sample *[La Point, 1994]*.

Borehole	Model 1	Nugget C_0	Sill C_1	Range a_1 (m)	Model 2	Sill C_2	Range a_2 (m)
KAS02-08	Spher.[1]	1.251	0.683	50	Spher.[1]	0.211	200
KAS02-08	Spher.[1]	1.252	0.680	50	Expon.[2]	0.298	200
KAS02-08	Spher.[1]	1.445	0.765	70			
KAS02-08	Expon.[2]	1.487	0.951	200			

[1] Spherical model
[2] Exponential model

The evaluated correlation ranges are around 20 to 70 m and the modellers assumed that isotropic conditions prevailed. However, the hydraulic conditions at the Äspö HRL are anisotropic and the correlation ranges may be different in different directions. The correlation range is fairly short compared with the cell size in the numerical model and, what is more important, the nuggets in the variogram models are large (generally about 60% of the total variance). The assumption of no correlation between the 20 • 20 • 20 m cells on the site scale numerical models seems justified, based on the correlation models mentioned above.

As a base case it is suggested that no spatial correlation is assumed and that the data used in a stochastic continuum model are scaled according to *Table 6-13*. The suggested properties for the population are shown in *Table 6-21*. The hydraulic conductivity is assumed to be of lognormal distribution. The effective hydraulic conductivity for domains SRD1-3 are based on the evaluated properties from the injection tests with 3 m packer spacing (see *Appendix A2*).

Considering the discussion in *Section 6.3.3 SRD2* should be modelled as an anisotropic feature with an average hydraulic conductivity that is less in the N-S direction than in the E-W direction. The values given probably represent the E-W direction. Values for the N-S direction has to be calibrated.

As there are no packer tests in the domain SRD4 the evaluated properties are based on tests in probe holes, excluding the deterministically defined hydraulic conductors, for tunnel chainage 700-1475 m.

There are no injection tests with 3 m packer spacing below a depth of 800 m on southern Äspö, 400 m in the Äspö shear zone and 600 m on northern Äspö,

and there are only a limited number of tests below 800 m in the entire area around Äspö. It is therefore suggested that the properties given in the regional model for depths below 600 m be used (see *Chapter 6.2* and *Appendix A2*).

At a depth of approximately 300 m within the tunnel spiral there is probably a larger body or a number bodies of fine-grained granite, according to *Chapter 4*. As the effective hydraulic conductivity is higher compared to other lithological units (see *Chapter 6.5*) it is suggested that the volume of the fine-grained granite is a domain, SRD5. Based on the results from the simulation with the Bayesian Markov Geo-statistical Model (Bay Mar) mentioned in *Chapter 4* the domain is approximated to an elliptical body 150 m long with its main axis in the E-W direction. The lengths of the minor axes are estimated to be 0.5 of the main axis length. The centre is estimated to be at a depth of 350 m and in the centre of the spiral. The volume and shape of the domain should be considered uncertain.

Table 6-21. Site scale hydraulic Rock mass Domain (SRD). Hydraulic conductivity - Spatial assignment method. d_b = depth to bottom level of numerical model, scale = test length, m = arithmetic mean of $Log_{10}(K)$, s = standard deviation of $Log_{10}(K)$.

Group of domains	Depth range (m)	Scale (m)	m(Log_{10}(K)) Log_{10}(m/s)	s(Log_{10}(K)) (-)	Comment
SRD1	0-600	3	-8.74	1.32	KAS03-"rock"
SRD2	0-600	3	-7.82	1.79	KAS04-"rock"
SRD3	0-600	3	-9.47	1.63	KAS02,05-08-"rock"
SRD4	0-600	15	-6.46	1.61	Probe holes-700-1475 m
SRD1-4	600-d_b	300	-7.33	0.72	Acc to regional model
SRD5	See text	3	-8.32	1.99	Fine-grained granite

However, there is most likely too little correlation in the stochastic model without any correlation structure for features with higher transmissivities when cell sizes in the numerical model are tens of metres or less with the modelling approach used so far. The radius of influence for a specific test depends on the hydraulic properties around the borehole. So far, the radius of influence has just been estimated roughly using the test section length as an indication of mean influence radius. Using the suggested relationships between hydraulic conductivity and specific storativity shown in *Table 6-17* the arithmetic mean influence radius is about 6, 22, 17 and 62 m for test scales 3, 15, 30 and 100 m respectively, using the simple approach of radial flow (see *Figure 6-52).* (Total test time was used if no upper time for the evaluation period was given.) The values above and in *Figure 6-52* should be seen as indications of influence

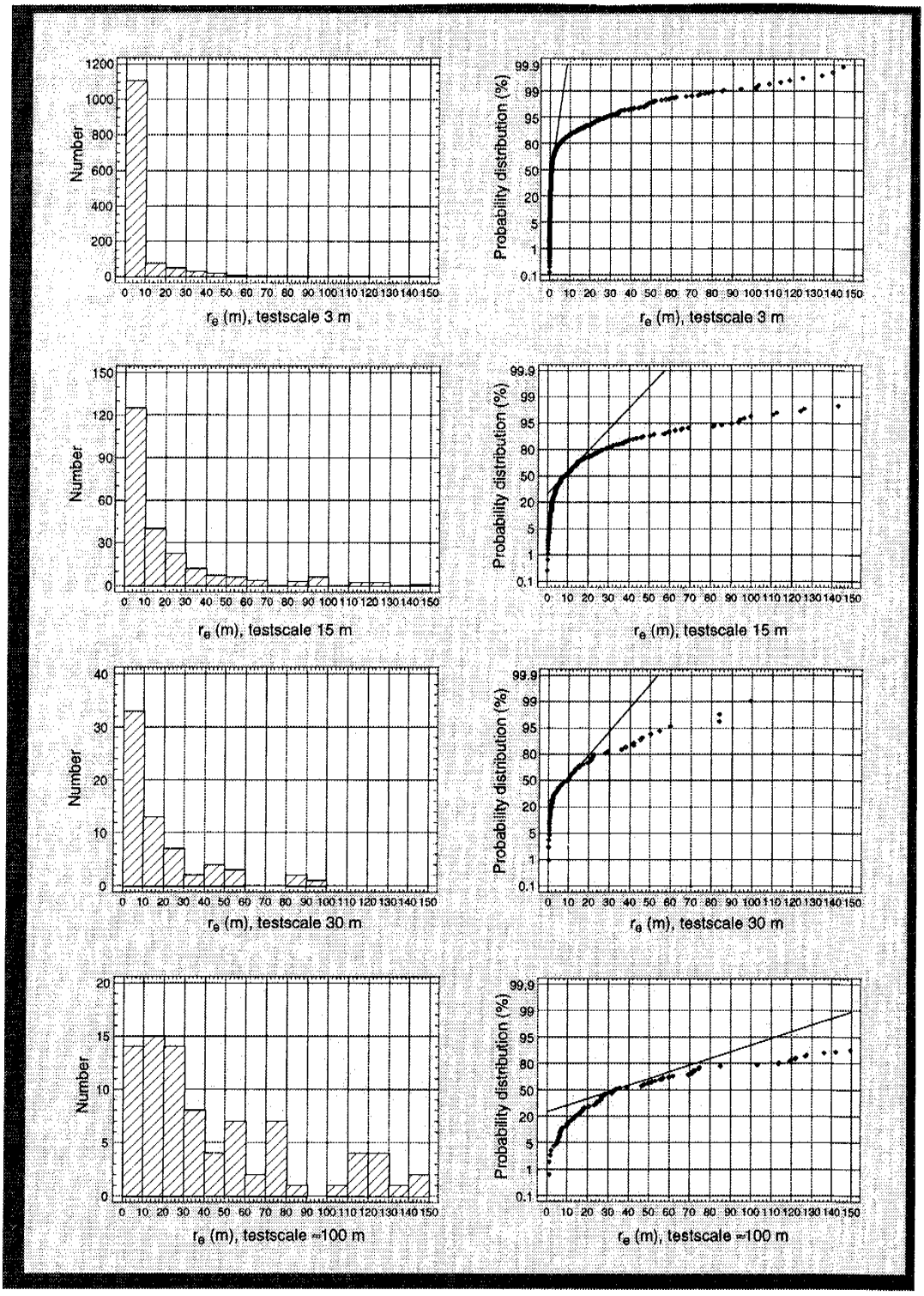

Figure 6-52. *Indication of radius of influence assuming a power law relationship between specific storativity and hydraulic conductivity according to Table 6-17 and radial flow. Data from the pre-investigation and construction phase at Äspö HRL. Total test time was used if no upper time for the evaluation period was given.*

region and not absolute values. The radius of influence linked to the evaluated hydraulic property can possibly be evaluated and incorporated into the model description, thus improving the base for a spatial correlation model.

The data has been used for groundwater flow modelling. Due to calibration some changes of the properties for the hydraulic rock mass domains were made, see *Chapter 8* and *Svensson /1997/.*

Specific storage

It is here suggested that the relationship between the hydraulic conductivity and specific storage shown in *Table 6-17* be used. However, the upper most 100 m or so should probably have higher values than indicated in *Table 6-17* because the conditions are not confined up to the bedrock surface. Possibly the specific yield (S_y) can be in the range 10^{-3} - 10^{-2} considering the low porosities that can be expected.

6.4 MODELS ON A BLOCK SCALE

6.4.1 General

The model comprises of the following geometrical concept:

- Hydraulic conductor domains.

The block scale comprises a description of the expected distance between hydraulic conductors with transmissivities (T) greater than a given value of T or within a given range for T. The purpose is to give a generic description of hydraulic characteristics of blocks within the site scale.

6.4.2 Distance between structures with a specified transmissivity

In the text below both arithmetic mean and median values are given. As the expected distance between structures with a certain transmissivity or greater than a specified value of the transmissivity is log/normally distributed, the median value is less than the arithmetic value. The median value and the standard deviation are useful for estimating where the next structure probably will turn up. The arithmetic mean value gives expected numbers of structures on a longer part of the tunnel.

The distance between hydraulic conductors has been estimated based on injection tests with 3 m packer spacing in KAS02, 04-08, 30 m packer spacing in KAS02, 03, KLX01 and also on the pressure build-up tests in the tunnel with a test scale of approximately 15 m.

For the 3 and 30 m tests the evaluated transmissivity and position of each test section were used for the statistics.

During the drilling of the probe holes the drill depth at which an increase in the amount of water flowing in was observed was documented (see *Figure 6-53*). The flow rate out of the borehole was also estimated and documented. The number of increasing flow-rate-steps was generally 1-6, but in a few of the probe holes it was not possible to define any position for the flow rate increase. The transmissivity of each fracture was calculated as:

$$T_f = T_i^j = \frac{T_i \cdot Q_i^j}{Q_i} \qquad (6\text{-}10)$$

Q_i^j is the estimated inflow during drilling from each fracture, Q_i the total inflow to the borehole and T_i the evaluated transmissivity of the borehole. The position of each inflow Q_i^j was projected on the tunnel line, and this position and T_i^j were then used to estimate the statistics.

Figures 6-54, *6-55* and *Table 6-22* show the statistics for the injection tests with 3 m packer spacing in KAS02, 04-08. It should be remembered that the statistics are based on tests of relatively short duration. Particularly the lower transmissivities do not necessarily represent fractures that are connected to other fractures. The results are probably biased to some extent for $T>10^{-4}$ m^2/s as the sample is small and located in only three of the holes. The statistics are also to some extent biased because the boreholes as well as the dominating numbers of water conducting fractures are subvertical, as was pointed out in *Section 6.3*. This means that the distance between the conductors has probably been overestimated to some extent as the boreholes are subvertical.

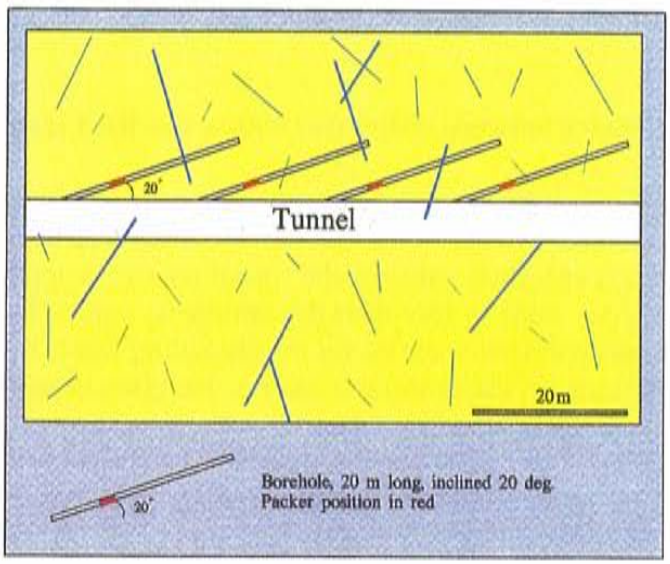

Figure 6-53. *Basic figure showing the way in which the probe holes were drilled in the left-hand tunnel wall. Probe holes were also drilled in the right-hand tunnel wall in the same manner. The figure also shows schematically the sparsely distributed water bearing fractures controlling the flow into the borehole and the section (packer in red) for which the pressure was measured, see Section 6.4.4.*

Figures 6-56 and *6-57* show the statistics for the injection tests with 30 m packer spacing in KAS02, 03 and KLX01. These holes are all more or less vertical. *Figure 6-56* shows that the transmissivity (T) should more or less always be expected to be greater than 10^{-10} m^2/s for each 30 m section and that the expected distance (median value) for $T>10^{-6}$ m^2/s is around 100 m. The expected distance (median value) for $T>10^{-6}$ m^2/s is around 10 m for the 3 m tests (see *Figure 6-54*). The arithmetic mean for the 3 m tests is around 20 m. One reason for this difference is that the samples are not from the same boreholes but if the data from KAS02 is compared the difference between 3 and 30 m tests can be studied. In KAS02 the expected distance (median value) for $T>10^{-6}$ m^2/s is around 10 m for the 3 m tests and around 60 m for the 30 m tests. The sample is, however, very small. The probable reason for the differences is that the fracture network has limited connectivity. Some fractures that are hydraulically active during a short duration test are not active during

a long test because they are not, or are only poorly, connected to fractures further away from the pumped section.

Figures 6-58 to *6-61* and *Table 6-23* show the statistics for pressure build-up tests in the tunnel, which were performed in more or less horizontal boreholes. As for the injection tests, results are probably biased to some extent for $T>10^{-4}$ m^2/s as the sample is small. The sample is also clearly biased for low transmissivities. Firstly, the method used (identifying transmissive structures in probe holes during drilling) leads to underestimation of low-conductivity structures, because they are masked by higher flow rates. This probably affects the statistics for low-transmissive structures. The statistics is probably not relevant for $T<10^{-7}$ m^2/s. Secondly, it has not been possible to drill every fourth round, which causes a few false 'long' distances.

Figures 6-58 and *6-59* indicate that the expected distance (median value) for $T>10^{-6}$ m^2/s is 10-20 m. The arithmetic mean is 35-55 m. As discussed in *Section 6.3* the rock mass is probably anisotropic due to most of the water-bearing fractures being subvertical. One could therefore expect to find shorter distances between conductive features with a specified transmissivity using probe hole data than with the data from the subvertical boreholes.

Table 6-22. Distance between hydraulic conductors with a transmissivity (T) greater than a specified value of the transmissivity (T_j) or within a range given by the transmissivities T_i and T_j. Data: Injection tests with 3 m packer spacing in cored boreholes KAS02, 05, 06, 07 and 08 for depth 200 to 500 m below sea level. (Observe that Figures 6-54 and 6-55 show the statistics for all observations in KAS02, 04-08. However, the distributions are almost identical to the samples shown in this table).

Distance between structures when $T>T_j$			Distance between structures when $T_i>T>T_j$			
	KAS02, 05-08				KAS02, 05-08	
T_j (m^2/s)	Arithmetic mean distance (m)	Median distance (m)	T_i (m^2/s)	T_j (m^2/s)	Arithmetic Mean distance (m)	Median distance (m)
1E-11	3.27	3.00	1E-10	1E-11	9.04	3.00
1E-10	4.11	3.00	1E-09	1E-10	8.35	3.00
1E-09	7.57	3.00	1E-08	1E-09	25.22	10.50
1E-08	9.82	3.00	1E-07	1E-08	26.39	9.00
1E-07	13.79	3.00	1E-06	1E-07	32.17	18.00
1E-06	20.88	9.00	1E-05	1E-06	28.89	12.00
1E-05	44.88	6.00	1E-04	1E-05	59.05	6.00
1E-04	156.00	120.00	1E-03	1E-04	156.00	120.00

Table 6-23. Distance between hydraulic conductors with a transmissivity (T) greater than a specified value of the transmissivity (T_j) or within an range given by the transmissivities T_i and T_j. Data: probe holes in tunnel section 1400-3600 m. Values for $T < 10^{-7}$ m²/s is uncertain.

Distance between structures when $T>T_j$			Distance between structures when $T_i>T>T_j$			
	Left tunnel wall				**Left tunnel wall**	
T_j (m²/s)	Arithmetic mean distance (m)	Median distance (m)	T_i (m²/s)	T_j (m²/s)	Arithmetic Mean distance (m)	Median distance (m)
1E-11	18.93	13.65	1E-10	1E-11	69.65	28.29
1E-10	19.86	14.14	1E-09	1E-10	152.57	123.83
1E-09	20.88	13.65	1E-08	1E-09	118.53	83.47
1E-08	24.41	13.24	1E-07	1E-08	83.14	80.26
1E-07	32.51	14.39	1E-06	1E-07	110.74	42.64
1E-06	36.62	19.19	1E-05	1E-06	56.68	50.21
1E-05	73.25	40.52	1E-04	1E-05	77.00	50.71
1E-04	No data	No data	1E-03	1E-04	No data	No data
	Right tunnel wall				**Right tunnel wall**	
T_j (m²/s)	Arithmetic mean distance (m)	Median distance (m)	T_i (m²/s)	T_j (m²/s)	Arithmetic Mean distance (m)	Median distance (m)
1E-11	20.05	13.09	1E-10	1E-11	100.05	87.98
1E-10	20.25	13.14	1E-09	1E-10	136.99	50.12
1E-09	22.01	11.73	1E-08	1E-09	119.15	86.79
1E-08	24.70	11.49	1E-07	1E-08	54.81	35.82
1E-07	36.16	12.65	1E-06	1E-07	65.37	37.00
1E-06	55.22	10.20	1E-05	1E-06	98.68	32.18
1E-05	77.73	24.08	1E-04	1E-05	155.47	83.72
1E-04	(33.84)*	(4.71)*	1E-03	1E-04	(40.60)*	(4.72)*

* Results based on few data points, see *Figure 6-58* and *6-60*.

If it is assumed that the statistical distribution of the transmissivity of individual fractures is the same for all fracture directions, the expected distance between structures with a defined transmissivity should be shorter for the horizontal boreholes than for the vertical ones. This seems possible, taking into account the scale dependency that seems to be present, as the expected distances in the probe holes are just somewhat larger than those from the 3 m tests.

A summarized presentation of the expected distances for features with a transmissivity greater than a specified value is shown in *Table 6-24*.

Table 6-24. The arithmetic mean distance between hydraulic conductors with a transmissivity (T) greater than a specified value of the transmissivity (T_j). Results for cored boreholes based on injection tests with 3 m packer spacing.

Probe holes T_j (m^2/s)	Arithmetic mean distance D_a (m^2/s)
$T > 10^{-5}$	70
$T > 10^{-7}$	35
$T > 10^{-9}$	(20)*
Cored boreholes T_j (m^2/s)	**Arithmetic mean distance D_a (m^2/s)**
$T > 10^{-5}$	45
$T > 10^{-7}$	14
$T > 10^{-9}$	8

* uncertain value

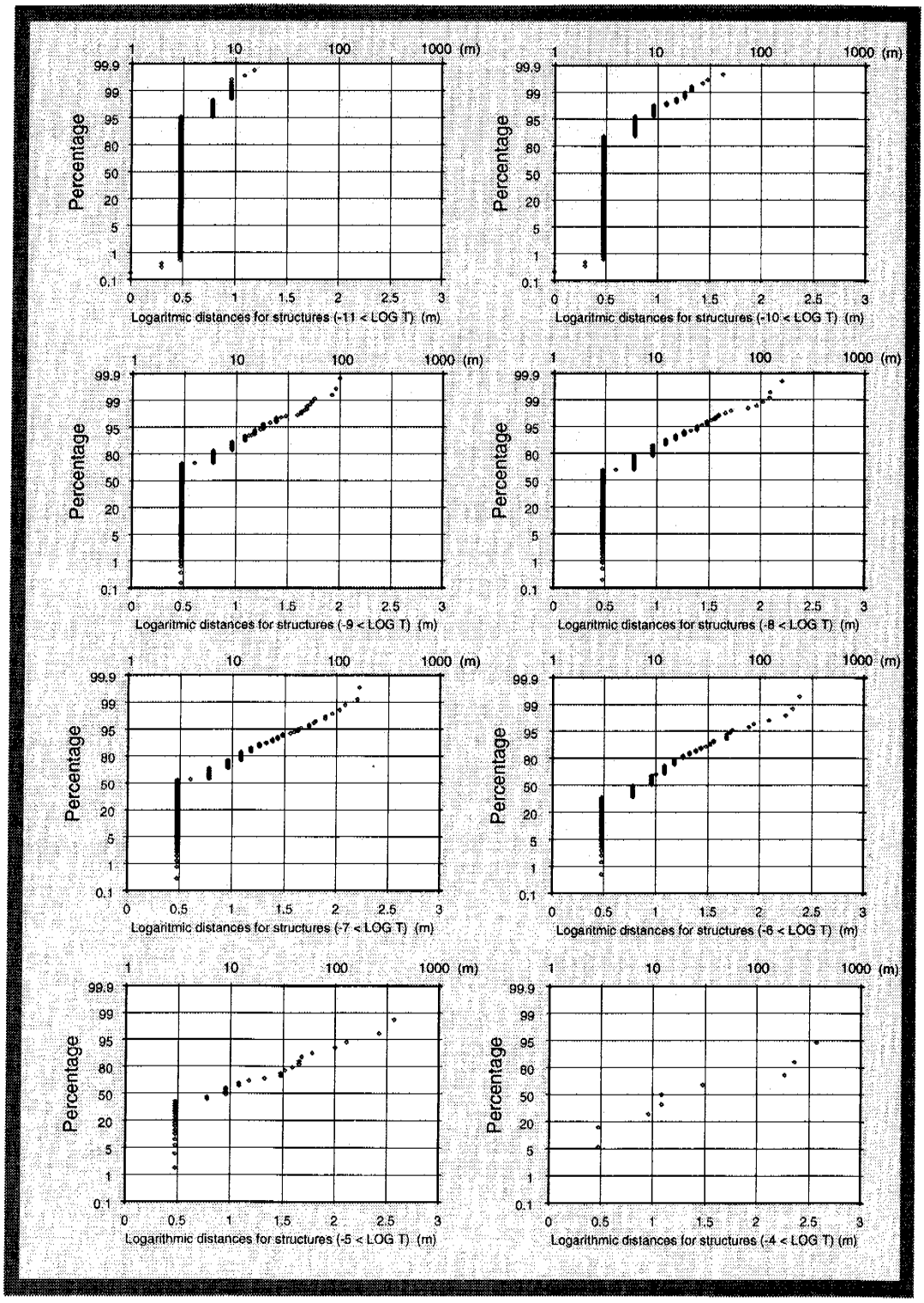

Figure 6-54. *The logarithmic distance (Log_{10} (D)) between conductors with transmissivities (T) greater than a specified value of the transmissivity. Data: Injection tests with 3 m packer spacing made in KAS02, 04-08. T: (m^2/s), Distance = D: (m).*

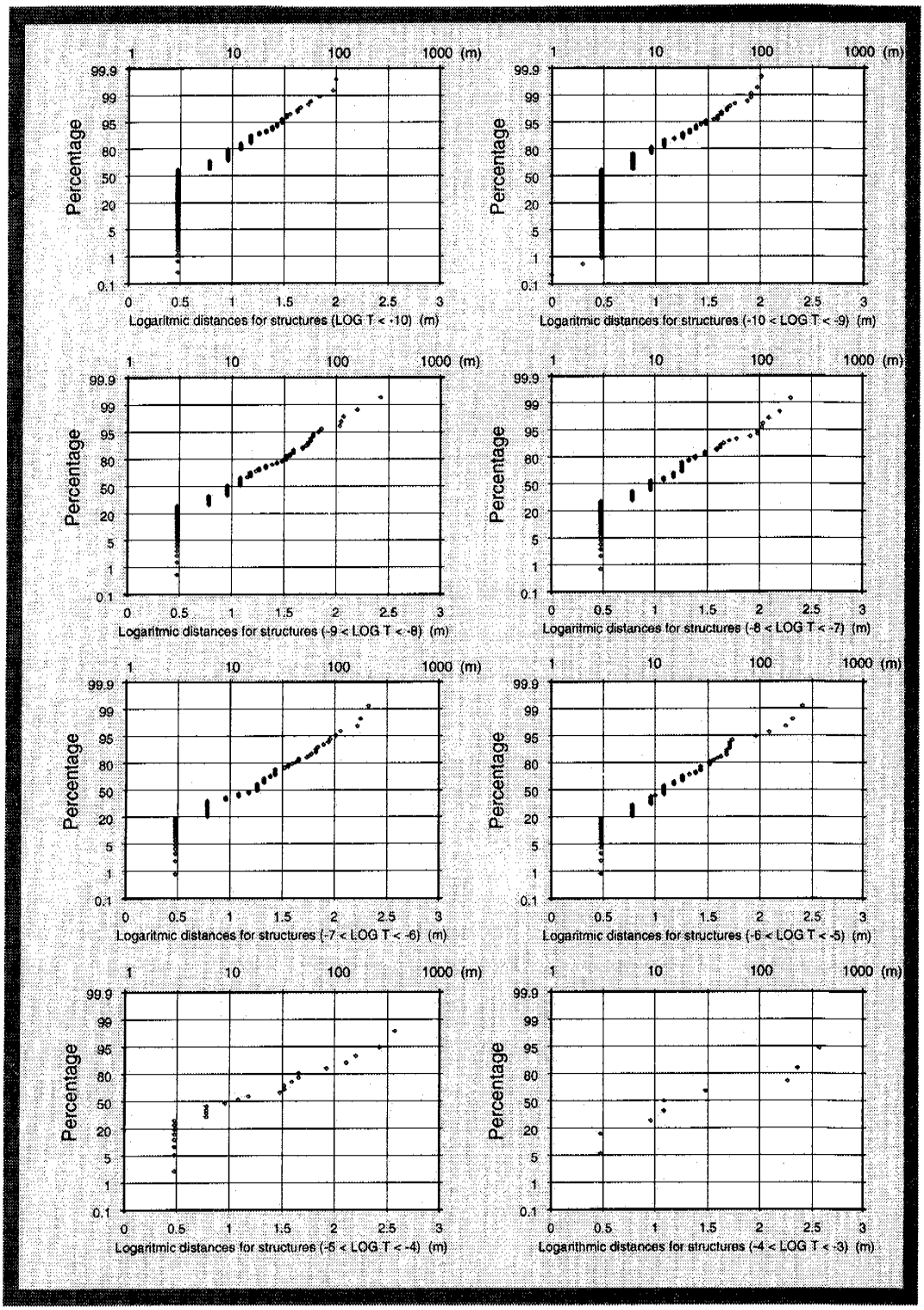

Figure 6-55. *The logarithmic distance (Log_{10} (D)) between conductors with transmissivities (T) within a specified range of the transmissivity.*
Data: Injection tests with 3 m packer spacing made in KAS02, 04-08. T: (m^2/s), Distance = D: (m).

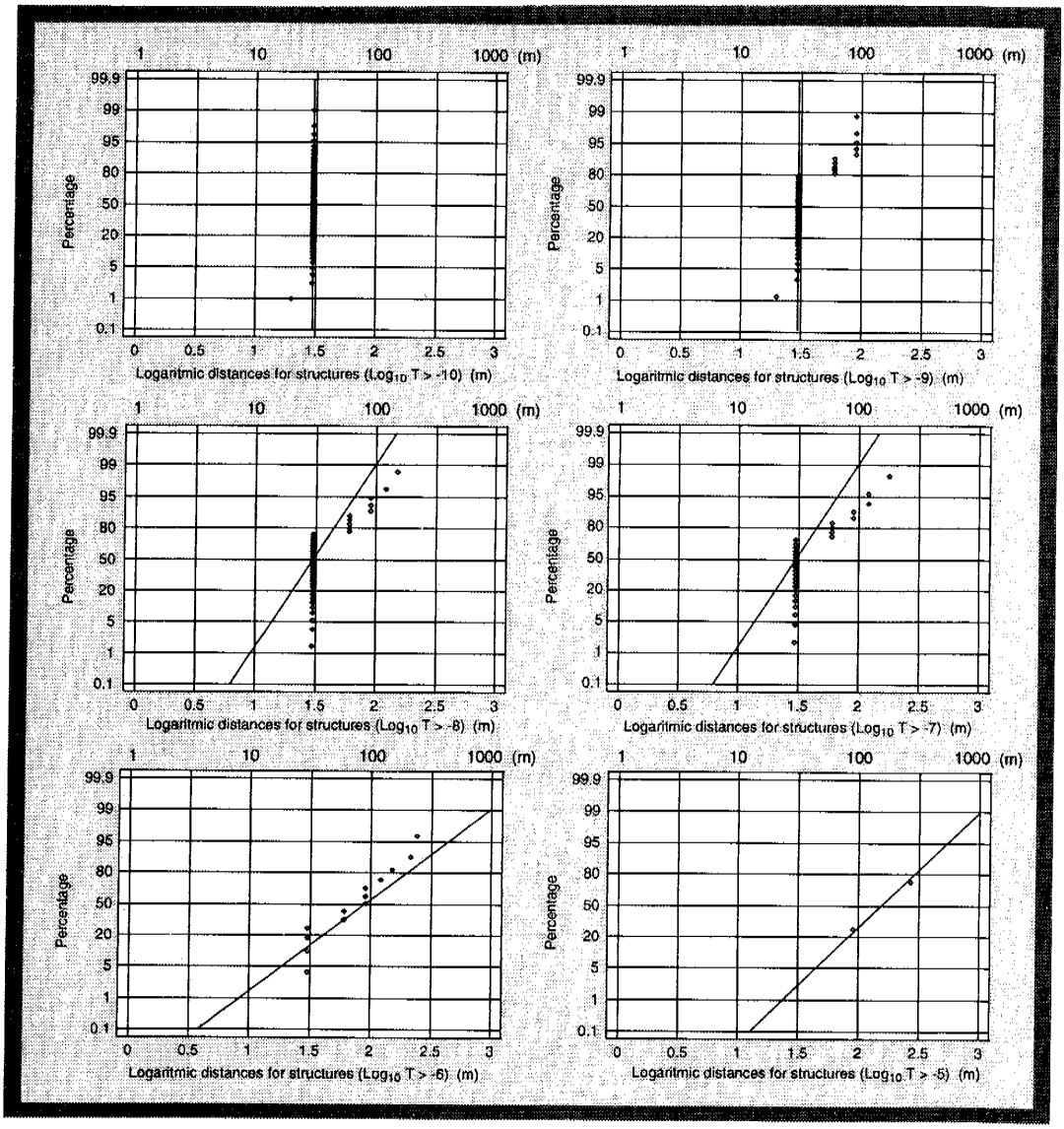

Figure 6-56. *The logarithmic distance (Log_{10} (D)) between conductors with transmissivities (T) greater than a specified value of the transmissivity. Data: Injection tests with 30 m packer spacing made in KAS02, 03 and KLX01. T: (m^2/s), Distance = D: (m).*

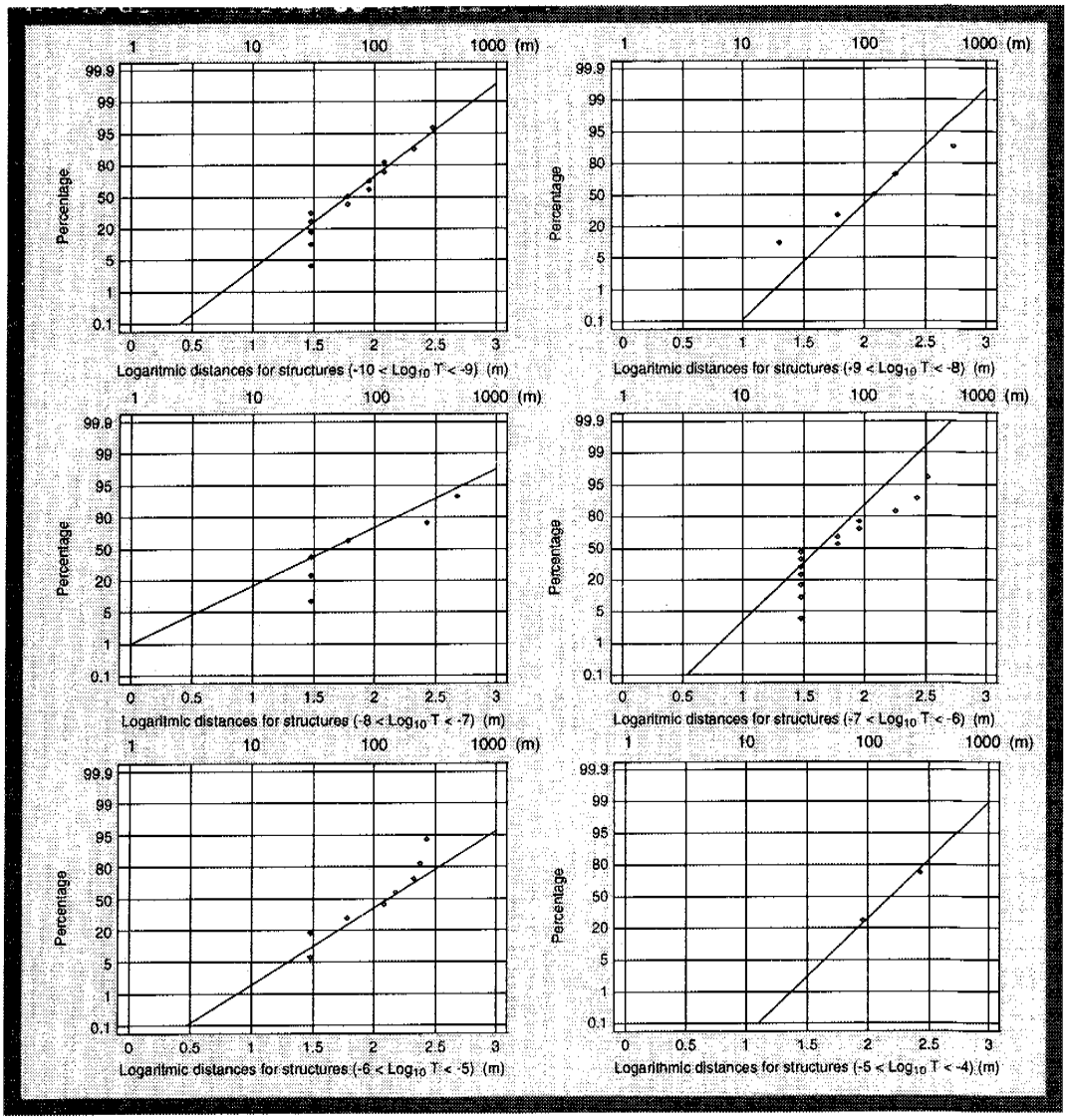

Figure 6-57. *The logarithmic distance (Log_{10} (D)) between conductors with transmissivities (T) within a specified range of the transmissivity.*
Data: Injection tests with 30 m packer spacing made in KAS02, 03 and KLX01.
T: (m^2/s), Distance = D: (m).

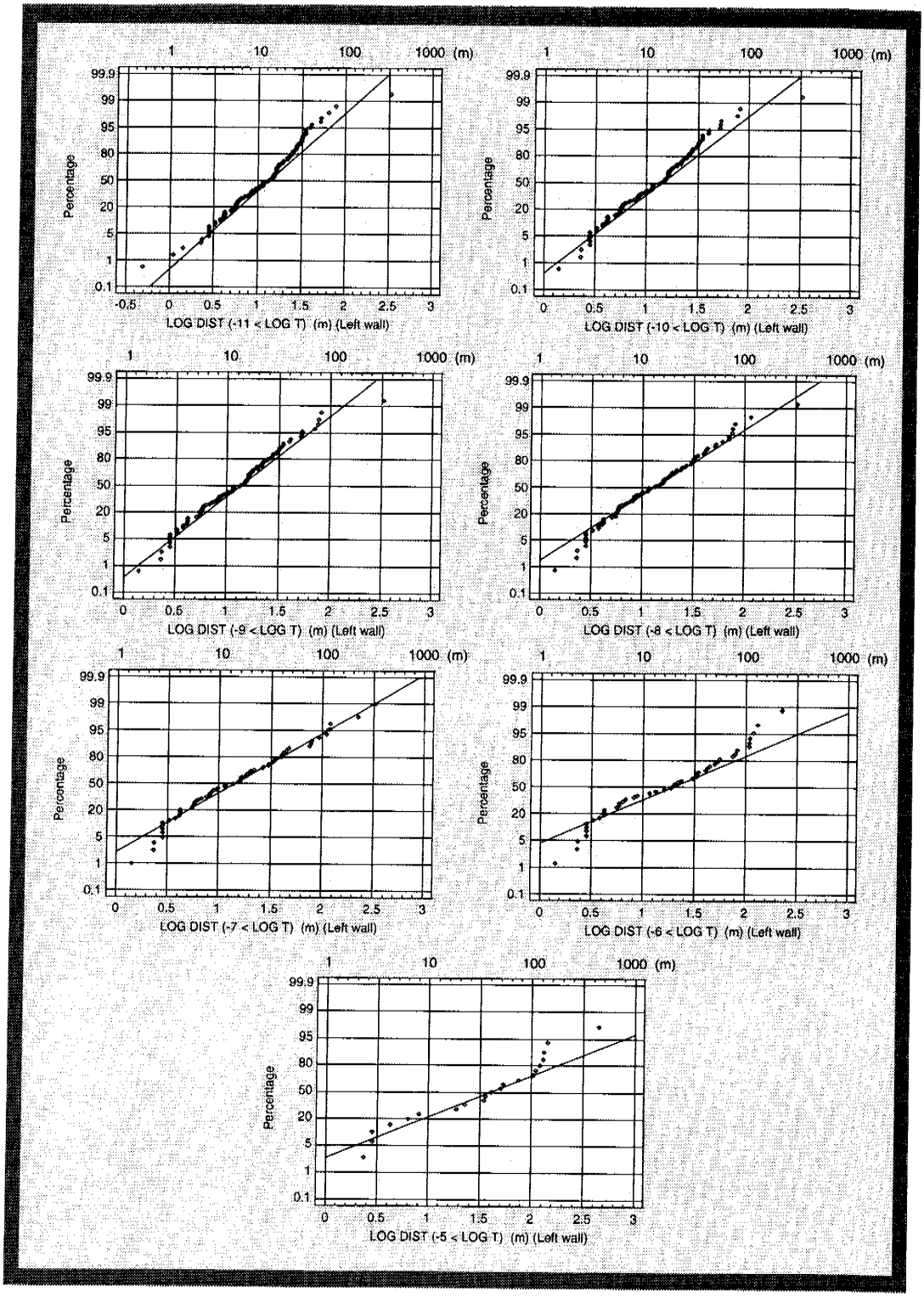

Figure 6-58. *The logarithmic distance (Log_{10} (D)) between conductors with a transmissivities (T) greater than a specified value of the transmissivity. Data: Pressure build-up tests in probe holes in the tunnel at chainage 1400-3600 m - left wall and centre of tunnel (TBM part). Test scale approximately 15 m. T: (m^2/s), Distance = D: (m). The number of features with T less than about 10^{-7} m^2/s is probably underestimated and makes the statistics uncertain in diagrams including such features.*

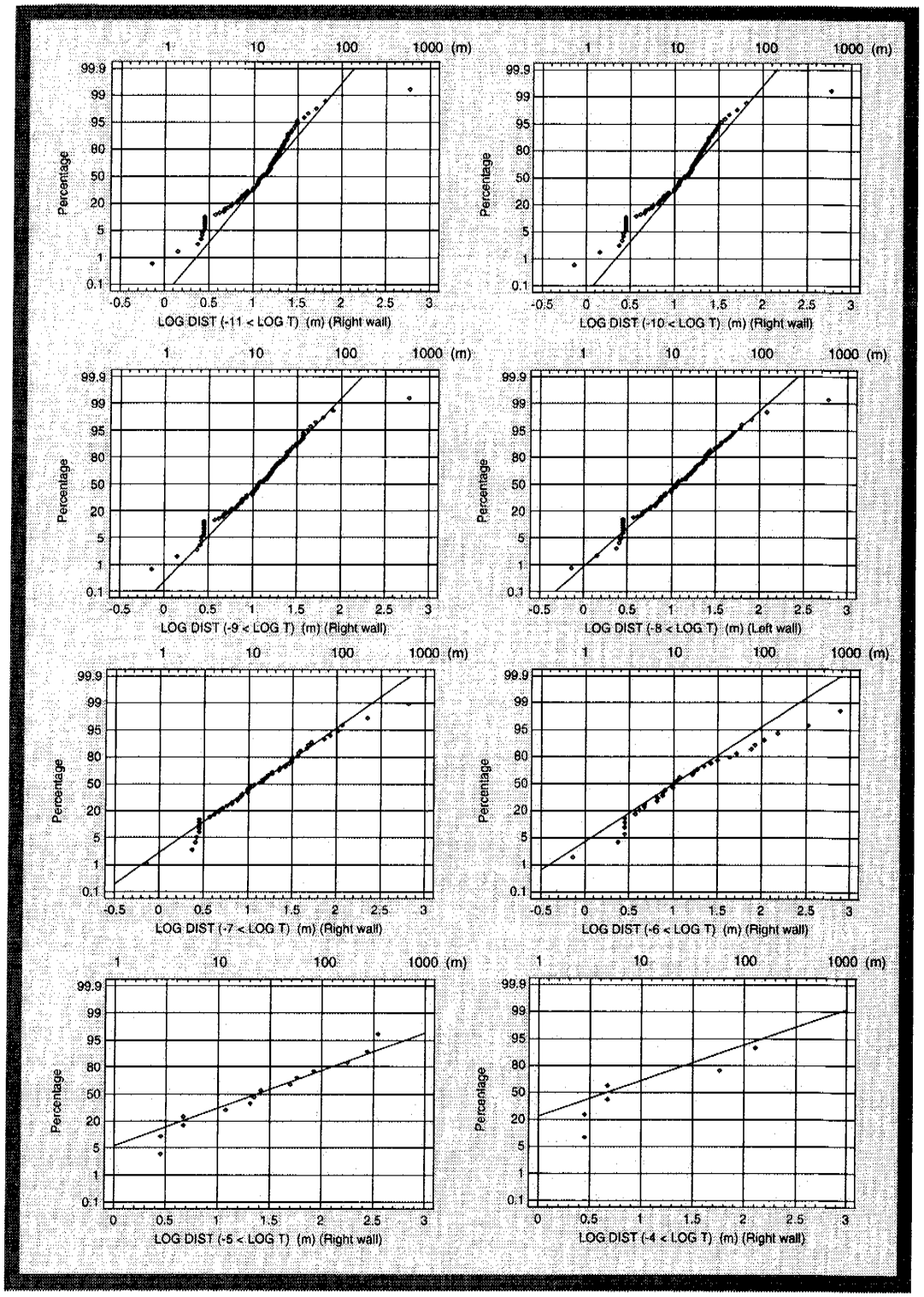

Figure 6-59. *The logarithmic distance (Log_{10} (D)) between conductors with a transmissivities (T) greater than a specified value of the transmissivity.*
Data: Pressure build-up tests in probe holes in the tunnel chainage 1400-2900 m - right wall. Test scale approximately 15 m. T: (m^2/s), Distance = D: (m). The number of features with T less than about 10^{-7} m^2/s is probably underestimated and makes the statistics uncertain in diagrams including such features.

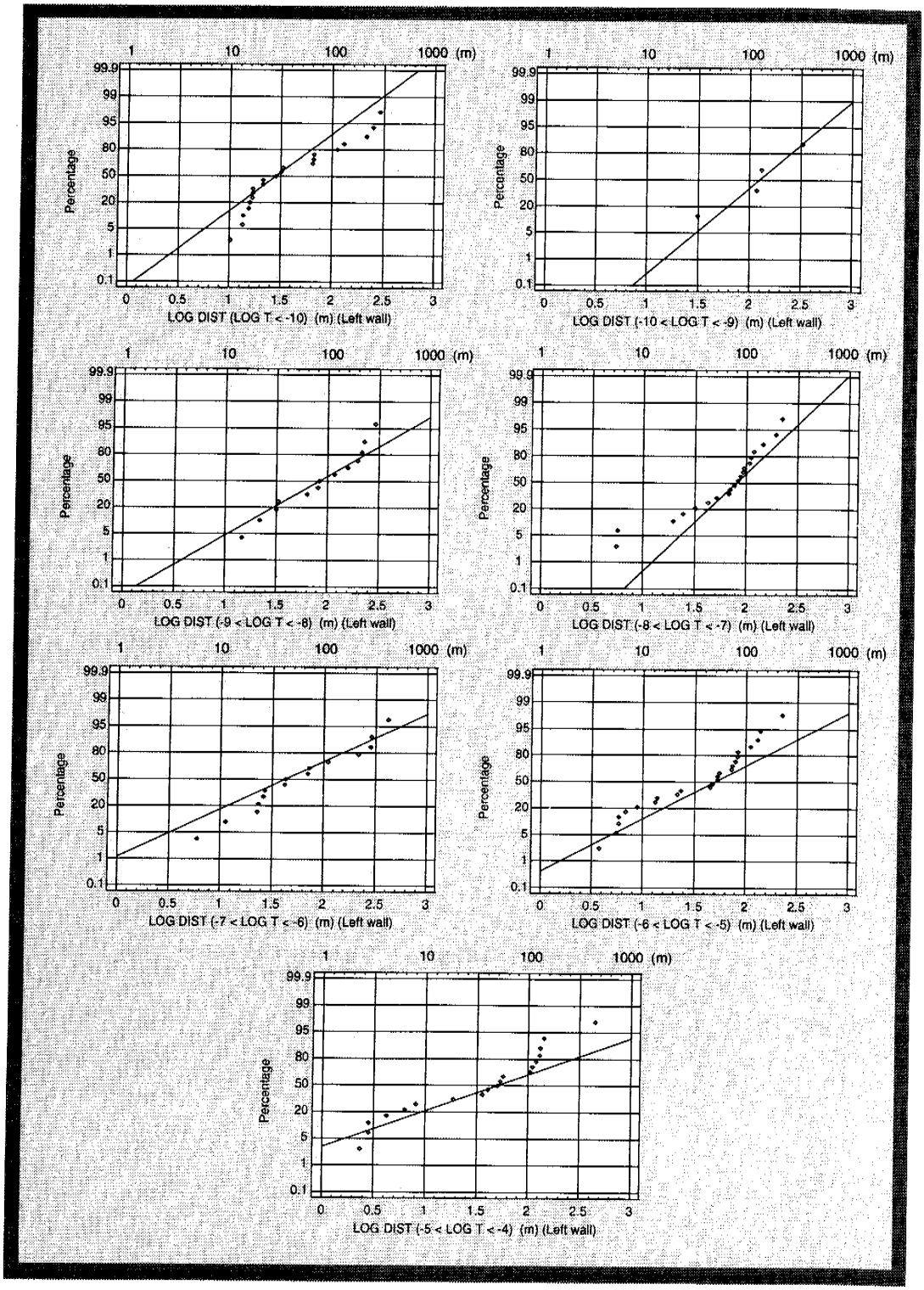

Figure 6-60. *The logarithmic distance (Log_{10} (D)) between conductors with a transmissivities (T) within a specified range of the transmissivity.*
Data: Pressure build-up tests in probe holes in the tunnel chainage 1400-3600 m - left wall and centre of tunnel (TBM part). Test scale approximately 15 m. T: (m^2/s), Distance = D: (m). The number of features with T less than about 10^{-7} m^2/s is probably underestimated and makes the statistics uncertain in diagrams including such features.

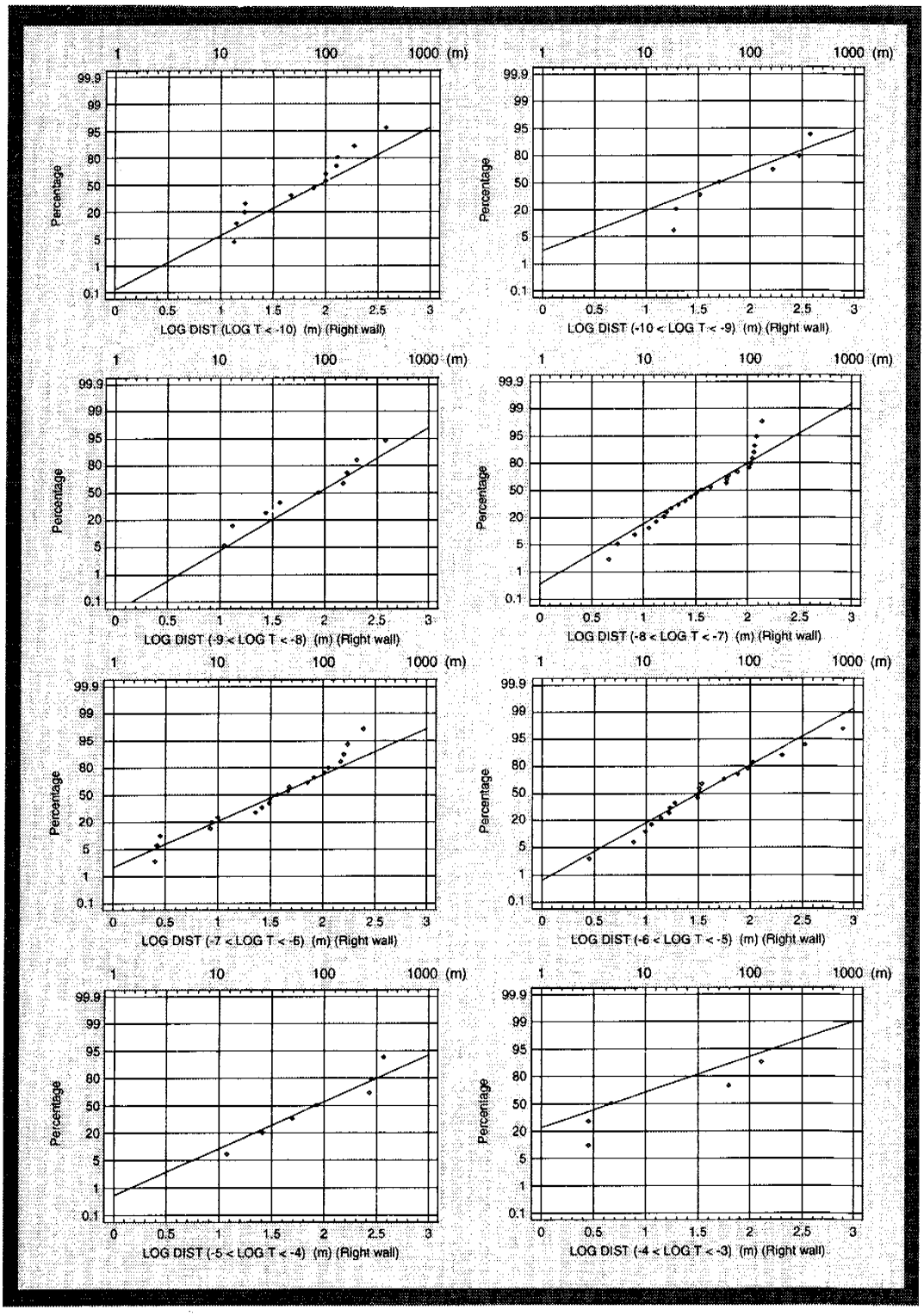

Figure 6-61. *The logarithmic distance (Log_{10} (D)) between conductors with a transmissivities (T) within a specified range of the transmissivity.*
Data: Pressure build-up tests in probe holes in the tunnel chainage 1400-2900 m - right wall. Test scale approximately 15 m. T: (m^2/s), Distance = D: (m). The number of features with T less than about 10^{-7} m^2/s is probably underestimated and makes the statistics uncertain in diagrams including such features.

6.4.3 Fracture characteristics of a block

In order to visualize a possible image of the fracture network at the Äspö site, a Discrete Fracture Network (DFN) model was used */Hermanson, 1996/*. The observed fracture directions in the TBM tunnel are shown in *Figure 6-62* and two DFN realisations are shown in *Figures 6-63* and *6-64*. The fracture orientations of the fractures in the DFN model were boot-strapped directly from the observed data as it was difficult to fit any orientation model to the data set.

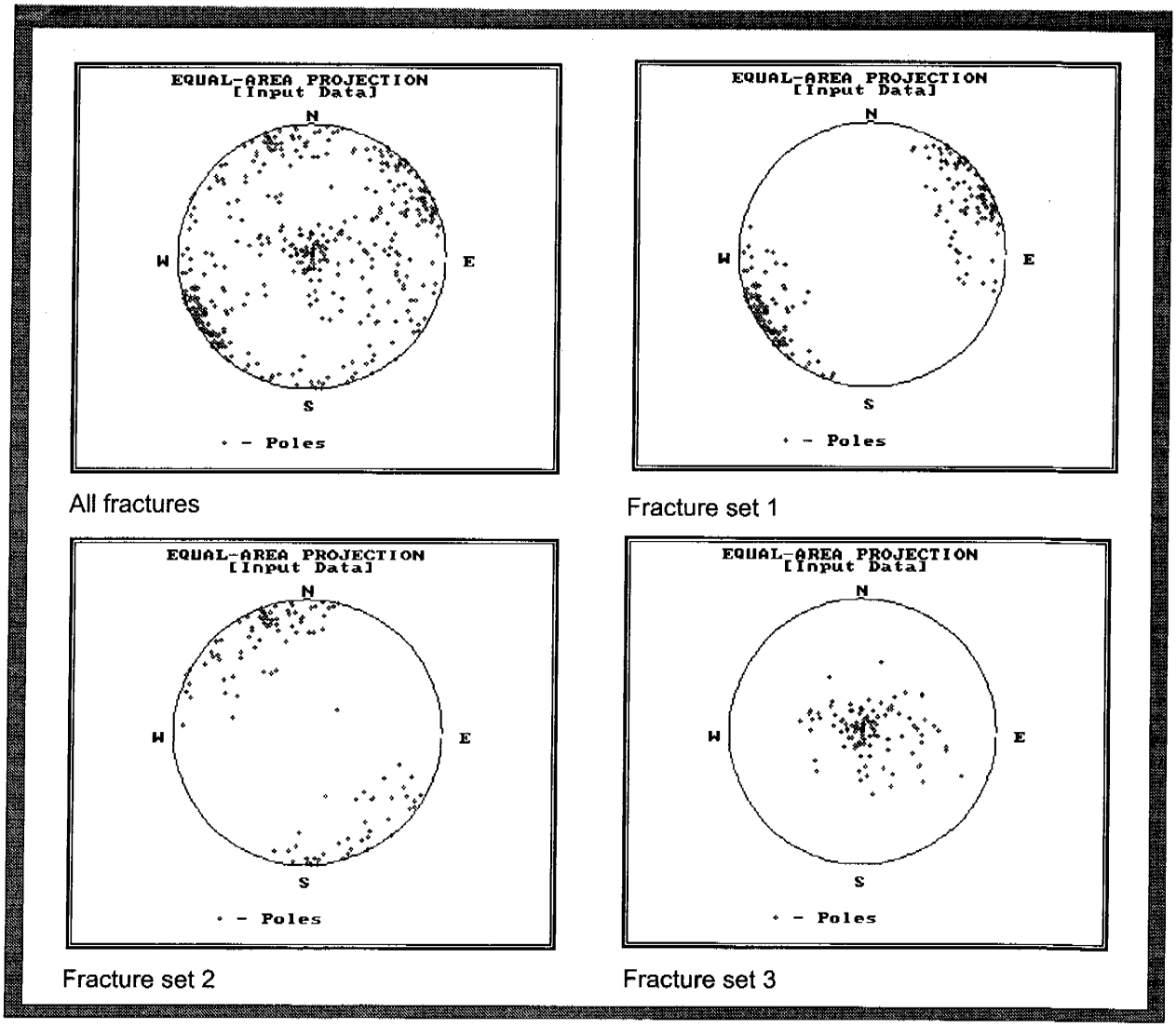

Figure 6-62. *Fractures in the TBM tunnel. Pole diagram for all fractures according to observations and fracture sets according to identified sets /Hermanson, 1996/.*

Analysis of the fracture traces in the tunnel indicted that the fracture size (=effective radius (R)), defined as the radius of a circular fracture with the area of the given fracture) had a log-normal distribution. The arithmetic mean of R was 6 m and the standard deviation of R was 3 m. (In order to use these data in the log-normal distribution the data has to be transformed to statistics for Log (R) (see */Hermanson, 1996/). La Point /1995/* found the same size distribution as above by analysing the conductive traces in the tunnel. *Uchida et al /1994/* estimated the mean fracture size to be 13.7 m and the standard deviation to be 12.7 m, based on fracture mapping of outcrops at Äspö. *Poteri /1996/* used a part of the drilled and blasted tunnel at the Äspö HRL and estimated the mean to be about 2.3 m and the standard deviation to be about 1 m. *Dershowitz et al /1996/* also used part of the drilled and blasted tunnel at the Äspö HRL and estimated the mean to be about 3.7 m and the standard deviation to be about 2 m.

Hermanson /1996/ estimated the volumetric fracture density (P_{32}) to be 0.48 m^{-1}. The location model used was Enhanced Beacher and the fracture termination percentage was set at 38%. As it was assumed that 10% of the fractures were conductive, based on evaluation of the observations of the fractures in the tunnel, P_{32} was set at 0.048 m^{-1} for conductive fractures and at 0.432 m^{-1} for non-conductive fractures (see the texts in *Figures 6-63* and *6-64* for further details). The mapping in the tunnel was made for fracture traces longer than about 1 m. If fracture traces down to dm size are available and used in the calculations P_{32} may increase considerably.

In order to study the statistics of the areal fracture density (P_{21}) and the linear fracture density (P_{10}) a tunnel and a number of boreholes were implemented in the DFN model.

Another set of realisations was also made with the same fracture intensity as in the drilled and blasted tunnel, but otherwise the same input data as for the model based on TBM data. The results are shown in *Table 6-25*. The values of P_{21} for the drilled and blasted tunnel in *Table 6-25* are close to the observed mean values for Småland granite and Äspö diorite in the drilled and blasted tunnel. The areal fracture density (P_{21}) and the linear fracture density (P_{10}) for the water-conducting fractures were not estimated as the sample in the model was so small. However, as the water-bearing fractures tend to be steep and strike NW to NNW, P_{10} should become about 10 times less than the values in *Table 6-25*, but relatively somewhat greater for boreholes 2, 6 and 7 and less for 1 in *Table 6-25*.

The observed fracture density in the drilled and blasted tunnel is probably to some extent overestimated due to some of the mapped fractures being induced by the blasting. The observed fracture density in the TBM tunnel is on the other hand possibly to some extent underestimated because of the difficulties in identifying fractures, at least small ones. It is also found that values of P_{10} in the cored boreholes are much greater than those in *Table 6-25*. This is probably due to drilling and handling of the core creating some new fractures, but also the fact that small fractures, not mapped or seen on the tunnel wall, are most likely included in borehole P_{10} .

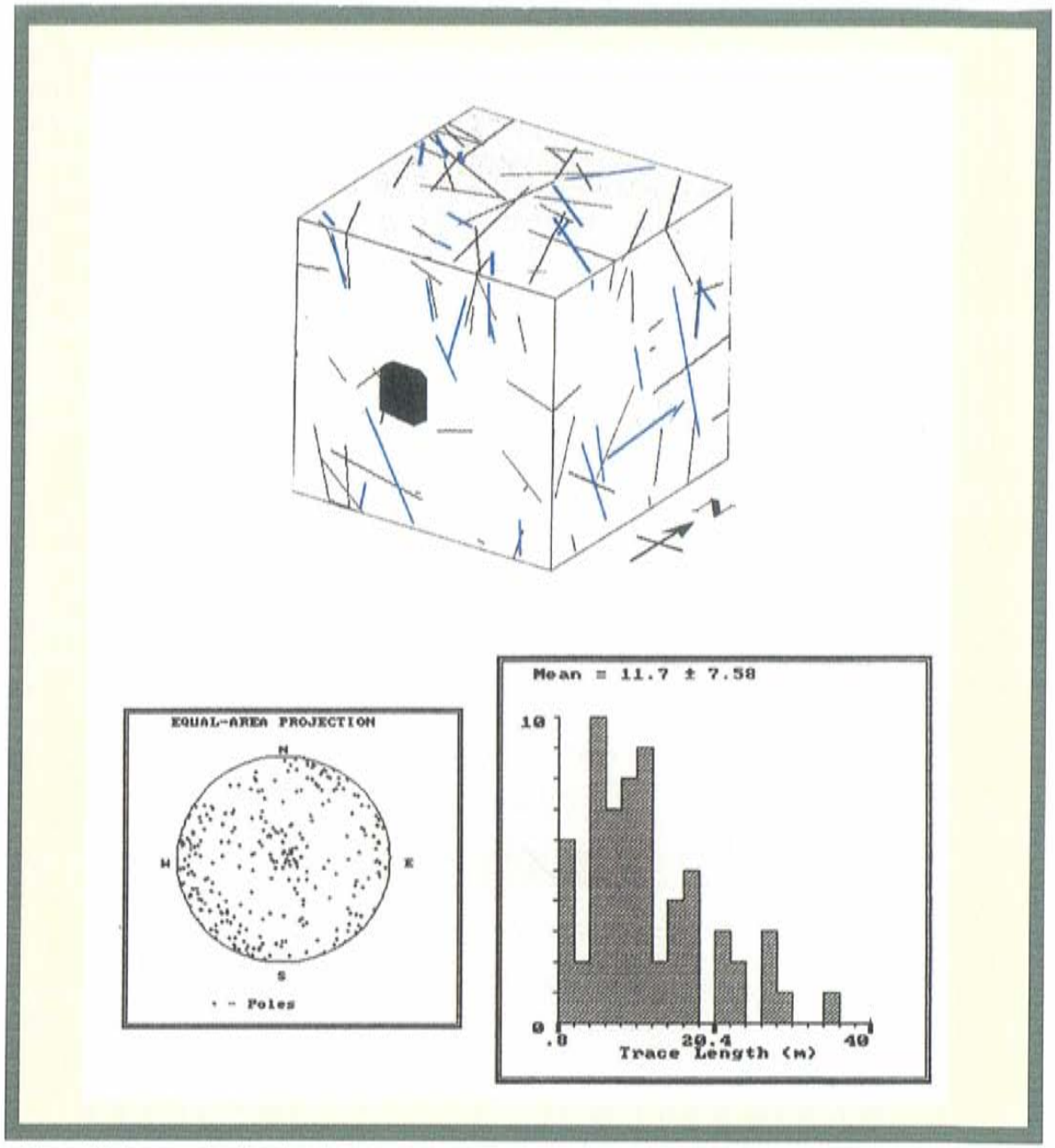

Blue : Water-conducting fracture
Black : All other fractures
Trace lenght : Traces on the faces of the cube
Pole diagram : All fractures

Figure 6-63. *Discrete Fracture Network (DFN) model. Realisation 1. Fracture size, intensity and spatial model for all fractures are based on data from the TBM tunnel. Fracture orientation for the non-conductive fractures are based on data from the TBM tunnel. 10% of all fractures are assumed to be conductive fractures, based on the mapped water-conducting fractures at tunnel chainage 1400-3600 m. Fracture orientations for the conductive fractures are based on data on the mapped water-conducting fractures at the tunnel chainage 1400-3600 m. The figure above shows non-conductive (black) and water-conducting (blue) fractures. The fracture statistics of trace length on the faces of the cube and a pole diagram of the generated fractures are also shown /Hermanson, 1996/.*

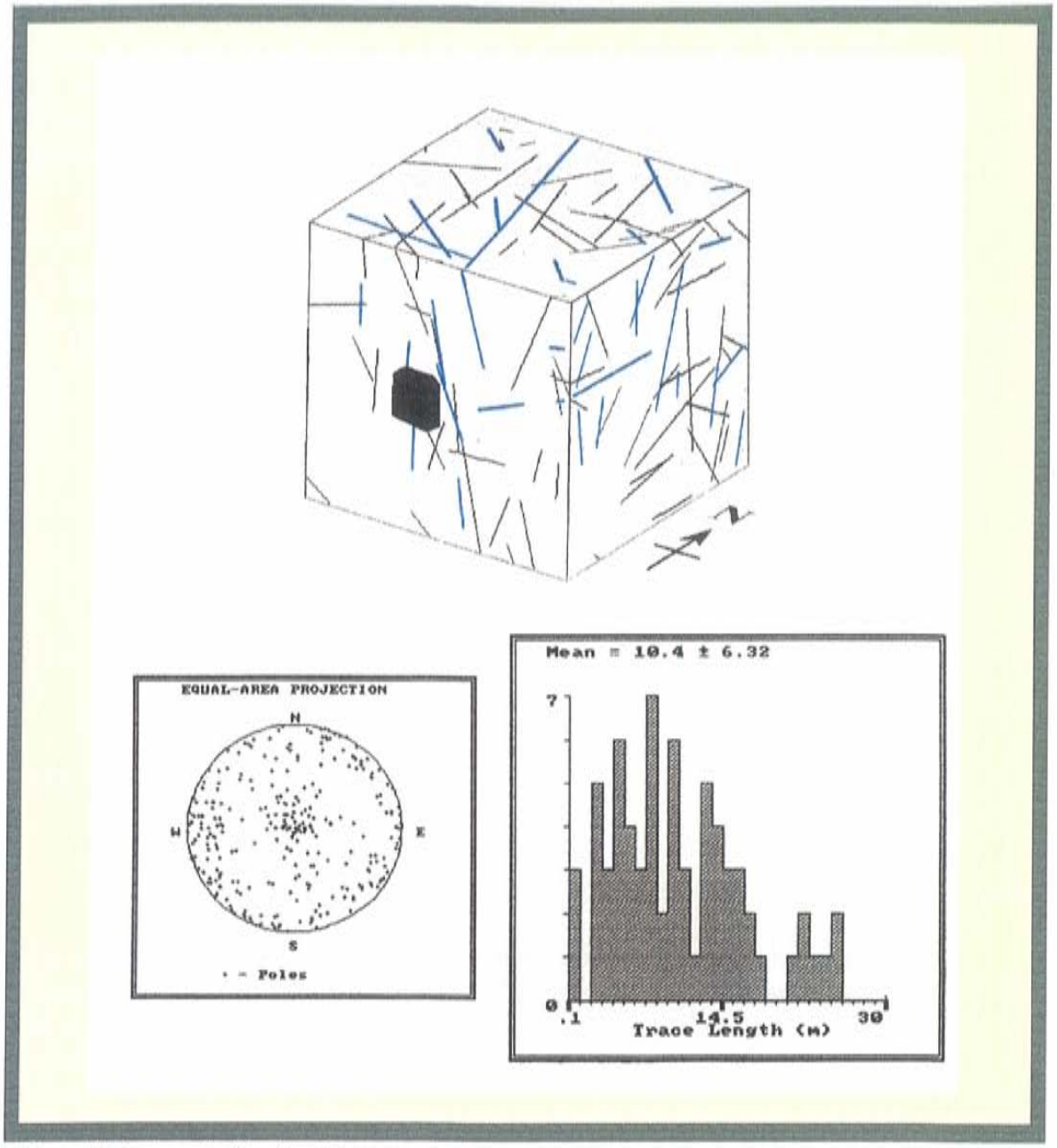

Blue : Water-conducting fracture
Black : All other fractures
Trace lenght : Traces on the faces of the cube
Pole diagram : All fractures

Figure 6-64. *Discrete Fracture Network (DFN) model. Realisation 2. Fracture size, intensity and spatial model for all fractures are based on data from the TBM tunnel. Fracture orientation for the non-conductive fractures are based on data from the TBM tunnel. 10% of all fractures are assumed to be conductive fractures, based on the mapped water-conducting fractures at tunnel chainage 1400-3600 m. Fracture orientations for the conductive fractures are based on data on the mapped water-conducting fractures at tunnel chainage 1400-3600 m. The figure above shows non-conductive (black) and water-conducting (blue) fractures. The fracture statistics of trace length on the faces of the cube and a pole diagram of the generated fractures are also shown /Hermanson, 1996/.*

Table 6-25. Areal fracture density (P_{21}) and the linear fracture density for (P_{10}) calculated from simulated sampling of a tunnel and 7 boreholes. Äspö coordinate system. Length = sampling length. TBM = TBM tunnel data. DBT= Drilled and blasted tunnel data. The model is based on mapped fracture traces longer than about 1 m.

Borehole /Tunnel	Trend (°)	Inclination (°)	Length (m)	TBM P_{10} (m^{-1})	TBM P_{21} (m^{-1})	DBT P_{10} (m^{-1})	DBT P_{21} (m^{-1})
Bh 1	0	90	50	0.28		0.46	
Bh 2	90	0	50	0.36		0.58	
Bh 3	0	0	50	0.30		0.47	
Bh 4	0	45	70.7	0.31		0.52	
Bh 5	180	45	70.7	0.31		0.49	
Bh 6	90	45	70.7	0.30		0.46	
Bh 7	270	45	70.7	0.37		0.58	
Tunnel	90	8	50		0.44		0.66

6.4.4 Water pressure outside the tunnel wall

At approximately every fourth round, two 20-m long probe holes were drilled about 4 m from the tunnel face, one in the left wall and one in the right wall. The main purpose of the probe holes was to estimate the hydraulic properties of the rock but the boreholes were also used for pressure measurements. Generally the borehole trend was around 20° from the tunnel line in the horizontal plane and with an inclination of approximately 10°. The packer was generally mounted about 5 m into the borehole (see *Figure 6-53*). During drilling the inflow of water (flow rate and position in the borehole) and the rock composition were estimated. In order to estimate the pressure distribution around the tunnel it was necessary to estimate a representative point of application. The flow rate distribution along the borehole and the borehole direction relative the tunnel centre line was used to estimate the point of application (see *Rhén et al /1997b/* for details). The estimated radial distance from the tunnel centre line to the point of application was around 10 m, that is about 7 m outside the tunnel wall. The packer position was about 2 m outside the tunnel wall.

The "undisturbed" pressure ahead of the tunnel face was estimated from the evaluation of the pressure build-up tests. The pressure in the probe holes were thereafter measured approximately twice a year. *Figure 6-65* shows the "undisturbed" pressure and the pressure measured in February 1995. As can be seen in both figures the spread is quite high. The reason is the high degree of heterogeneity in the rock mass (see *Figure 6-53*). The figures also show that the

average pressure has decreased by about 40%. If the pressures from February 1995 are compared with the pressures, measured more or less directly after the tunnel face passed the bottom of the probe hole, the difference is much smaller. These pressures are just somewhat higher than the pressures measured February 1995. It has been found that on average the pressures are slowly decreasing, even though there are examples of pressure increases */Rhén (ed), 1995/*.

Figures 6-66 to *6-67* show the statistics for the pressure or the relative pressure (pressure divided by the hydrostatic head) for four sections of tunnel, 0-700 m, 700-1400 m (below the Baltic Sea), 1400-2300 m (first tunnel spiral) and 2300-3600 m (second tunnel spiral). As can be seen in *Figure 6-66* the pressure ahead of the tunnel face was generally about 60% of hydrostatic pressure in the spiral, but below the sea it was nearly hydrostatic. These were the pressures encountered during the pre-grouting of the tunnel. The pressure conditions outside the tunnel 1995 (see *Figure 6-67)* show that the pressure was generally about 40% of hydrostatic pressure in the spiral, but below the sea it was around 75%.

The pressure observations were also divided into two groups. Observations in reinforced rock mass and not-reinforced rock mass (see *Figure 6-68*). As can be seen in the figure the pressures in the reinforced rock mass were about 50% higher than the pressures in the non-reinforced rock mass.

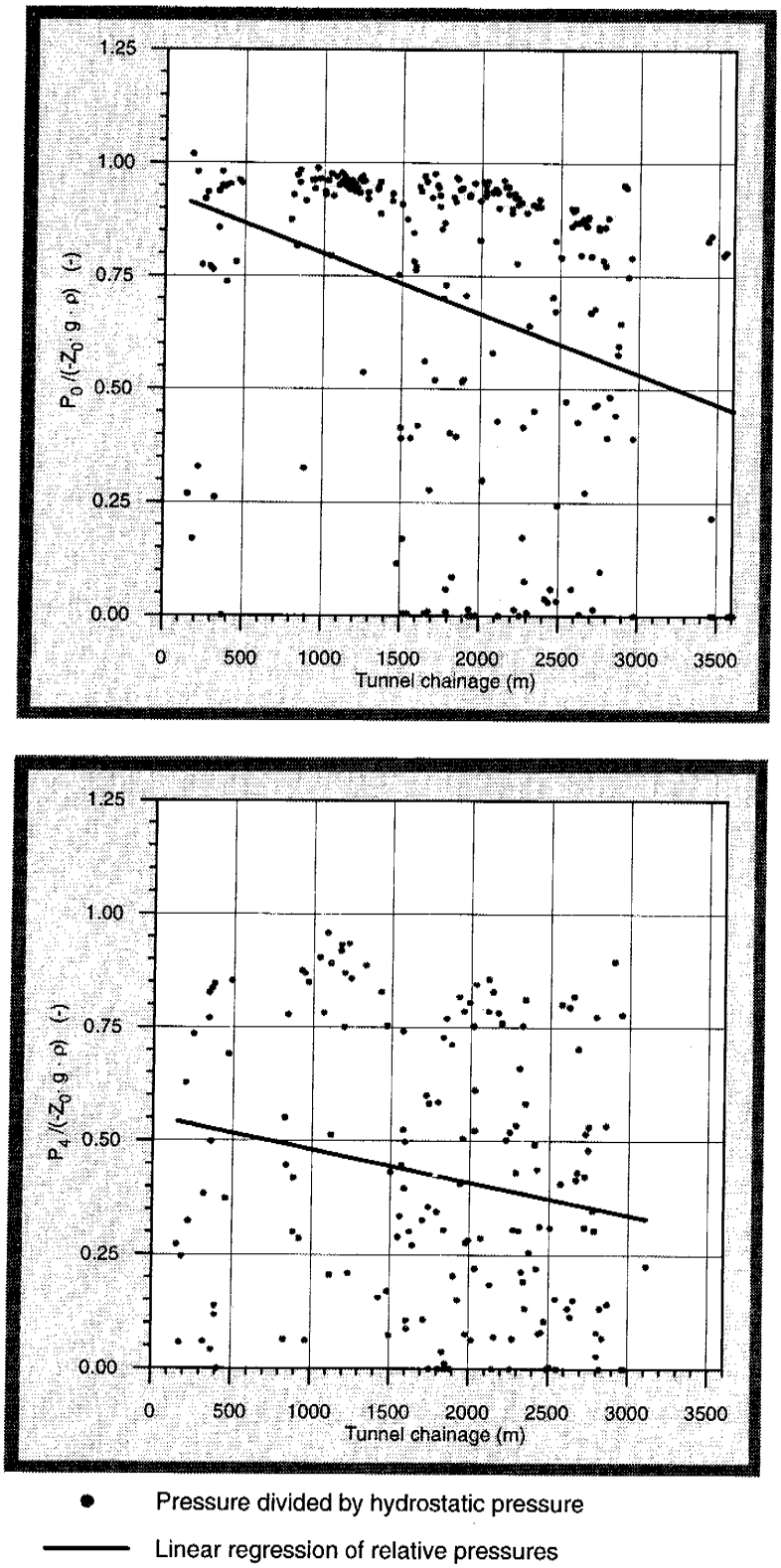

Figure 6-65. *Relative water pressure outside the tunnel wall. Data: tunnel chainage 0-3600 m. The line in the figure is a linear regression of the relative pressures as function of tunnel chainage.* z_o *= the level of the borehole below sea level,* $\rho = 1000\ kg/m^3$.
Top : Pressure ahead of the tunnel face (2-16 m) measured during excavation. Bottom: Pressure measured February 1995.

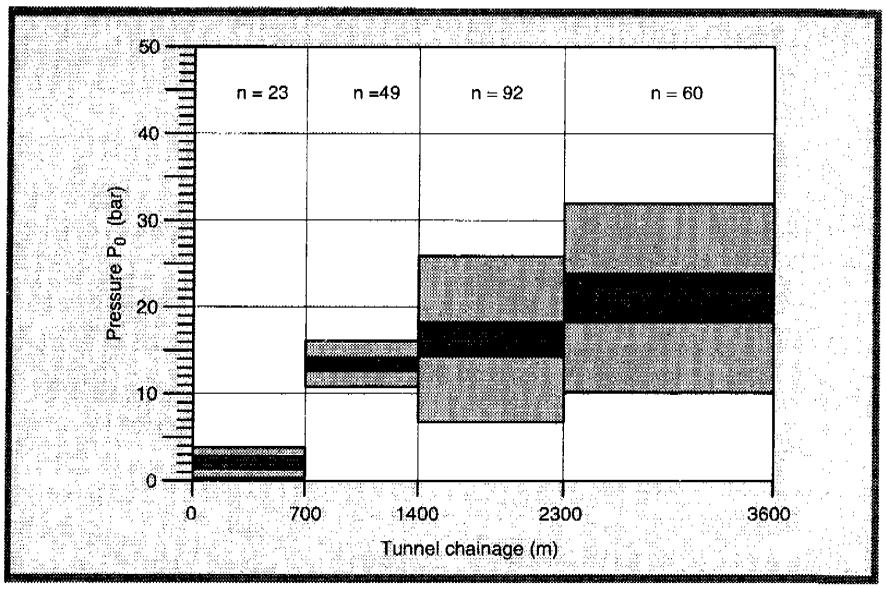

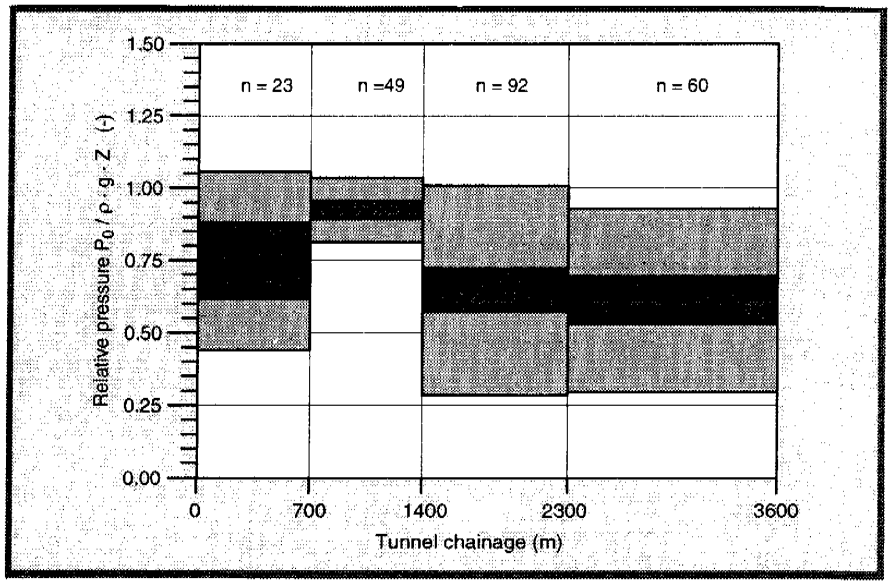

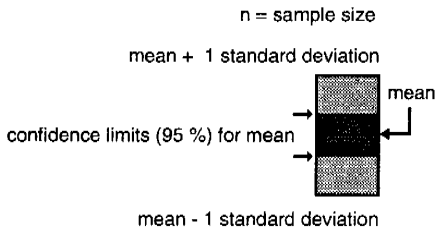

Figure 6-66. *Water pressure outside the tunnel wall. Data: tunnel chainage 0-3600 m. Pressure ahead of the tunnel face (2-16 m) measured during excavation. Z = the level of the borehole below sea level, ρ = 1000 kg/m^3.*
Top : Pressure. Standard deviation and confidence limits for mean.
Bottom: Relative pressure. Standard deviation and confidence limits for mean.

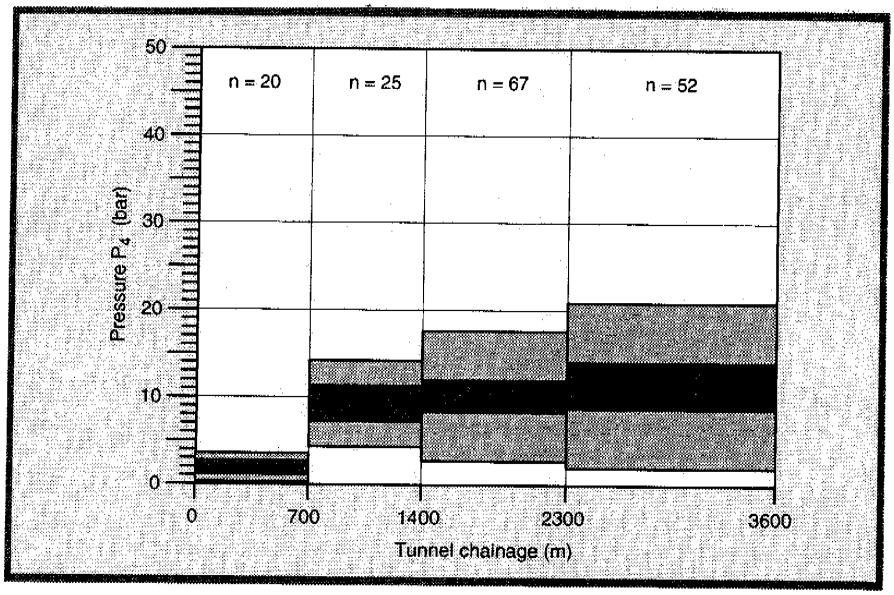

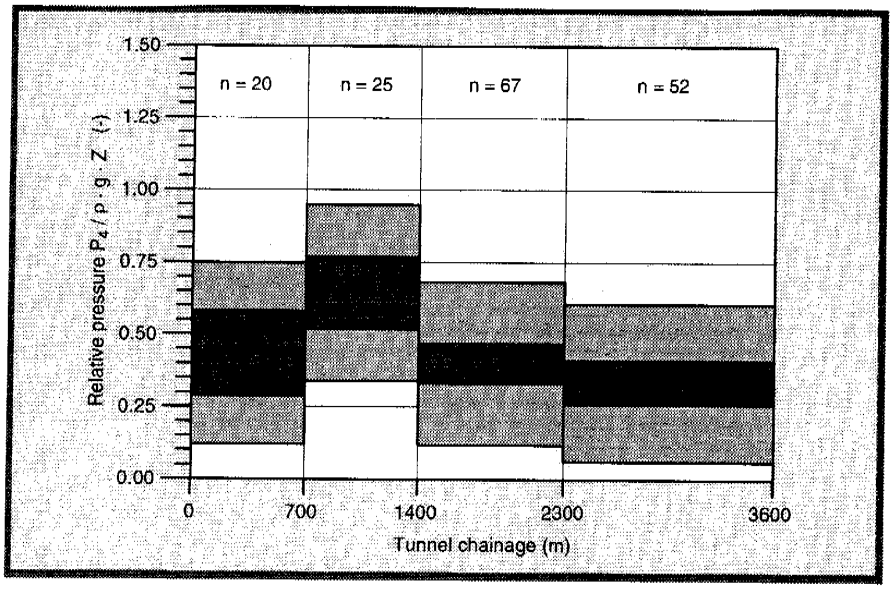

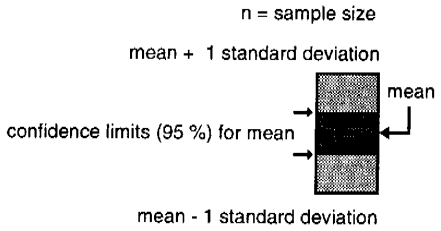

Hel sida

Figure 6-67. *Water pressure outside the tunnel wall. Data: tunnel chainage 0-3600 m. Pressure measured on February 1995. Z = the level of the borehole below sea level, ρ = 1000 kg/m^3.*
Top : Pressure. Standard deviation and confidence limits for mean.
Bottom: Relative pressure. Standard deviation and confidence limits for mean.

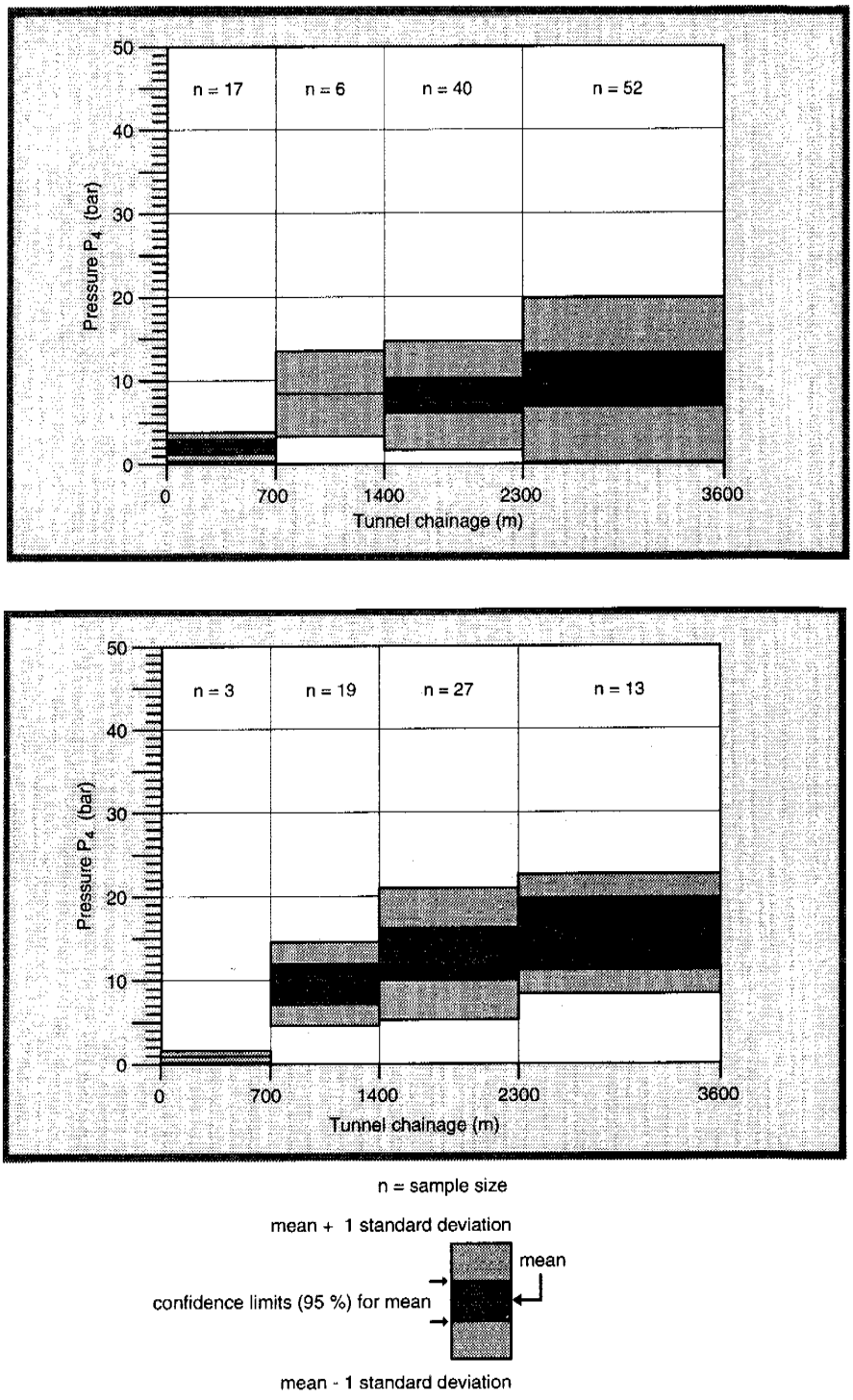

Figure 6-68. *Water pressure outside the tunnel wall. Data: tunnel chainage 0-3600 m. Pressure measured on February 1995.*

Top : Pressure - Non-reinforced rock. Standard deviation and confidence limits for mean.

Bottom: Pressure - Reinforced rock. Standard deviation and confidence limits for mean.

6.5 MODELS ON DETAILED SCALE - LITHOLOGICAL UNITS

6.5.1 General

The model comprises of the following geometrical concept:

- Hydraulic rock mass domains.

The detailed scale comprises a description of the expected hydraulic conductivity (K) for each lithological unit. The purpose is to provide a generic description of the hydraulic characteristics of lithological units within the site scale.

6.5.2 Lithological units

The statistics shown in *Figure 6-69* are based on all injection tests with 3 m packer spacing made in boreholes on Äspö. The detailed statistics are shown in *Appendix A2*. As can be seen in the figure the most conductive lithological unit, excluding mylonite, is fine-grained granite. The mylonite sample is more or less from one borehole, KAS04, intersecting one of the larger fracture zones. The sample is thus possibly not representative.

6.5.3 Characteristics as seen on the tunnel wall

Wet area in the tunnel

The wet area of the tunnel was estimated for each rock type, see *Table 6-26*. The wet areas were estimated during the documentation for all objects except when the inflow was clearly identified as inflow spread over a part of a fracture length (L_w). In such a case the area was set to $L_w \cdot 0.1$ m. As can be seen in *Table 6-26* fine-grained granite appears to be the wettest, which mainly is due to the more intense fracturing of the rock unit compared with the others. The value for greenstone and pegmatite are somewhat uncertain as the area in the tunnel of these two rock units is relatively small, see *Table 6-27*.

It may be noted that the mapped wet tunnel area is much smaller for the TBM-tunnel than for the drilled and blasted tunnel, but the inflow rate is comparable to that of the drilled and blasted tunnel.

Mapped inflow by rock type

The mapped inflow by rock type is shown in *Table 6-28* and by using the total areas of each rock type and the values in *Table 6-28* the inflow per square metre of rock type can be calculated as shown in *Table 6-29*. As can be seen, greenstone and pegmatite have the lowest mapped inflow per square metre. (Pegmatite may not be representative because its sparse appearance in the tunnel.)

Äspö diorite and Småland granite seem to be fairly equally represented, although Äspö diorite seems on average to have a smaller inflow. Fine-grained granite has both higher and lower inflow rates than Småland granite and Äspö diorite for the tunnel sections shown, but its average inflow is the greatest.

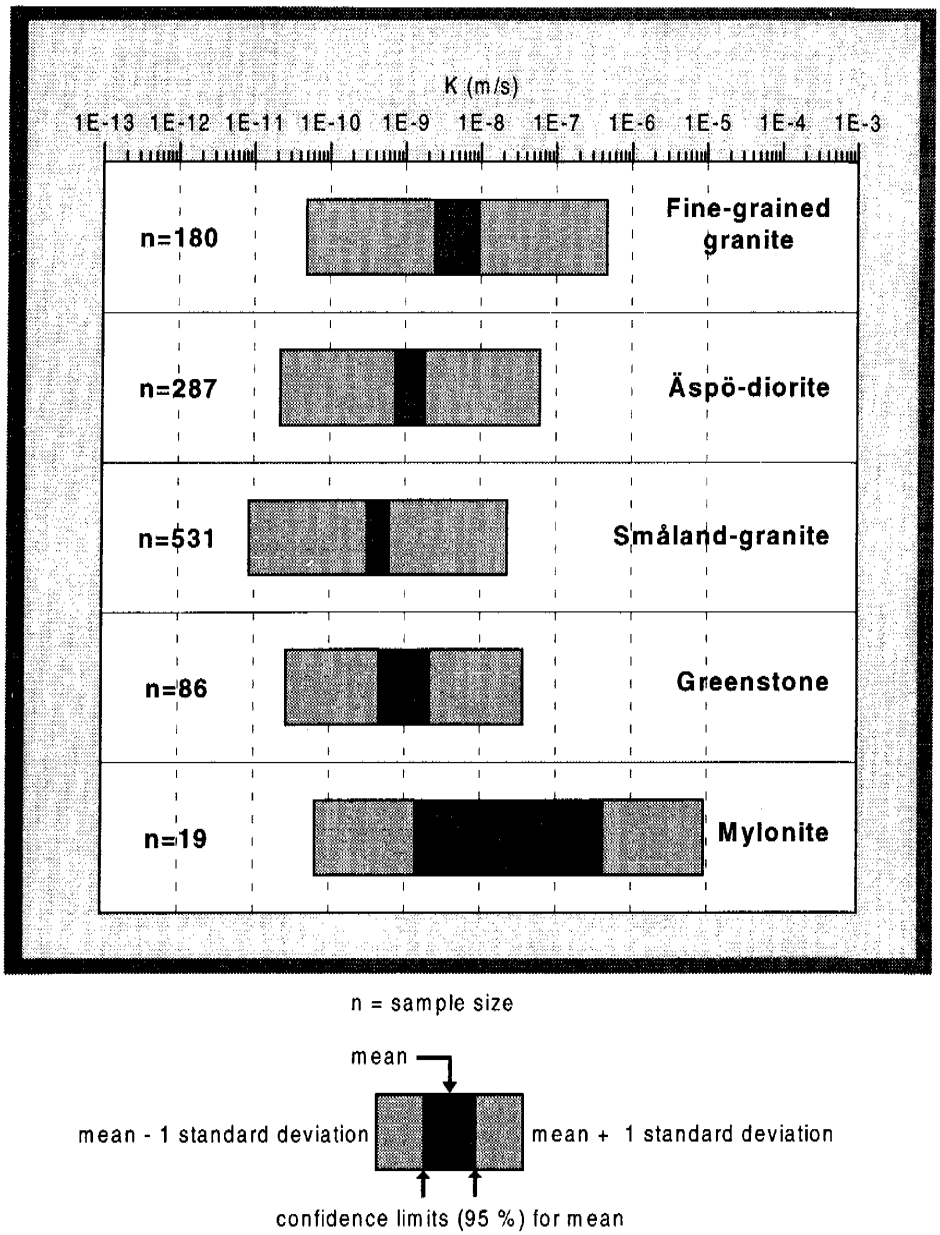

Figure 6-69. *Statistics for the main lithological units on Äspö. Data: injection tests with 3 m packer spacing in KAS02-08.*

Table 6-26. Mapped wet area by rock type. (% value: Wet area by rock type/total area by rock type) /*Rhén (ed), 1995*/.

	700-1475		1475-2265		2265-2875		2875-3600		700-3600	
	(m^2)	(%)	(m^2)	(%)	(m^2)	(%)	(m^2)	(%)	(m^2)	(%)
Fine-grained granite	280.2	13.5	105.1	6.3	88.2	15.0	2.1	0.3	475.6	9.5
Småland granite	154.5	5.5	65.1	2.6	141.6	12.6	1.0	0.1	362.2	4.7
Äspö-diorite	276.4	5.7	134.3	2.3	84.4	3.2	73.1	0.9	568.2	2.7
Greenstone	14.1	6.1	28.0	3.3	7.4	7.0	2.5	0.8	52.0	3.5
Pegmatite	0.0	0.0	0.2	0.3	0.0	0.0	0.0	0.0	0.2	0.1
Total	725.2	7.2	332.6	3.1	321.6	7.2	78.7	0.8	1458.2	4.1

Table 6-27. Mapped total area by rock type. (% value: Area by rock type/total mapped tunnel area) /*Rhén (ed), 1995*/.

	700-1475		1475-2265		2265-2875		2875-3600		700-3600	
	(m^2)	(%)	(m^2)	(%)	(m^2)	(%)	(m^2)	(%)	(m^2)	(%)
Fine-grained granite	2070.4	20.6	1660.1	15.2	588.0	13.1	702.5	7.0	5021.0	14.1
Småland granite	2810.1	28.0	2480.4	22.8	1127.7	25.2	1357.9	13.4	7776.1	21.9
Äspö-diorite	4884.0	48.7	5861.8	53.8	2631.9	58.7	7727.4	76.4	21105.1	59.4
Greenstone	232.1	2.3	837.4	7.7	104.9	2.3	315.2	3.1	1489.6	4.2
Pegmatite	43.7	0.4	58.9	0.5	29.3	0.7	4.8	0.1	136.7	0.4
Total	10040.3	100	10898.6	100	4481.8	100	10107.8	100	3552852	100

Table 6-28. Mapped inflow to the tunnel by rock type /*Rhén (ed), 1995*/.

	Tunnel chainage									
	700-1475 m		1475-2265 m		2265-2874.6 m		2875-3600 m		700-3600 m	
	(l/min)	(%)	(l/min)	(%)	(l/min)	(%)	(l/min)	(%)	(l/min)	(%)
Fine-grained granite	208.	44.3	11.02	8.8	7.48	21.6	0.06	0.1	226.56	36.0
Småland granite	72.5	15.4	52.65	42.3	17.27	50.0	2.3	1.9	144.72	22.6
Äspö diorite	184.	39.1	60.2	48.3	9.15	26.4	110.2	93.2	363.55	40.3
Greenstone	5.75	1.2	0.66	0.6	0.72	2.0	5.68	4.8	12.81	1.1
Pegmatite	0	0	0	0	0	0	0	0	0	0
Total	469.76	100	124.53	100	34.62	100	118.24	100	747.15	100

Table 6-29. Mapped inflow to the tunnel by rock type and in proportion to the total area of the rock type /*Rhén (ed), 1995*/.

	Tunnel chainage				
	700-1475 m l/(min•m²) x • 10^{-3}	1475-2265 m l/(min•m²) x • 10^{-3}	2265-2874.6 m l/(min•m²) x • 10^{-3}	2875-3600 m l/(min•m²) x • 10^{-3}	700-3600 m l/(min•m²) x • 10^{-3}
Fine-grained granite	100.4	6.6	12.8	0.1	45.1
Småland granite	25.8	21.2	15.3	12.4	21.9
Äspö diorite	37.7	10.3	3.5	12.7	16.5
Greenstone	24.8	0.8	6.9	17.9	8.6
Pegmatite	0	0	0	0	0
Total	46.8	11.4	7.7	12.0	21.2

Mapped inflow by leakage objects

The mapped leakage into the tunnel was separated into fracture "zones", "fractures" and "rock contacts" and diffuse leakage which could not be related to the first three objects. The last object was called "rock" in *Table 6-30*. This table shows the total mapped inflow from these four types of leaking object. As can be seen leakage related to rock contacts was very small. The major part of the inflow is from "fractures", but it is only just greater than "rock" and "zone".

Table 6-30. Mapped flow into the tunnel separated on objects "Rock", "Contact", "Fracture" and "Zone". (Zone includes all objects with the identification code ZI, that is fracture zones and increased fracturing.) /Rhén (ed), 1995/

Object	Tunnel section									
	700-1475 m (l/min)	(%)	1475-2265 m (l/min)	(%)	2265-2874.6 m (l/min)	(%)	2874.6-3600 m (l/min)	(%)	700-3600 m (l/min)	(%)
Rock	71.4	15	46	37	8.3	24	15.96	13.5	141.3	19
Contact	0	0	0	0	0.3	1	0.0	0	0.3	(0.04)
Fracture	123.9	26	39.3	32	14	40	79.27	67	256.5	34
Zone	274.4	59	39.2	31	12	35	23.01	19.5	352.3	47
Total	469.7	100	124.5	100	34.6	100	118.24	100	750.2	100

Trace length of water-conducting fractures

The trace length of fractures in the tunnel was documented during the construction of the tunnel. The length of the wetted part of a water-conducting fracture was also estimated if possible. The median length of the wetted part of a water-conducting fracture was about 0.3-1.5 m compared with the total trace length of the water-conducting fracture, which was 4-5 m */Rhén et al, 1993a,b, 1994a and 1995/.*